FINAL/TECHNICAL REPORT

Cryogenic Carbon Capture Development

Principle Authors	Larry L. Baxter – Principal Investigator Andrew Baxter Ethan Bever Stephanie Burt Skyler Chamberlain Dave Frankman Christopher Hoeger Eric Mansfield Dallin Parkinson Aaron Sayre Kyler Stitt
Date Prepared	28 September 2019
DOE Award Number	DE-FE0028697
Project Title	Cryogenic Carbon Capture Development
Submitting Organization	Sustainable Energy Solutions, LLC 1489 W 105 N Orem, UT 84057
Submitted To	U.S. Department of Energy National Energy Technology Laboratory 626 Cochrans Mill Road Pittsburgh, PA 15236-0940

Acknowledgement and Disclaimer

This material is based upon work supported by the Department of Energy under Award Number DE-FE0028697.

Executive Summary

This project extends and leverages the work completed under funding from ARPA-E and other sources by exploring aspects of the Cryogenic Carbon Capture™ (CCC) process and issues discovered during those projects, but that were not within the scope or budget of previous projects or that became apparent during field tests. Our successful completion of the tasks outlined in this project has increased the reliability, efficiency, and scalability of the CCC process and we are better prepared for pilot-scale testing. The first phase of this project improved key areas of the process through iterative design and experiment, culminating with recommendations for improvements to the existing skid-scale system developed under non-federal funding. The second phase of this project implemented the improved unit operations into the Cryogenic Carbon Capture External Cooling Loop (CCC ECL™) skid and field tests the improved system at a coal-fired power plant. The specific areas of work in this project are:

Budget Period 1:

- Selection of the most energy-efficient drying system for ambient-pressure flue gas.

  Sustainable Energy Solutions, LLC (SES) has successfully demonstrated a dryer that removes bulk water using a low-temperature brine to remove about 99% of the water followed by a mol sieve 3A desiccant dryer to remove the remaining 1% water.

- Selection and demonstration of efficient solution to fouling due to dissolved CO_2 in system.

  SES has tested several commercial heat exchangers that purport to be able to handle fouling issues similar to those experienced in the contact liquid chiller. Replicated tests using the CCC ECL™ skid and dimpled brazed plate heat exchangers demonstrate that quick throttling of refrigerant combined with a burst of clean gas mitigate the fouling caused by CO_2 solubility in contact liquid with only minor increases in parasitic load. SES models indicate that parasitic load would increase by approximately 0.0125 GJ/tonne, an order of magnitude less than what was determined to be the maximum allowable additional parasitic load caused by this system (i.e., approximately 0.1 GJ_e/tonne).

- Selection and demonstration of efficient and scalable solid–liquid separation system.

  The screw press technology met or exceeded the 70% solids loading benchmark during several test runs exceeding 24 hours as well as the initial stages of a 50-hour test run while capturing 0.5 tonne/day CO_2 on the CCC ECL™ skid. The average solids loading during the entire 50-hour run was 67%. The energy demand for this system is less than 0.1 GJ_e/tonne of CO_2 processed, all of which involves turning the auger.

- Optimize design and demonstration of patented desublimating heat exchangers.

  SES has a preliminary fluid bed heat exchanger designed, but we have decided to stop further development of this design because it will require more time and resources than we have available to develop to an appropriate stage for testing as part of this project.

  We have also designed and built a hybrid spray tower that combines the fast cooling of SES' patented bubbling desublimating heat exchanger and the efficient heat exchange of a spray tower. The hybrid spray tower/bubbler was tested over many hundreds of hours and a 50-hour continuous test run was completed capturing over 0.5 tonne CO_2/day at >90% capture.

- Continue testing of current system and improved reliability through optimization of controls.

  We have installed a Coriolis flow meter at the inlet feed to the solid–liquid separation system and two turbine flowmeters at the liquid output of each screw press. These flowmeters have already improved the reliability of the screw presses and allowed us to better characterize their performance. These performance results will help educate our design for scaling up the solid–liquid separation system. We have also installed mass flow controllers for injecting pollutants into our simulated flue gas stream and created new FTIR methods for measuring their concentrations.

- Plan for safe dilution of oxygen-depleted, cleaned flue-gas stream.

The AERSCREEN simulator developed by the EPA modeled the dispersion of oxygen-depleted flue gas from the CCC process at a commercial plant. SES performed these simulations with review and essential guidance from Tri-State and Sargent & Lundy. The results indicate that this plan effectively mitigates the flue gas hazards.

- Simulation of and experimental work related to multi-pollutant capture.

  SES programmed an upgrade to its solid/vapor/liquid equilibrium (SVLE) algorithm, moving from single-component to multi-component modeling. This enables simultaneous modeling of multiple pollutants (i.e., CO_2, SO_x, NO_x, Hg, HCl). The multi-component SVLE model does not provide any improvement in the capabilities of the in-house modeling software, but it does increase the time it takes to converge and increases the complexity of the bookkeeping requirements for the software. Thus, we decided instead to implement a simpler approach using a hybrid vapor/liquid and solid/vapor equilibrium (VLE/SVE) algorithm to model pollutant capture in the CCC process. The multi-component SVLE solver remains an option within the program but the more efficient hybrid solver is the method of choice for most computations that do not require detailed analyses of the multipollutant aspects of CCC. The results of both approaches compare well with experimental data and predict reasonable pollutant concentrations in the outlet streams from the CCC ECL™ process.

- Update techno-economic analysis with third-party validation.

  The Budget Period 1 techno-economic analysis has been completed. It confirms the potential large reduction in energy and cost of the CCC process compared with leading alternatives and that the estimates and estimation techniques are reliable.

Budget Period 2:

- Finalize the plans for modifying the CCC ECL™ skid for field testing, implement the modifications, and complete shakedown testing of the modified skid.

  The plans for modifying the CCC ECL™ skid were finalized and put into place. Shakedown testing of the updated CCC ECL™ skid occurred at SES using closed-loop mode (i.e., using a synthetic flue gas consisting of only N_2 and CO_2) and at the Hunter Power Plant using flue gas from the coal-fired boiler. Shakedown testing took longer than expected due to delays in receiving equipment and unexpected equipment performance in the field. Shakedown testing was completed in May 2019.

- Operate the CCC ECL™ skid in the field.

  Longer testing of the CCC ECL™ skid occurred at the Hunter Power Plant. Multiple tests exceeding 35 hours were completed, with a total of over 600 hours of CO_2 capture completed using flue gas at the Hunter Power Plant with an average CO_2 capture rate of over 91% during those hours. Extensive notes and documentation were acquired informing improved methods for controls, startup, operation, and shut down.

- Determine figures of merit and quantify process improvement.

  SES defined figures of merit for unit operation performance and overall CCC ECL™ process performance. All figures of merit were achieved or surpassed, except for 500 continuous hours of demonstration at the Hunter Power Plant.

- Update techno-economic analysis with third-party validation.

  The techno-economic analysis was continuously updated as more information was obtained during testing.

- Complete an Environmental Health and Safety Risk assessment by a third party.

  Tri-State completed an Environmental Health and Safety Risk assessment.

Table of Contents

Executive Summary i
1. Introduction 10
2. Budget Period 1 – Results and Discussion 13
Task 1. Project Management & Planning 13
Task 2. Drying 13
Desiccant Drying 14
Direct-Contact Phase-Change Drying 14
Prototype Testing of Direct-Contact Phase-Change Dryer and Two-Stage Dryer 18
Task 3. Dissolved Carbon Dioxide 20
Shell and Tube Self-Cleaning Heat Exchanger 21
Alternative Brazed Plate Heat Exchanger Testing 22
Process Controls Techniques to Prevent Fouling 23
Modeling Energy Penalty from Heat Exchanger Fouling Mitigation 25
Success Criteria 26
Task 4. Solid Liquid Separations 27
Task 5. Heat Exchanger Testing 28
Fluidized Bed Desublimating Heat Exchanger 29
Multi-Stage Desublimating Heat Exchanger 29
Spray Tower 30
Task 6. Instrumentation and Controls 34
Task 7. Light-Gas Dispersal 34
Task 8. Multi-Pollutant Capture 36
Pollutant Modeling 36
Pollutant Capture Measurements 37
Task 9. Phase 1 Techno-Economic Analysis 38
Improved In-House Software 38
SES TEA effort 39
Independent TEA Effort 49
Comparison of EPRI and SES Results 51
3. Budget Period 2 – Results and Discussion 52
Task 1. Project Management & Planning 52
Task 10. Skid Modification and Shakedown 52
Finalize Plans to Modify Skid and Complete Skid Modification 52
Complete Skid Shakedown Testing 79
Task 11. Skid Operation 82

Test Plan 82
Finalize Host Site Agreement 85
Skid Operation 86
Task 12. Quantify System Figures of Merit and Improvement 93
Figures of Merit Definition 93
Demonstrate Figures of Merit 93
Task 13. Phase 2 Techno-Economic Analysis 95
Updating the CCC ECL™ Techno-Economic Modeling 95
Energy Performance Comparisons 97
Conclusion 100
Task 14. EH&S Risk Assessment 101
Air, Water, and Solid Waste Identification for a Cryogenic Carbon Capture™ (CCC) System for a 550 MW Coal-Fired Power Plant 101
Toxicological Effects of Components in the CCC Process 102
U.S. EH&S Law Compliance and Regulation Implication for the CCC Process 105
Engineering Analysis and Controls for the CCC-ECL Process 108
Handling and Storage for the CCC-ECL Process 109
4. References 109

List of Figures

Figure 1. High-level flow diagram of the CCC ECL™ process. 10
Figure 2. Hunter Power Plant Unit 3 with preliminary testing locations marked. (red) Flue gas lines. (purple) Power lines to supply the skid. 13
Figure 3. Isotherm for water adsorption capacity of SYLOBEAD® 3A molecular sieve [1]. 14
Figure 4. DCPC drier schematic diagram. 15
Figure 5. Predicted water vapor pressures over ice (yellow) and aqueous methanol (orange) and ethanol (blue) mixtures as a function of temperature. 16
Figure 6. Phase diagram of the LiCl–H_2O system temperature from 160 to 400 K. L: Liquid, L0: LiCl(cr), L1: LiCl H2O(cr), L2: LiCl 2H2O(cr), L3: LiCl 3H2O(cr), L5: LiCl 5H2O(cr) [2]. 16
Figure 7. Phase diagram including potassium acetate and water (squares) [3]. 17
Figure 8. Freezing points of water–alcohol mixtures [4]. 17
Figure 9. Heats of solution for HCl and LiCl at 25 °C [5]. 18
Figure 10. Process flow diagram of the DCPC dryer testing system. 19
Figure 11. Dewpoint measured at the outlet from the combined DCPC dryer followed by a mol sieve dryer [6]. 19
Figure 12. Dewpoint measured at the outlet from the DCPC dryer [6]. 20
Figure 13. Shell and tube heat exchanger designed for testing ball cleaning. The contact liquid with dissolved CO_2 will run through the tube side and a boiling refrigerant will be on the shell side. Passing PTFE balls through the tubes should clean any CO_2 deposits from the tube walls. These balls are then captured and recirculated through the system. 22
Figure 14. Differing plate geometries. High Θ represents better heat transfer per unit of surface area, but has a greater fouling tendency. Extra low Θ has lower heat transfer per unit of surface area, but has a lesser tendency to foul [7]. 22
Figure 15. Pressure drop measured in psi across the uncoated heat exchanger. 24
Figure 16. Pressure drop measured in psi across the coated heat exchanger. 24
Figure 17. CO_2 capture during 27-hr test using a single coated heat exchanger with an average 96.5% CO_2 capture. 25
Figure 18. Effects of fouling mitigation techniques on temperature of system 26
Figure 19. Mass fraction of CO_2 exiting the solid–liquid separations system for a 50-hour test run at 0.5 tonne/day CO_2 [6]. 28
Figure 20. Mass fraction of CO_2 exiting the solid–liquid separations system for representative 15- to 30-hour test runs at 0.5 tonne/day CO_2 [6]. 28
Figure 21. CAD drawing of fluidized bed heat exchanger. 29
Figure 22. Still image taken from the camera feed inside the desublimating heat exchanger showing the cold contact liquid/solid CO_2 slurry entering the heat exchanger (from the left side of the image). 29
Figure 23. Spray tower during installation. 30
Figure 24. Contact liquid droplet visual measurement. 31
Figure 25. Spray plate for optimal spatial distribution of contact liquid droplets. 32
Figure 26. Hybrid spray tower/bubbler half section. 32
Figure 27. Percent CO_2 capture over 50-hour run [6]. 33

Figure 28. CO_2 capture by mass accumulation rate and total mass [6]. 33
Figure 29. Model output predicting the maximum N_2 concentration at each distance from the stack when emitting the clean CCC gas up the stack at the power plant [6]. 35
Figure 30. Calculated minimum O_2 concentration using the predicted the maximum N_2 concentration at each distance from the stack when emitting the CCC clean gas up the stack at the power plant [6]. .. 35
Figure 31. Example output from a Distillation Column unit operation simulation. 38
Figure 32. Partial output from SES' standalone Spray Tower simulator calculating the CO_2 and contact liquid content in the clean gas exiting the spray tower. 39
Figure 33. Comparison of the primary energy demands in an air-separation-based unit and in the CCC process 40
Figure 34. Pollutant Capture at CCC temperatures 41
Figure 35. Histograms of overall HHV plant efficiencies for all utility-scale bituminous coal, subbituminous coal, lignite, and natural gas plants operated in the first 8 months of 2017 in the US, with a total of 277 coal plants and 299 natural gas plants. The plant efficiency assumed in the NETL report is 0.41. 43
Figure 36. COE of different case studies broken into component parts. 47
Figure 37. Cost of CO_2 48
Figure 38. Renderings of the new refrigeration/cooling coldbox. 53
Figure 39. Coldbox after removing the refrigerant pump. The brazed plate heat exchanger is shown in the back (dark orange). 53
Figure 40. Skid layout without skid walls. Upper panel shows the view from above. The upper cold box is shown in the lower panel and is housed above the screw press. 54
Figure 41. A screenshot from the SES dryer model, showing temperature and moisture profiles of the desiccant bed at a moment in time during the regeneration phase. (top left) Temperature as a function of bed location. (top right) Desiccant loading in kg water/kg desiccant. (bottom left) Partial pressure of water in the gas phase. (bottom right) Dew point of the gas phase. During regeneration, flow enters from the right (zone 49) 55
Figure 42. Model output representing the dryer after any number of loading and regeneration cycles at 1 tonne CO_2/day using a portion of the clean nitrogen from the process outlet to regenerate the desiccant. 56
Figure 43. CAD rendering of the mol sieve desiccant dryer 56
Figure 44. Mol sieve dryer integrated with the CCC ECL™ Skid. Both beds are covered with blankets of gray fiberglass insulation. 57
Figure 45. Flue gas conditioning portion of the CCC ECL™ skid. Two cyclonic separators were added during shakedown testing to improve water removal and dryer performance. 58
Figure 46. Updated process flow diagram of the recuperator and spray tower for the CCC ECL™ skid. . 59
Figure 47. (left) Recuperator heater casing design, (middle) actual heater, and (right) installed. 59
Figure 48. Airec asymmetrical heat exchanger. 60
Figure 49. Recuperator (red box, left) and new secondary "precuperator" (red box, right). 60
Figure 50. Vapor–liquid separator for removing entrained contact liquid from the clean gas stream. 61
Figure 51. Drawing of the spray tower coldbox. The vessel in the front on the right is the spray tower. The vessel partially obscured behind and to the left is the vapor–liquid separator. 62
Figure 52. Image of the spray tower interior after the polished lining was inserted into the spray tower. . 63
Figure 53. Polished cap of spray tower. 63

Figure 54. Spray nozzle assembly prior to mounting in the spray tower. The liquid to be sprayed enters at the compression fitting in the center of the image. The air motor that turns the drive shaft is on the left and the spray head and drive gear is located on the right. 64
Figure 55. Interior of the spray tower showing the cleaning spray. 64
Figure 56. View of complete hybrid spray tower with a single impact air knocker installed at the top (green). The air knocker extends above the insulation surrounding the heat exchanger. 65
Figure 57. Operating mechanism for the external-gear pumps originally installed on the CCC ECL™ skid. 65
Figure 58. External gear pump bearing showing uneven wear, as evidenced by the thinner wall towards the upper right. 66
Figure 59. Heat exchanger designed and constructed at SES. 67
Figure 60. Shell and tube heat exchanger with extended ends for including scrapers or brushes. 68
Figure 61. Rendering from PT&M of the 1 tonne/day screw press. 69
Figure 62. FEA analysis for the filter support cylinder. 70
Figure 63. (left, center) Mesh pressure testing apparatus. (right) Example of pressure-tested mesh showing permanent deformation. 70
Figure 64. Completed filters for new screw press 71
Figure 65. 6-inch screw press installed on its mount before insulation was applied. 71
Figure 66. Melter section with cameras and instrumentation attached. 72
Figure 67. Internal view of the melter plunger. 72
Figure 68. Microscope images of a shiny portion of the mesh with the microscope focus moving down (L to R) through the layers of the mesh. 73
Figure 69. High-level Process Flow Diagram of the Distillation Column and Surrounding Systems 74
Figure 70. Fully assembled distillation column before adding side panels and loose perlite insulation. 75
Figure 71. Distillation column (foreground) installed at the Hunter Power Plant 76
Figure 72. Contact liquid P&ID showing the location of the two pollutant removal and sampling units installed inside the distillation column cold box. 77
Figure 73. One of the pollutant settling tanks with a vapor–liquid separation drain and filter on the bottom. 78
Figure 74. Data output from the SES historian showing data during the test on June 3–4, 2019. Both plots have units of hours and minutes for the x axis. The y axis of the top plot is CO_2 capture (%). The y axis of the bottom plot is flue gas flow rate (kg/hr). 78
Figure 75. Screenshot of the SCADA software developed by SES. Clockwise from upper-left: process flow diagram, historical trends, issues, watch window, alarm window, log window. 79
Figure 76. Test duration comparison while conducting shakedown and skid operation testing on site at the Hunter Power Plant 80
Figure 77. Mass fraction of the slurry over a 24-hour period while the impulse vibrater on the spray tower operates every 10 minutes. 81
Figure 78. Temperatures into and out of the cooling heat exchanger over time compared with the increase in pressure drop across the heat exchanger. 82
Figure 79. Aerial photograph of Unit 3 at the Hunter Power Station with scale blocks representing the skids. 83

Figure 80. Timeline of the on-site testing. 84
Figure 81. CCC ECL™ skid PFD with instrumentation locations. 85
Figure 82. Cumulative hours testing CCC ECL™ skid capturing CO_2 from flue gas at the Hunter Power Plant. 86
Figure 83. Pressure before (PT-913) and after (PT-904) the contact liquid heat exchanger compared with the contact liquid temperature (TT-912). 87
Figure 84. Sample of contact liquid chilled in a freezer to −40 °C. The amber liquid is a separate liquid phase; its composition will be determined by future analytical tests. 88
Figure 85. Test data from May 28–29, 2019. 89
Figure 86. Test data from May 31–June 1, 2019 90
Figure 87. Test data from June 1–3, 2019. 91
Figure 88. Test data from June 3–4, 2019. 92
Figure 89. Representative plots of pressure drop through the shell and tube heat exchanger: (top) May 31–June 1, 2019, (middle) June 1–3, 2019, (bottom) June 4–5, 2019. 94
Figure 90. Predicted CO_2 outlet compared with test data 96
Figure 91. Pressure drop through the non-fouling heat exchanger 96
Figure 92. COE of different case studies broken into component parts (updated from Figure 36 in the Budget Period 1 TEA). 98
Figure 93. Cost of CO_2 (updated from Figure 37 in the Budget Period 1 TEA). 99

List of Tables

Table 1. Comparison of alternative brazed plate heat exchangers used in testing. 23
Table 2. Time to return to baseline and average temperature from mitigation 26
Table 3. Sensitivity analysis output from AERSCREEN. For each variation, all other factors were held constant at the typical value. 36
Table 4. Pollutant concentrations as predicted using the in-house model and measured from pollutant-capture testing of the skid-scale CCC ECL™ process. 37
Table 5. Pollutant concentrations in the purified CO_2 outlet. 38
Table 6. Pollutant levels at 90% CO_2 capture 42
Table 7. List of Parasitic Loads for CCC 44
Table 8. Summary of Energy Penalty of CCS technologies 45
Table 9. Energy requirements for amine-based CCS technologies, based on reports from the US, Europe, China, and Australia [12]. 45
Table 10. Cost comparison between NETL Cases B12A and B12B as well as estimates for the CCC process, both as a greenfield installation and as a retrofit installation. 48
Table 11. Cost of CO_2 comparison for greenfield cases. 48
Table 12. Increase in COE for amine-based CCS installations [12] and CCC. 49
Table 13. CCC system performance summary. 50
Table 14. CO_2 capture auxiliary load. 50
Table 15. Revised stages for distillation startup procedure. 77

Table 16. Control system specifications 79
Table 17. Key measured parameters and their locations in the ECL skids. 84
Table 18. Figures of merit for individual unit operations and the CCC process as a whole used to quantify the improvements achieved during this project. 93
Table 19. Quantitative results from operating the CCC ECL™ skid at the Hunter Power Plant for the figures of merit for individual unit operations and the CCC process as a whole. 93
Table 20. List of Parasitic Loads for CCC (updated from Table 7 in the Budget Period 1 TEA). 97
Table 21. Summary of Energy Penalty of CCS technologies (updated from Table 8 in the Budget Period 1 TEA). 98
Table 22. Cost comparison between NETL Cases B12A and B12B as well as estimates for the CCC process, both as a greenfield installation and as a retrofit installation (updated from Table 10 in the Budget Period 1 TEA). 99
Table 23. Cost of CO_2 comparison for greenfield cases (updated from Table 11 in the Budget Period 1 TEA). 100
Table 24. Increase in COE for amine-based CCS installations [12] and CCC (updated from Table 12 in the Budget Period 1 TEA). 100
Table 25. Composition and flow rate for the clean light gas out 101
Table 26. Composition and flow rate for CO_2 final product 102
Table 27. Composition and flow rate of water out after flue gas pre-cooler 102
Table 28. Composition and flow rate of pollutant capture/waste stream 102
Table 25. Regulator overview for components of CCC system 105
Table 26. Criteria to be considered characteristic hazardous waste under RCRA Subtitle C. 107

1. Introduction

Cryogenic Carbon Capture™ (CCC) is a promising, transformational post-combustion carbon capture technology. The CCC process can reduce CO_2 emissions by over 95% at a cost of less than $45/tonne of CO_2 avoided and has a parasitic load of less than 17%. This is about half the energy and cost of currently available technologies and meets the DOE goals for carbon capture systems. Additionally, the CCC process easily retrofits existing plants, recovers water from flue gas, enables energy storage, and robustly handles most impurities in the gas stream.

The CCC External Cooling Loop (CCC ECL™) process (Figure 1) dries and cools flue gas from existing systems to near ambient temperature, provides pressure sufficient to overcome pressure drop, cools it to a temperature slightly above the point where CO_2 forms a solid, condenses CO_2 in a desublimating heat exchanger as it further cools the gas, precipitating CO_2 as a solid, separates the solid from the gas, pressurizes the CO_2, and reheats the CO_2 and the remaining flue gas by cooling the incoming gases. A thermodynamic feature of CO_2 in most flue gases (<16% CO_2 on a dry basis) is that CO_2 will not form a liquid phase at any temperature or pressure. Rather, the CO_2 desublimates in a thermodynamically pure solid phase or remains as a vapor. The CCC process produces CO_2 in a high-pressure, liquid phase and the remaining flue gas at ambient pressure. Both streams are near ambient temperature. CO_2 capture efficiency depends primarily on the coldest temperature the flue gas obtains. At 1 bar, the process captures 99% of the CO_2 from typical coal flue gases at −207 °F (−133 °C) and 90% at −179 °F (−117 °C). Furthermore, the captured CO_2 is typically 99.4–99.99% pure.

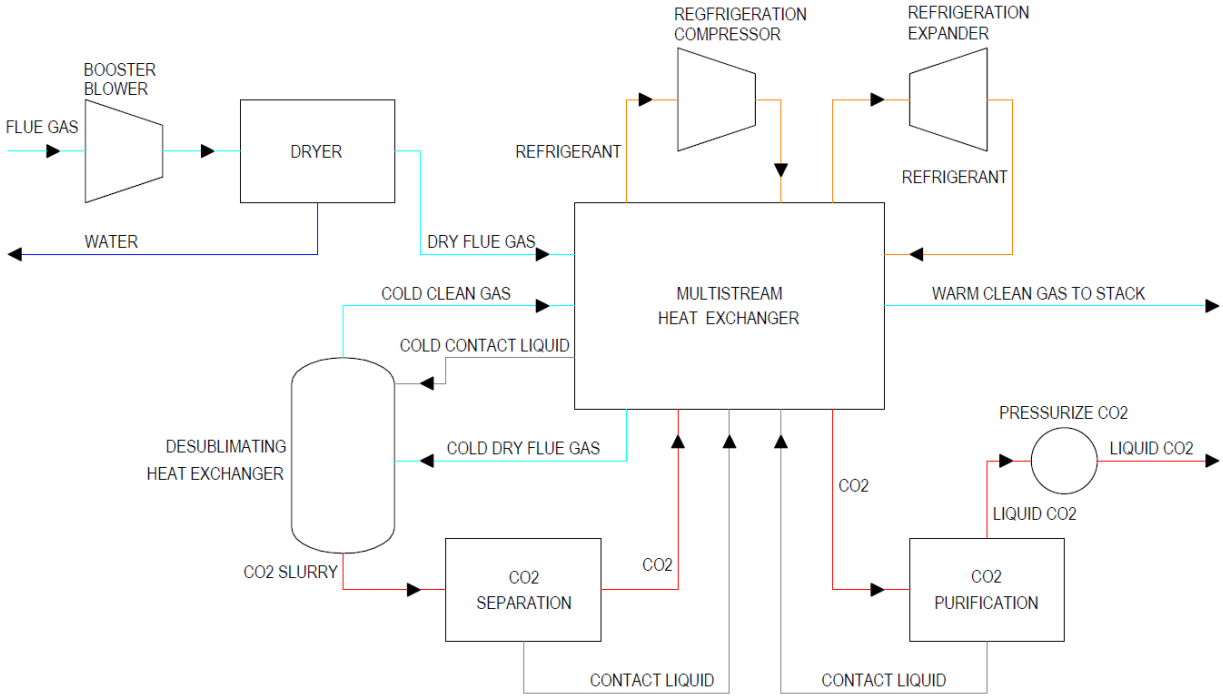

Figure 1. High-level flow diagram of the CCC ECL™ process.

These are relatively mild conditions compared with competing oxyfuel technologies, which require temperatures of about −200 °C with a slightly larger volumetric flow rate of gas and requires substantial purification steps after the combustor. Most carbon capture technologies also produce a gaseous CO_2 stream that requires compression to 100–150 bar whereas CCC produces a liquid CO_2 stream that requires fewer resources to compress, including capital and operating costs and energy. Additionally, most alternative processes exhibit rapidly increasing costs and energy demands as capture increases above 90%. Due to the

relatively small difference in temperature as the capture increases (~15 °C between 90% and 99% capture), CCC does not exhibit this same rapid increase.

This project extends and leverages the work completed under funding from ARPA-E and other sources by exploring aspects of the CCC process and issues discovered during those projects, but that were not within the scope or budget of previous projects or that became apparent during field tests. Successfully completing the tasks outlined in this project will increase the reliability, efficiency, and scalability of the CCC process and prepare it for pilot-scale testing. The first phase of this project improves individual unit operations through iterative design and experiment, culminating with recommendations for improvements for the existing, skid-scale system developed under non-federal funding. The specific areas of work in this project are:

Budget Period 1:

- Selection of the most energy-efficient drying system for ambient-pressure flue gas.
    - *Specific Objectives:* The objective of this task is to decrease the energy consumption and CO_2 absorption in the final flue gas drying stages of CCC.
- Selection and demonstration of efficient solution to fouling due to dissolved CO_2 in system.
    - *Specific Objectives:* The objective of this task is to eliminate the accumulation of dissolved CO_2, solid CO_2, and other possible impurities in the CCC process.
- Selection and demonstration of efficient and scalable solid–liquid separation system.
    - *Specific Objectives:* The objective of this task is to improve the reliability and performance and to decrease the energy consumption of the solid–liquid separation process.
- Optimized design and demonstration of patented desublimating heat exchangers.
    - *Specific Objectives:* The objective of this task is to explore the relative merits of the three desublimating heat exchanger designs in a commercial-scale implementation of CCC.
- Continue testing of current system and improve reliability through optimization of controls.
    - *Specific Objectives:* The objective of this task is to extend the skid testing time through improved controls, and instrumentation.
- Plan for safe dilution of oxygen-depleted, cleaned flue-gas stream.
    - *Specific Objectives:* The objective of this task is to explore issues with light-gas dispersal when the gas temperature is near room temperature
- Simulation of and experimental work related to multi-pollutant capture.
    - *Specific Objectives:* The objective of this task is to develop models that describe CCC capture of pollutants other than CO_2 and to validate these models with experimental data.
- Update techno-economic analysis with third-party validation.
    - *Specific Objectives:* The objective of this task is to maintain techno-economic analyses during development of the CCC process.

Budget Period 2:

- Finalize the plans for modifying the CCC ECL™ skid for field testing, implement the modifications, and complete shakedown testing of the modified skid.
    - *Specific Objectives:* The objective of this task is to modify the existing skid system to incorporate the improvements identified in Budget Period 1 and to shakedown the resulting system.
- Operate the CCC ECL™ skid at SES and in the field.
    - *Specific Objectives:* The objective of this task is to test the improved skid in house and in the field, with at least one test consisting of a minimum of 500 continuous hours.
- Determine figures of merit and quantify process improvement.
    - *Specific Objectives:* The objective of this task is to quantify the improvements in the skid system and in the unit operations identified above.
- Update techno-economic analysis with third-party validation.

  - *Specific Objectives:* The objective of this task is to quantify theoretical improvements in techno-economic performance of the CCC process based on the work in Budget Period 1 and the results in Budget Period 2.
- Complete an Environmental Health and Safety Risk assessment by a third party.
  - *Specific Objectives:* The objective of this task is to assess the environmental friendliness and safety of the proposed process.

2. Budget Period 1 – Results and Discussion

Task 1. Project Management & Planning

Specific Objectives: The objective of this task is to manage, coordinate, and report on the technical scope, budget, and schedule consistent with a task-oriented work breakdown structure to accomplish the work effectively and to ensure that project plans, results, and decisions are appropriately documented, and that project reporting and briefing requirements are satisfied.

The Project Officer has approved the Project Management Plan (PMP).

Larry Baxter and Kyler Stitt attended the project kick-off meeting held on December 9, 2016 at the National Energy Technology Laboratory (NETL) in Pittsburgh, PA.

Kyler Stitt and Larry Baxter held a conference call with all the subcontractors. We met with individuals from Rocky Mountain Power (RMP) to prepare for field testing at one of their power plants. RMP is providing in-kind cost share for this project. In addition, RMP is funding a separate project that extends the SES field test at their unit by several months. SES visited the Hunter Power Plant in Castle Dale, UT and tentatively selected the third unit of the plant, which is the only unit exclusively owned by PacifiCorp, as the test site. This unit and preliminary testing locations appear in Figure 2. A finalized contract with PacifiCorp describes the insurance and general on-site safety requirements.

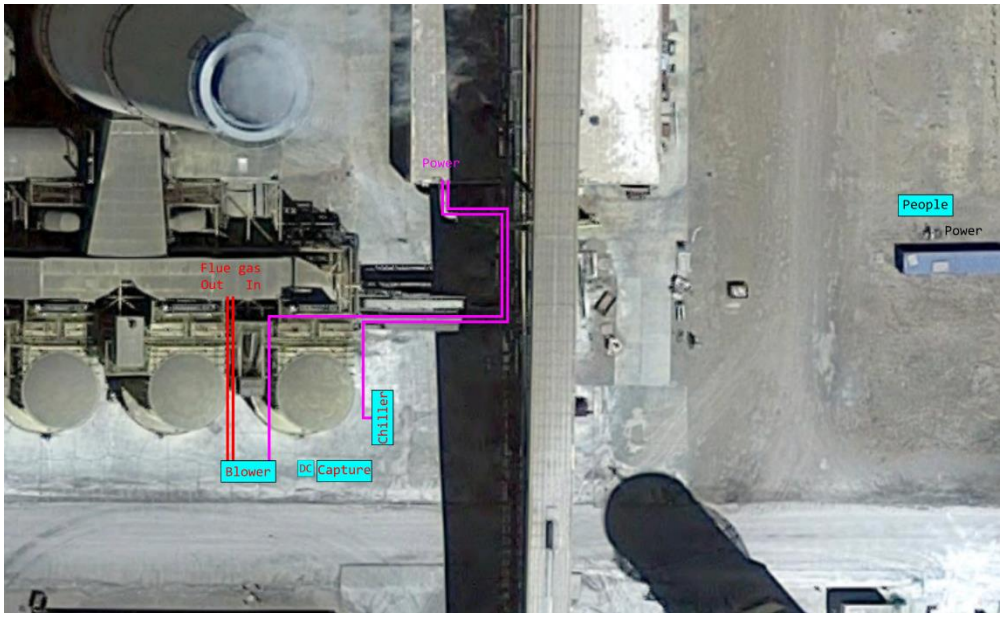

Figure 2. Hunter Power Plant Unit 3 with preliminary testing locations marked. (red) Flue gas lines. (purple) Power lines to supply the skid.

SES is also working closely with Tri-State as they become better acquainted with the CCC ECL™ process and are working through an external analysis of the process and its economic and environmental impacts.

We submitted a Budget Period 2 continuation application. A Budget Period 1 project review meeting with NETL occurred on August 8, 2017 via WebEx and teleconference. In addition, Larry Baxter presented the project status at the 2017 NETL CO_2 Capture Technology Project Review Meeting in Pittsburgh on August 24, 2017.

Task 2. Drying

Specific Objectives: The objective of this task is to decrease the energy consumption and CO_2 absorption in the final flue gas drying stages of CCC.

Desiccant Drying

We sized a system with molecular sieve 3A to achieve our dew point target while minimizing the thermal mass of the system. Because the ability of most desiccants to capture water is proportional to the amount of water vapor in the air being dried, significantly more desiccant is required to take the gas from 100 ppmv to 10 ppbv H_2O than is required to get from 10,000 ppmv to 100 ppmv. We reviewed isotherm data (Figure 3) for the molecular sieve to estimate the smallest dryer size to minimize the thermal mass and pressure drop of the system.

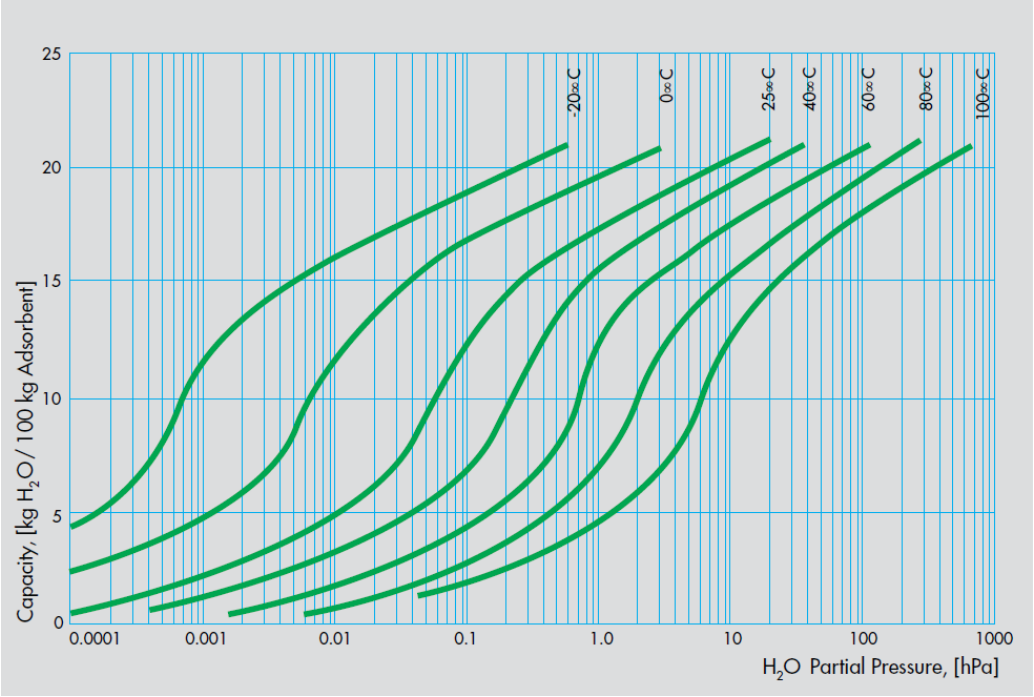

Figure 3. Isotherm for water adsorption capacity of SYLOBEAD® 3A molecular sieve [1].

Direct-Contact Phase-Change Drying

SES developed the direct-contact phase-change (DCPC) drier, which simultaneously cools and dries a gas (Figure 4). The process has some similarities to the desublimating heat exchangers used for CO_2 removal. Moist flue gas enters the process at the bottom of the direct-contact heat exchanger in the upper portion of in this figure. The flue gas contacts a counter-current, low-temperature, aqueous liquid and moisture from the flue gas condenses as a liquid well below the freezing point of water. Dry flue gas exits the direct-contact heat exchanger and goes to the CO_2 removal stages of the process. After CO_2 removal, flue gas returns to the bottom of the heat recovery heat exchanger where it warms as the aqueous liquid cools. This heat exchanger may or may not be a direct-contact design, depending on the choice of the liquid, as described later.

The cold aqueous liquid enters the top of a direct-contact heat exchanger and cools the flue gas, condensing some residual moisture in the process. This heat exchanger is a packed column, spray tower, or similar low-pressure-drop but efficient contacting device, possibly with an internal finned-tube heat exchanger near the bottom to help condense the moisture. The aqueous liquid exits the direct-contact chamber near the flue gas entrance temperature. A membrane, distillation column, flash drum, or some other suitable device partially dewaters the aqueous liquid at either this stage or in the cold leg of the process, removing the moisture that the aqueous liquid collected in the direct-contact heat exchanger. The aqueous liquid then enters a second heat exchanger and cools as it warms the treated flue gas. The cold aqueous solution then recycles to the first heat exchanger. An alternative means of dewatering the solution at warm temperatures is to freeze some water out of the solution in this recirculation leg.

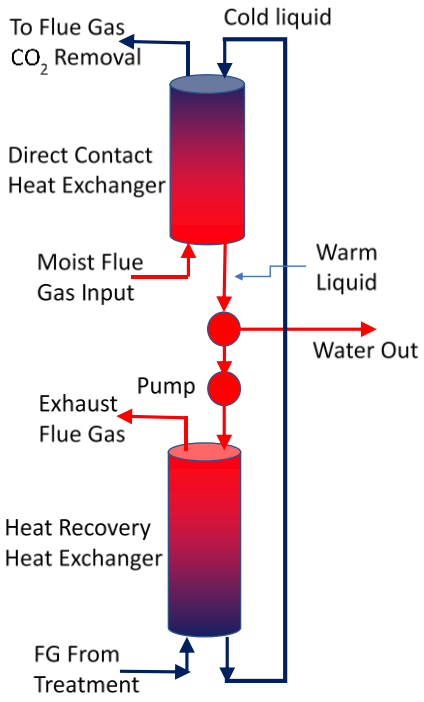

Figure 4. DCPC drier schematic diagram.

The DCPC can use several aqueous fluids. This discussion illustrates two brine solutions and two alcohol mixtures that are economical and have minimal environmental or safety hazards. The brine solutions have essentially zero salt vapor pressure while the two alcohols can achieve lower temperatures without freezing and are less corrosive. Both condense water to vapor pressures below those of pure water/ice at the same temperature (Figure 5) and both provide efficient water removal with lower pressure drop and energy demand than adsorption systems. The flue gas enters the desublimating heat exchanger at about −100 °C. These dryers/coolers should prevent ice formation at this temperature. To do so, the methanol and ethanol systems need only equilibrate with the gas at −87 °C and −78 °C, respectively, providing a large safety margin for operation if they are used to cool the gas to −100 °C or preventing ice formation in a traditional heat exchanger if it is used for the final cooling step. In the temperature range of interest to this application, the liquids SES reviewed have low vapor pressures and relatively low viscosity. The two brines include a lithium chloride/water brine (Figure 6) and a potassium acetate/water solution (Figure 7). Non-ionic systems of interest include an ethanol/water solution and a methanol/water solution, both of which can reach −100 °C without freezing (Figure 8). The vapor pressures of the alcohol solutions exceed the near-zero vapor pressures of the salt in the brine solutions and therefore require a non-contact heat exchanger during heat recovery to prevent the warm liquid phase from losing alcohol vapor to the gas phase. A non-contact heat exchanger is both larger and less efficient than a direct-contact heat exchanger, but the non-contact (traditional) heat exchanger eliminates vapor loss and maintains different pressures in the two streams. The four aqueous phase-change drying solutions all require less energy, have a smaller footprint, and have much lower pressure drops than the sorbent systems they would replace.

A calorimeter (built by SES) verified the salt heats of solution over a range of concentrations near the eutectic points. The LiCl/H_2O heat of solution is highest for concentrations of 1–3 moles H_2O to 1 mole LiCl. As the water concentration increases, the heat of solution decreases. SES tested the range of 6.7 to 15.7 mol H_2O + LiCl. The literature heats of solution data are included in Figure 9.

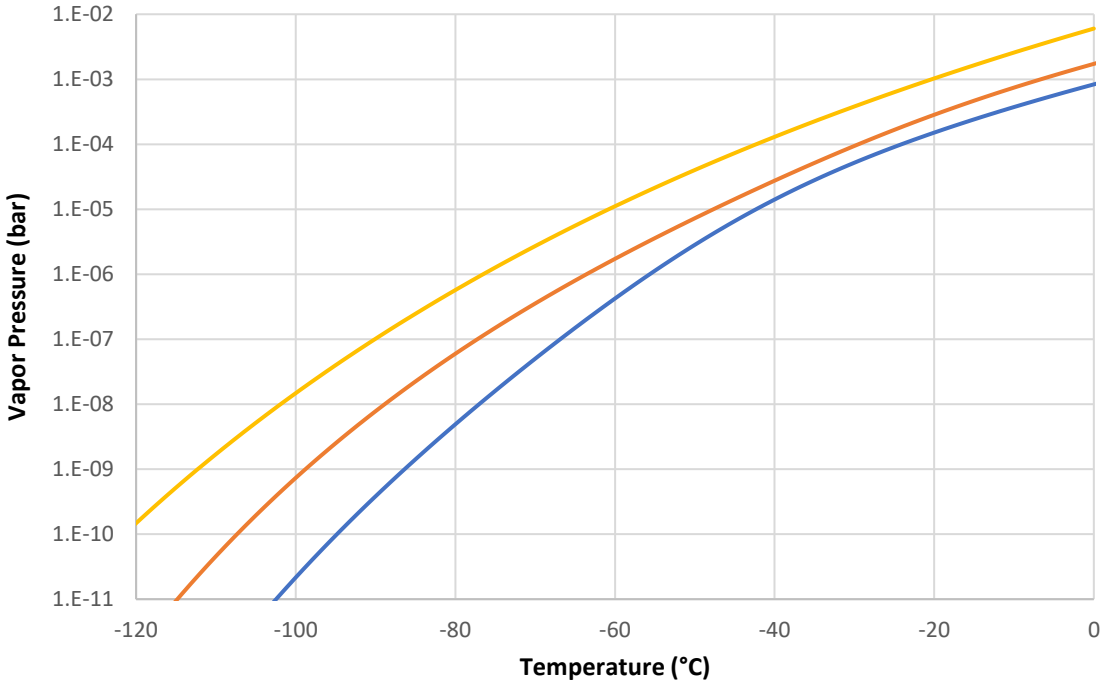

Figure 5. Predicted water vapor pressures over ice (yellow) and aqueous methanol (orange) and ethanol (blue) mixtures as a function of temperature.

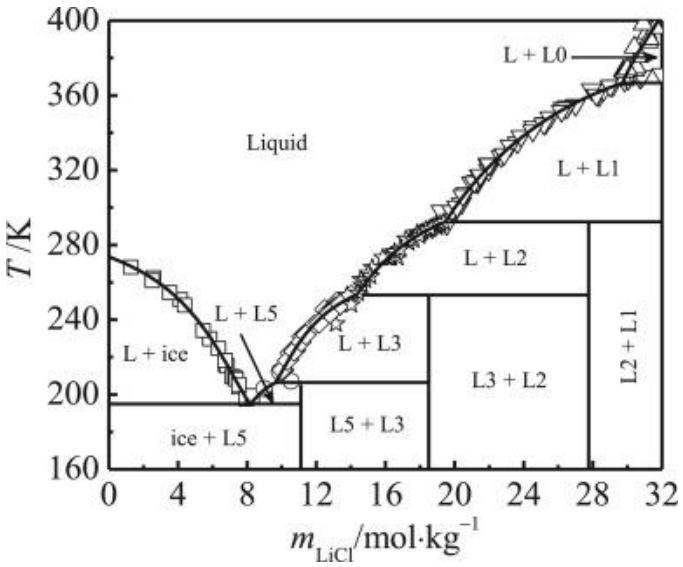

Figure 6. Phase diagram of the LiCl–H_2O system temperature from 160 to 400 K. L: Liquid, L0: LiCl(cr), L1: LiCl H2O(cr), L2: LiCl 2H2O(cr), L3: LiCl 3H2O(cr), L5: LiCl 5H2O(cr) [2].

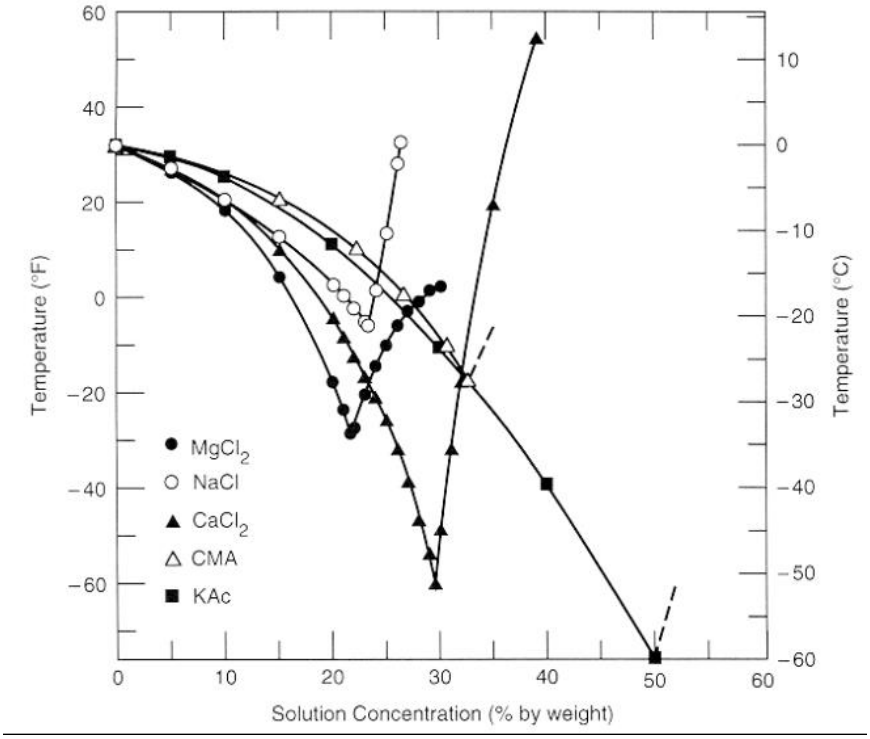

Figure 7. Phase diagram including potassium acetate and water (squares) [3].

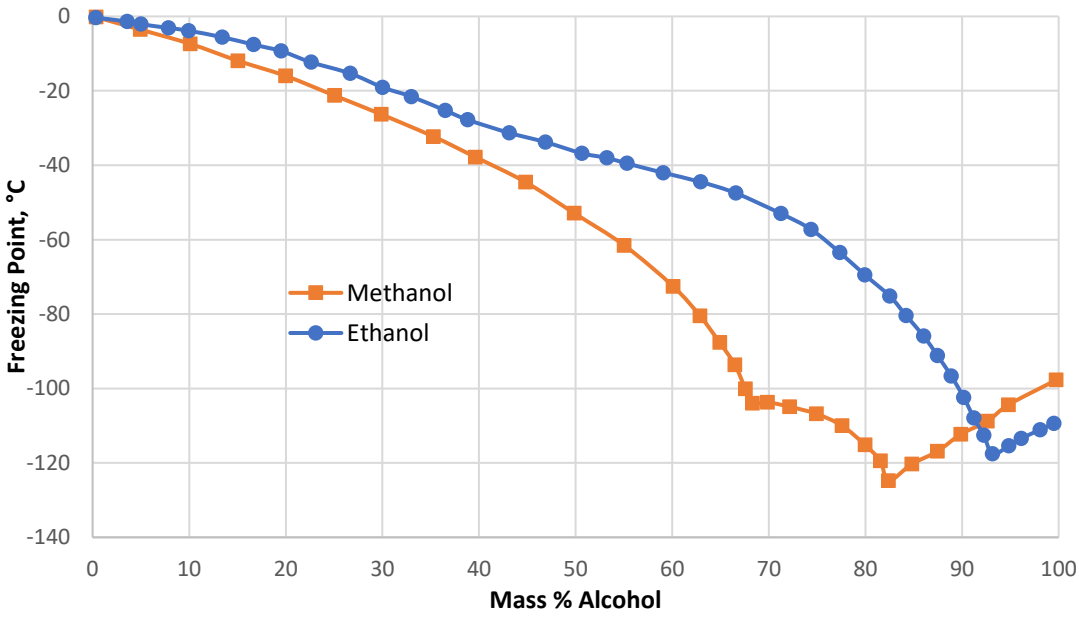

Figure 8. Freezing points of water–alcohol mixtures [4].

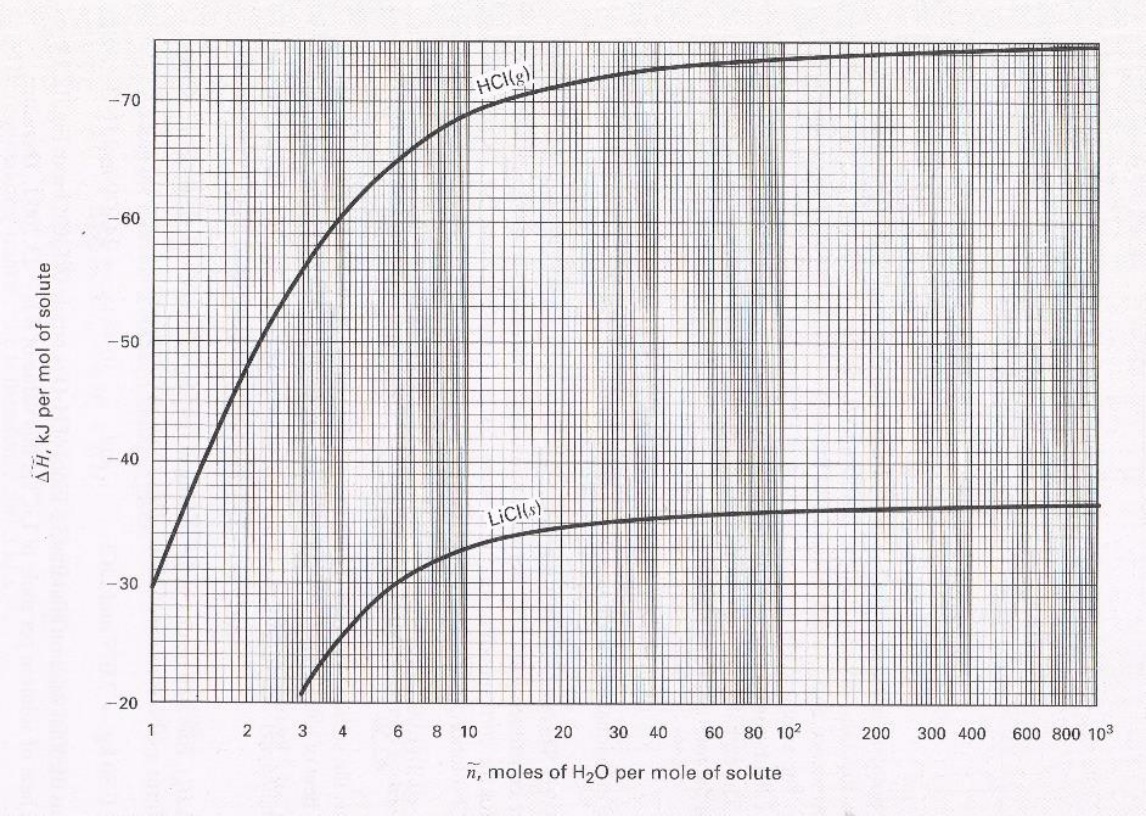

Figure 9. Heats of solution for HCl and LiCl at 25 °C [5].

Prototype Testing of Direct-Contact Phase-Change Dryer and Two-Stage Dryer

SES designed and built a bench-scale test dryer for a 1 SCFM stream of simulated flue gas. Two thermal mass flow controllers create a stream of N_2 and CO_2 from gas cylinders. That stream bubbles through a humidifier that saturates the stream with water at a given temperature and pressure. That stream then enters the prototype DCPC dryer. In some tests, the gas then flows through a small desiccant bed to further dry the gas. Figure 10 shows the process flow diagram for the bench-scale dryer tests.

Figure 11 shows data from the prototype DCPC dryer followed by a small mol sieve 3A packed bed. A statistics program called R performed the data analysis [6]. The hydrator saturated the stream with water to a dew point above 20 °C at 148 kPa (>23,339 ppmv H_2O). Nitrogen purged the dew point transmitter until the brine temperature reached about −35 °C (225 ppmv H_2O). The transmitter then switched to the dryer outlet and recorded a dew point below −70 °C (< 2.7 ppmv). The dew point transmitter responds slowly at low dew points. This approach provided the outlet gas measurements near the end of the experiment (Figure 11) for the DCPC stage and the mol sieve (Figure 12). The dew point after the DCPC closely matched the expected dew point of −35 °C (about 255 ppmv), which demonstrates that the DCPC removed about 99% of the water, with the remaining water removed in the desiccant stage (going from 255 to 2.7 ppmv). The actual dew point is lower than the measured dew point because the dew point sensor slowly sheds water over time. Even with a N_2 purge, the sensor requires hours to get to a measured dew point of −70 °C and significantly longer to reach a dew point of −80 °C. While we recorded dew points below −70 °C, it is very possible the actual dew point was much lower.

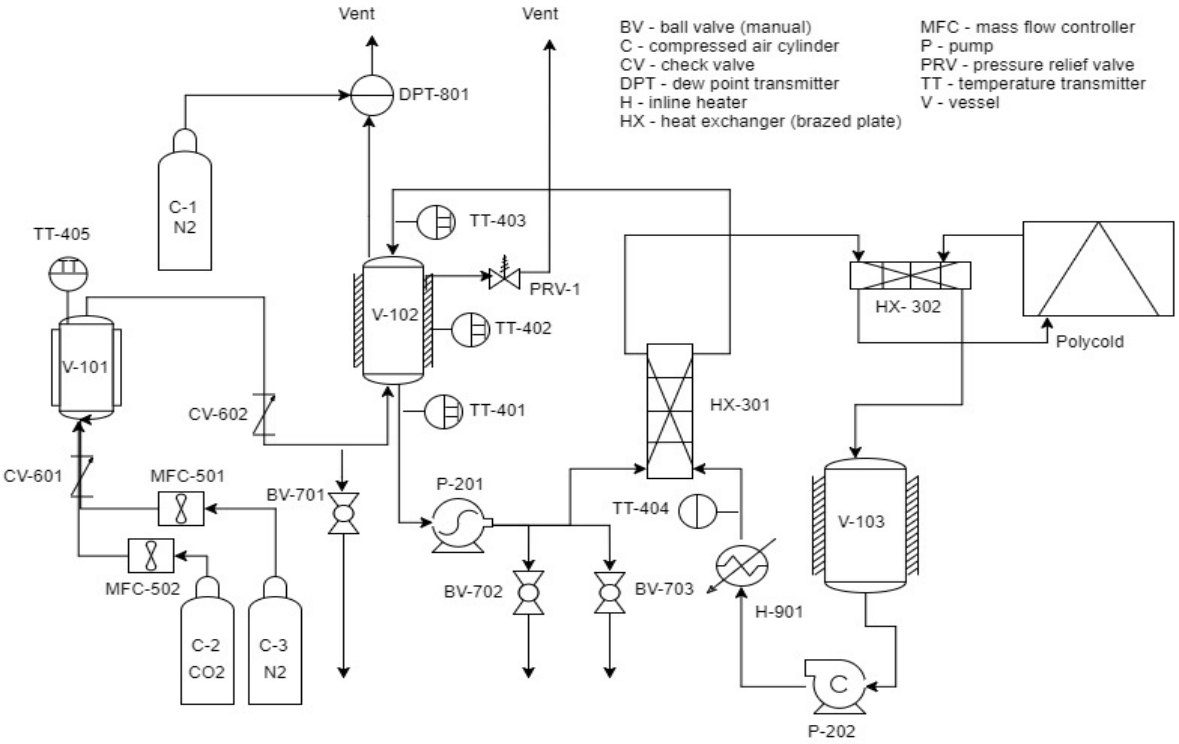

Figure 10. Process flow diagram of the DCPC dryer testing system.

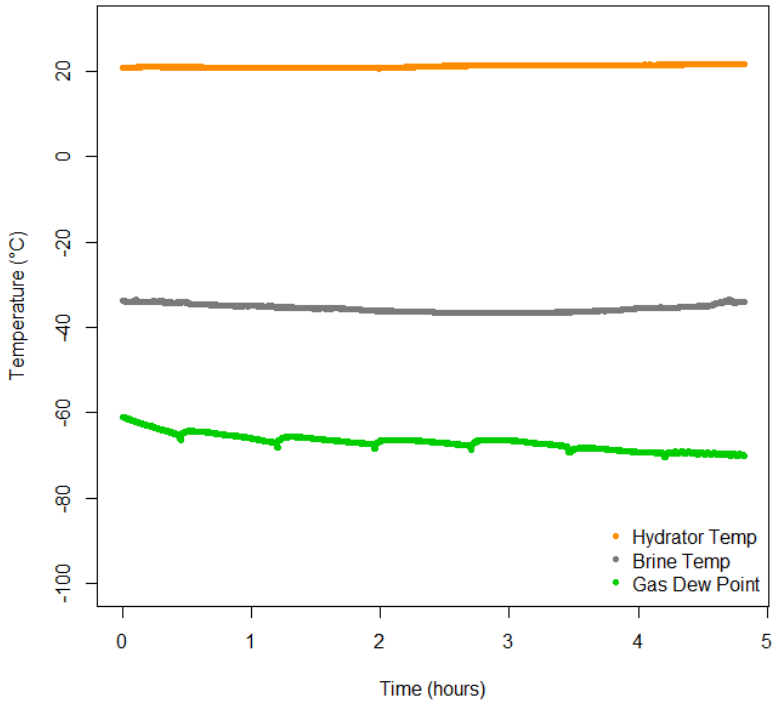

Figure 11. Dewpoint measured at the outlet from the combined DCPC dryer followed by a mol sieve dryer [6].

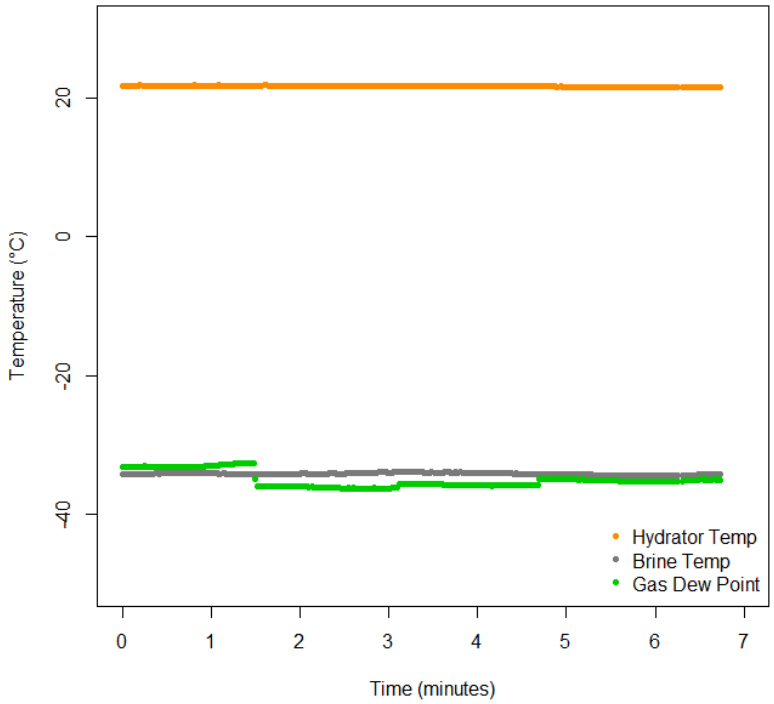

Figure 12. Dewpoint measured at the outlet from the DCPC dryer [6].

By removing over 99% of the water in the DCPC, we significantly reduce the pressure drop of the system. While we have to increase the cooling load to account for the heat of mixing of the phase change of the water, the decreased pressure drop more than makes up for the extra cooling required. To quantify the energy penalty of the dryer, we optimized a CCC process simulation with a completely dry flue gas. We then optimized the same CCC process with the same flue gas but include the water and the DCPC followed by a polishing desiccant dryer. Our best estimates assume that the packed bed needed after the DCPC will have a pressure drop of 0.5 psi for each time the flue gas must pass through (both for drying and regeneration) and that 50% of the exhaust gas is needed for regeneration. Using this metric, and including the extra cooling required, the energy demand for the dryer is 0.0668 GJ_e/tonne of CO_2. A worse-case scenario would be a 1 psi pressure drop for each pass through the dryer. Even with this higher pressure drop, the energy demand for the dryer is 0.0884 GJ_e/tonne. Both estimates fall comfortably below the success criteria of 0.247 GJ_e/tonne CO_2. The alcohol system is still under development, but they require no polishing desiccant and have lower heats of mixing. The simulated energy demand for the entire system is less than 0.08 GJ_e/tonne of CO_2.

Task 3. Dissolved Carbon Dioxide

Specific Objectives: The objective of this task is to eliminate the accumulation of dissolved CO_2, solid CO_2, and other possible impurities in the CCC process.

The main impact of dissolved CO_2 is fouling of the heat exchangers used to re-cool the contact liquid in the process. SES investigated several variations to the cooling heat exchangers, as well as improved dissolved CO_2 concentration diagnostics.

Traditionally, CCC uses brazed plate heat exchangers to cool the contact liquid. This project explored variations of brazed plate heat exchangers that prevent and/or reduce fouling. These include coatings on the heat exchanger surfaces and alternative surface configurations (i.e., dimpled and chevron corrugations). This project also explored methods for physically cleaning these heat exchangers during operation, including meeting with vendors who offer self-cleaning heat exchangers that utilize either fluidized bed mechanisms to clean the heat exchanger surfaces or installing balls or brushes to periodically clean tubes.

Finally, the project explored operational means of cleaning the heat exchangers in several configurations, including periodically blasting them with gas or warmer contact liquid.

Shell and Tube Self-Cleaning Heat Exchanger

Industry commonly mitigates fouling with shell and tube heat exchangers and a system of circulating balls or similar objects. This increases the time between maintenance cycles and improves heat exchanger efficiency. A typical implementation includes slightly compressed foam rubber balls. The compressed sides of the ball form a seal against the walls of the tube and the pressure difference from the front to the back of the ball pushes the ball through the tube. A vortex forms downstream of the ball and, in combination with the ball rubbing on the surface, cleans deposits that have begun to form, thus restoring heat transfer in the heat exchanger. This project considered this technology as a possible method for cleaning CO_2 deposits that form inside of the contact liquid coolers.

Some challenges exist for using this technology for the CCC process. One primary concern is that these heat exchangers require a significantly larger footprint, have much higher thermal mass, and are more expensive than are their brazed plate counterparts. Also, while this technology has been used in a variety of settings, it has not been used at CCC temperatures. The cold temperatures preclude the use of a compressible sponge rubber ball. In addition, commercial shell and tube heat exchangers sized for our current scale feature tubes that are too small to test the ball cleaning technology. Vendors indicate that these systems require at least 3/8” tube diameters. Ultimately, these challenges precluded the shell and tube heat exchanger with these cleaning systems for the contact liquid coolers.

The commercial nature of the shell and tube systems represents its most compelling attribute. These systems can use balls near the tube diameter that require no compression. Vendors manufacture these systems using polytetrafluoroethylene (Teflon) balls. SES has positive experience using polytetrafluoroethylene (PTFE) at cryogenic temperatures in other applications. Therefore, SES worked with vendors to design a potential test system for these balls using a shell and tube heat exchanger constructed by SES.

Liquid nitrogen boils on the shell side of the heat exchanger as it cools the contact liquid. The temperature difference between the nitrogen and the outer tube surface drives the boiling rate. The heat flux increases as the temperature difference increases until the boiling heat transfer drops dramatically during film boiling. Nitrogen reaches film boiling at a temperature difference of 2–10 °C. Thus, film boiling is a likely possibility at any time. As a result, the heat exchanger design assumes film boiling with the associated relatively small heat flux.

The drawing of the shell and tube heat exchanger in Figure 13 illustrates the design. The designs for this system were developed in parallel with competing designs using brazed plate heat exchangers. The brazed plate systems cleared CO_2 particles well enough to terminate research into the shell and tube systems.

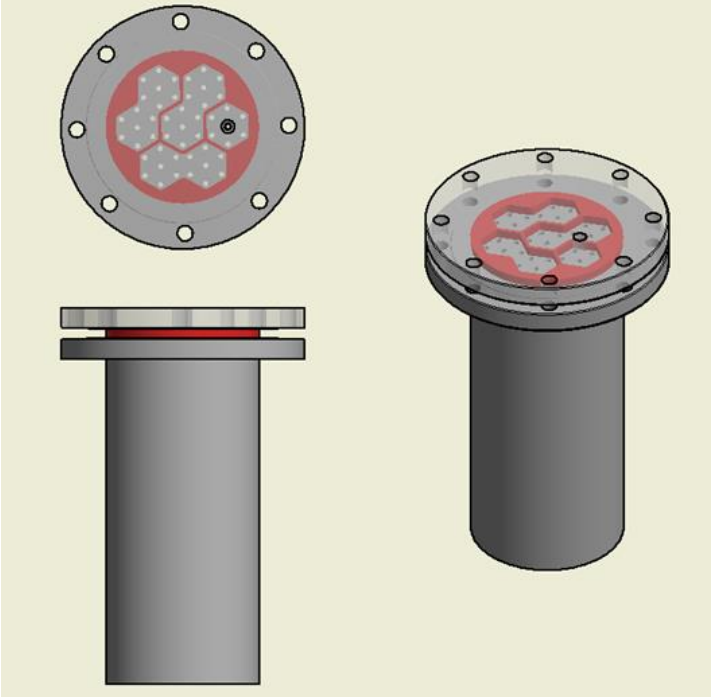

Figure 13. Shell and tube heat exchanger designed for testing ball cleaning. The contact liquid with dissolved CO_2 will run through the tube side and a boiling refrigerant will be on the shell side. Passing PTFE balls through the tubes should clean any CO_2 deposits from the tube walls. These balls are then captured and recirculated through the system.

Alternative Brazed Plate Heat Exchanger Testing

Traditionally, brazed plate heat exchangers cool the contact liquid in the CCC system. There are many possible variations of these brazed plate heat exchangers and they affect internal fouling. This project explored coatings on the internal walls of the heat exchanger, which might prevent or reduce fouling, and alternative geometries, which replaces the chevron style of a standard brazed plate system with a dimpled system to reduce both pressure drop and fouling potential (Figure 14). The plates on the left, labeled "High Θ" have more contact points between the plates, leading to higher heat transfer per unit of surface area, but they also have a more tortuous path for the working fluid, greater pressure drop, and more areas for dissolved CO_2 to settle and freeze onto the plate surface.

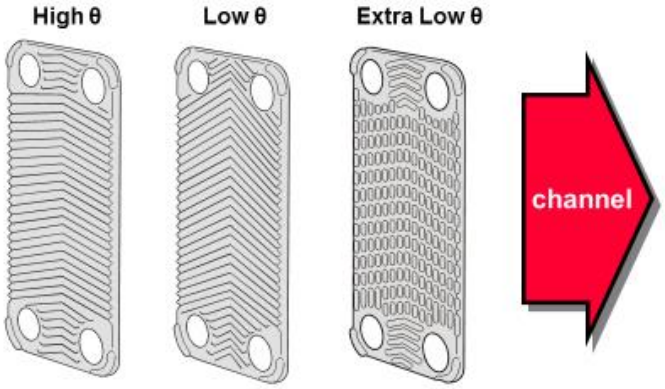

Figure 14. Differing plate geometries. High Θ represents better heat transfer per unit of surface area, but has a greater fouling tendency. Extra low Θ has lower heat transfer per unit of surface area, but has a lesser tendency to foul [7].

SWEP, Inc. provided four different heat exchangers to quantify this performance. SWEP provided the proprietary coating in exchange for testing information for this application. The heat exchangers replaced the current versions in the CCC ECL™ skid system during a total of over 200 hours of testing. Table 1 qualitatively summarizes the tests of these four heat exchangers.

Table 1. Comparison of alternative brazed plate heat exchangers used in testing.

Plate Style	Coating	Results
Chevron, High Θ	Coated	Not effective at reducing fouling
Chevron, High Θ	Uncoated	Not effective at reducing fouling
Dimpled, Extra Low Θ	Coated	Moderately effective, best when used with other techniques
Dimpled, Extra Low Θ	Uncoated	Moderately effective, best when used with other techniques

Five extended test runs, each with two heat exchangers in parallel, determined if the coated heat exchangers from SWEP can perform as described. The tests included alternating between heat exchangers during a single run, which largely eliminates any run-to-run operational variations from affecting the data. The tests indicated no statistically significant differences in fouling rate between the coated and uncoated heat exchangers of the same plate geometry. However, the high Θ heat exchangers exhibited a higher fouling rate than the extra low Θ exchangers. Additionally, the process-control–based mitigation techniques described above had virtually no effect on the high Θ heat exchangers, while they were very effective for removing fouling in the extra low Θ heat exchangers. The tests indicate that none of the heat exchangers completely mitigate fouling without additional process mitigation techniques.

Process Controls Techniques to Prevent Fouling

Four control-based techniques were developed to mitigate solid CO_2 fouling. These techniques were combined with optimally designed heat exchangers to prevent fouling. In addition, the first and second techniques can be used simultaneously for even more robust results.

The first technique temporarily throttles the refrigerant. This warms the heat exchanger walls, allowing any built-up CO_2 to slough off. The CO_2 appears to clear within the first few seconds of closing the refrigerant valve. This technique facilitated a 28-hour run on a single heat exchanger. However, this technique briefly increases the temperature of the slurry recycle to the desublimating heat exchanger, which, in turn, decreases the system capture efficiency for a few minutes.

The second technique is to inject gas at the heat exchanger slurry inlet. This agitates the flow and cleans the heat exchanger walls. This technique has proved to be just as effective as the cycling technique mentioned above, while avoiding the short drop in capture efficiency associated with temperature cycling.

The third technique uses warmer CO_2-lean contact liquid to flush the heat exchangers. This dissolves the CO_2 that is stuck on the heat exchanger surfaces. This technique is not as effective as the other techniques discussed above. However, it can be used to supplement them when needed.

The fourth technique sequentially decreases and increases the fluid velocity in the heat exchanger. This technique proved to have very little utility.

To test the usefulness of these techniques, we ran over 200 hours of tests using the four heat exchangers from SWEP, Inc. Figure 15 and Figure 16 illustrate data from two of these runs performed on the coated and uncoated extra low Θ heat exchangers, respectively. The data indicate a pressure drop across the cooling heat exchanger where the fouling occurs. Over time, this pressure drop increases as the dissolved CO_2 solidifies on the heat exchange surfaces. However, the extra low Θ geometry plates mitigate fouling when the process-control–based techniques described above are also used.

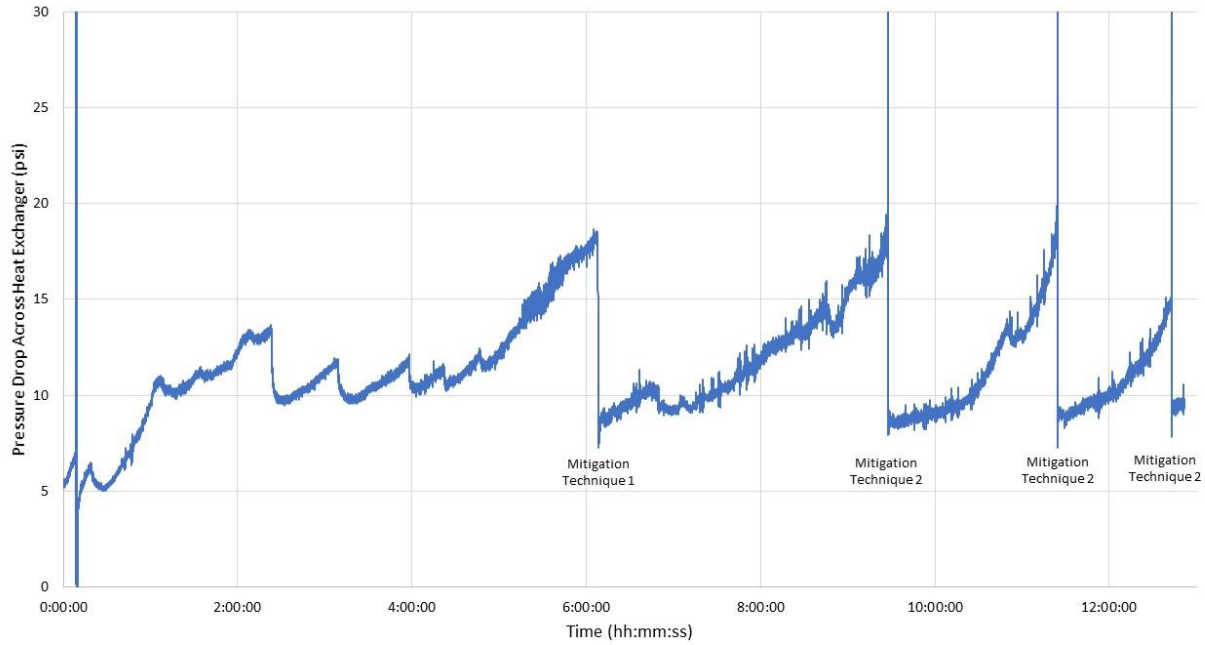

Figure 15. Pressure drop measured in psi across the uncoated heat exchanger.

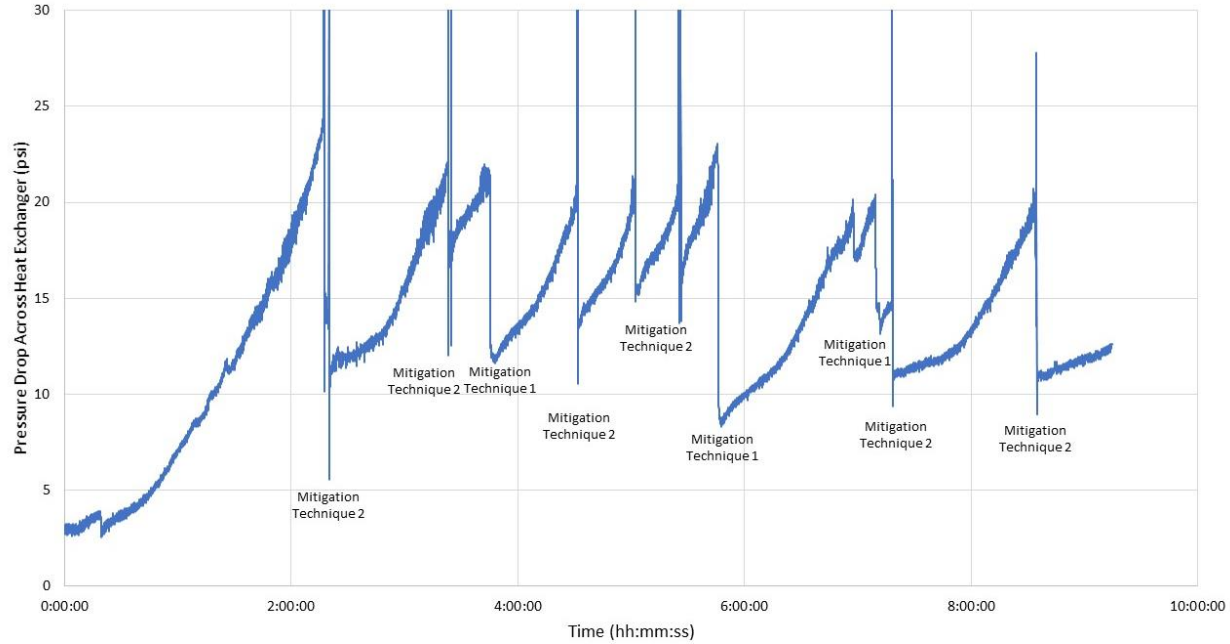

Figure 16. Pressure drop measured in psi across the coated heat exchanger.

Figure 15 illustrates data from approximately 12 hours of continuous runtime on the uncoated heat exchanger. During the first hour of runtime, the pressure drop rapidly climbs to about 9 psi. During this time, solid CO_2 builds up in the slurry to its steady-state value of approximately 10–15% solids. No mitigation techniques are required from 0 to 6 hours of runtime. These six hours saw some small decreases in pressure drop perhaps caused by some of the CO_2 breaking off on its own without any intervention. These self-clearing events are typical of these runs. Around hour 6, a refrigerant throttling technique produces an immediate pressure drop to ~9 psi. Short nitrogen bursts (Technique 2) at about 9:30, 11:30, and 13:00 similarly reduce pressure drop to ~9 psi. The data suggest that 9–12 psi is the approximate base pressure

drop without any fouling. This number depends on the slurry viscosity, which is primarily affected by solids loading. For example, 10% and 15% solids produce about 9 and 12 psi pressure drops, respectively. Each mitigation event reduces the pressure drop to the base value.

Figure 16 contains data from approximately 9 hours of continuous runtime on the coated heat exchanger. This test deliberately involved conditions that promote fouling faster than the previous test to determine the long-term efficacy of the mitigation techniques. A combination of Techniques 1 and 2 mentioned above controls the pressure drop.

Proprietary techniques with a single heat exchanger provided 27 continuous operating hours with an average capture rate of 96.5% on a simulated flue gas with a flow rate of 30 SCFM and a CO_2 inlet concentration of 10%. One process upset lasted 20 minutes, but this upset was not related to the heat exchanger. A controlled shutdown after approximately 28 hours terminated the run. The capture data from the run appear in Figure 17. The average runtime on the non-coated, chevron style heat exchangers before a defrost cycle is required is 3–4 hours.

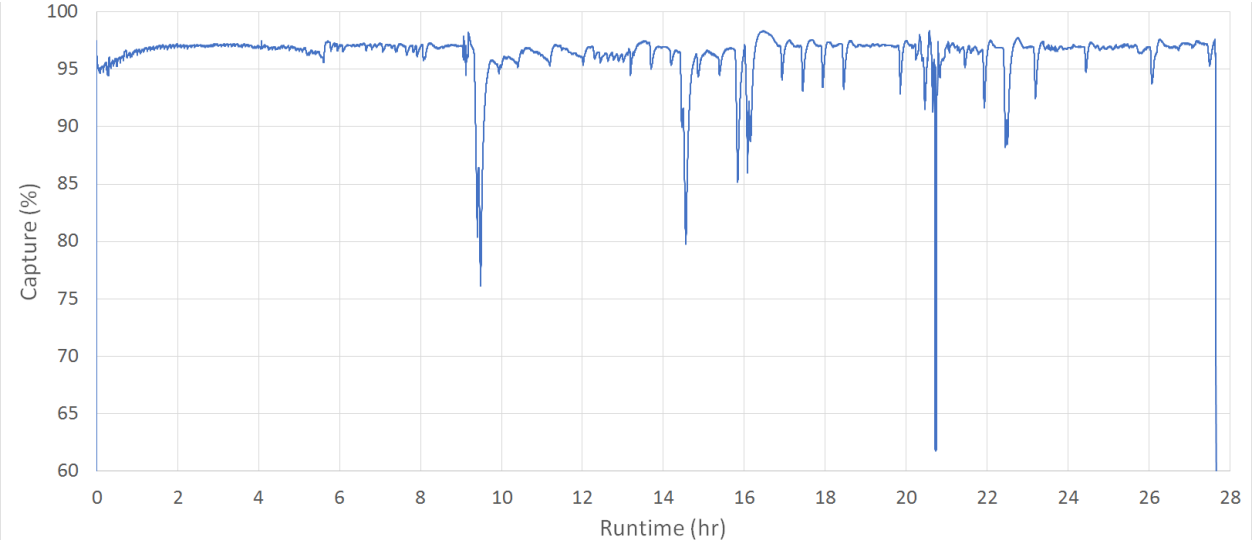

Figure 17. CO_2 capture during 27-hr test using a single coated heat exchanger with an average 96.5% CO_2 capture.

Modeling Energy Penalty from Heat Exchanger Fouling Mitigation

The different mitigation techniques affect the overall energy demand in different ways. Techniques 1 and 2, refrigerant throttling followed by a single or multiple gas bursts, combined with a low Θ heat exchanger produce the best results. Figure 18 shows the effects of this combination of heat exchanger and mitigation techniques. These were used in rapid succession to see the overall response time required for full recovery to steady-state process operation.

Samples from each of the mitigation techniques appear in Table 2. These show an average increase of 4 °C during a mitigation step, which lasts on average 5 min. These results provided a basis for modeling the effects of these cycles on energy demand.

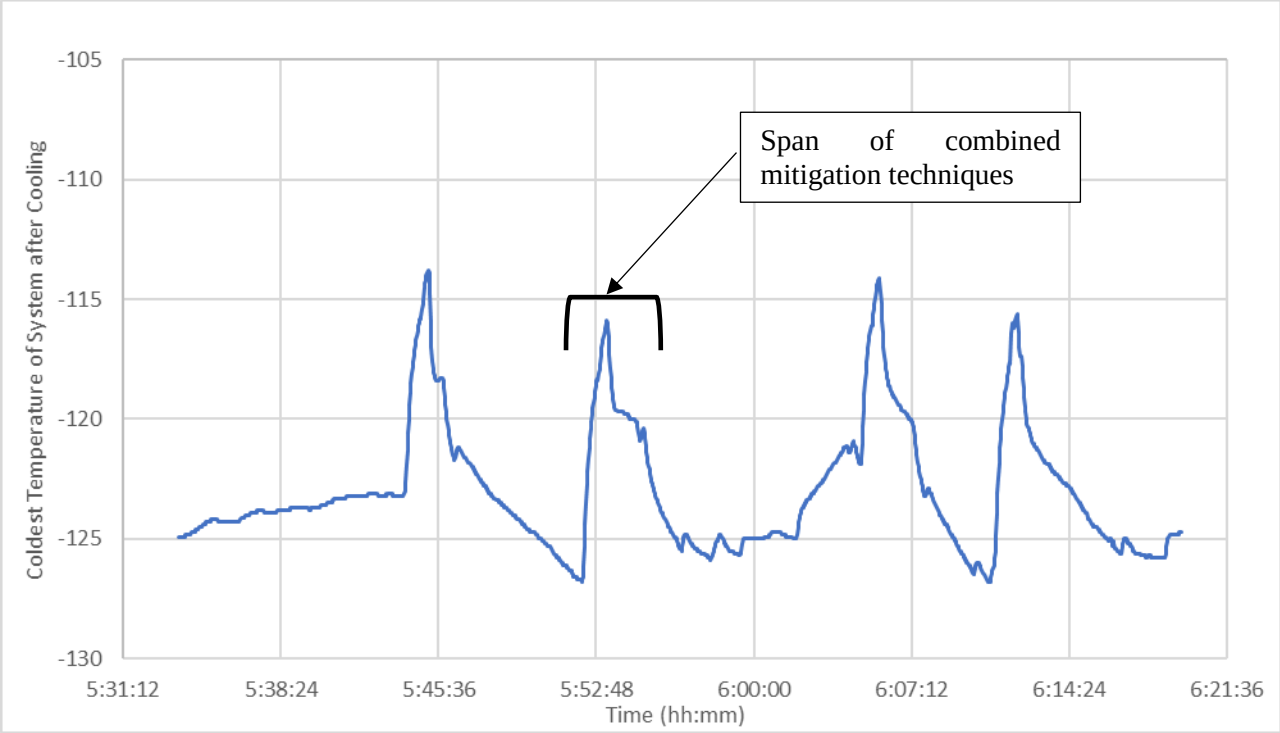

Figure 18. Effects of fouling mitigation techniques on temperature of system

Table 2. Time to return to baseline and average temperature from mitigation

Start (H:MM:SS)	End (H:MM:SS)	Duration (H:MM:SS)	Mean Temp (C)	Delta T (C)
5:52:16	5:56:05	0:03:49	−120.5	4.5
6:01:57	6:08:56	0:06:59	−121.0	4.0
6:11:04	6:16:00	0:04:56	−121.5	3.5

The data suggest that the observed 4 °C increase in contact liquid temperature results in a change of capture from 90% to approximately 78% on average for the duration of the mitigation step. This increases the system energy cost because of the slight CO_2 capture decrease. The mitigation steps occur approximately once every 30 min, and each last 4 minutes on average. This results in a reduced capture rate lasting 11.8% of the run. The pressurized gas bursts are approximately 0.12 mol per burst at 130 psia at the skid level, or 3138 mol per burst at full scale. A very small slip steam of the light gas exhaust from the CCC process supplies this gas in the model.

Comparing these rates with full-scale numbers, we find that a typical run with no mitigation steps results in an overall capture rate of 133.51 kg/sec, with an energy load of approximately 0.8 GJ/tonne CO_2 captured. Using Techniques 1 and 2, we have a capture rate of 131.41 kg/sec and an increased load of 13.9 kW, resulting in an energy usage of 0.812 GJ/tonne CO_2 captured. This represents an estimated increase of 1.57% or 0.0125 GJ/tonne. A worst-case scenario of having to perform mitigation steps every 10 min results in an increase of only 3.81% and 33.7 kW or 0.03 GJ/tonne CO_2 captured.

Success Criteria

The original success criterion for this task was to "experimentally demonstrate a contact liquid cooling system that operates reliably and reduces the parasitic load to less than 0.1 GJ_e/tonne CO_2." SES tested several commercial heat exchangers that purport to be able to handle fouling issues similar to those experienced in the contact liquid chiller. Replicated tests over many hours using the CCC ECL™ skid and specifically the SWEP dimpled heat exchangers demonstrate that quick throttling of refrigerant combined

with a burst of clean gas mitigate the fouling caused by CO_2 solubility in the contact liquid without significantly increasing parasitic load. SES will use a larger, uncoated SWEP heat exchanger during Budget Period 2 of this project.

SES models indicate approximately an energy penalty of 0.0125 GJ_e/tonne CO_2 captured for this process, an order of magnitude less than the required 0.1 GJ_e/tonne.

Task 4. Solid Liquid Separations

Specific Objectives: The objective of this task is to improve the reliability and performance and to decrease the energy consumption of the solid–liquid separation process.

SES performed a series of tests running the CCC ECL™ process at a variety of conditions (e.g., gas flow rates, CO_2 content in the flue gas stream, contact liquid flow rates) to increase the outlet solids fraction exiting the screw press separator. SES has designed, built, and tested three versions of these screw presses, with two copies of the most reliable design currently installed in the skid. Instrumentation in these unit operations measures flow rates and conditions. This includes turbine meters, thermocouples, and pressure transducers. SES also better insulated these units and their associated piping by immersing them under perlite in a cold box rather than wrapping the screw presses with insulation. The separation process achieves 70% solids in this stage. The screw press meets the reliability and performance requirements and will continue to provide solid–liquid separation in future designs.

SES worked with Press Technology and Manufacturing (PT&M) to improve the current screw-press separations method. This collaboration should improve the solid–liquid separation system at skid and large-pilot scale. The design work emphasizes the final stage of the device as well as the filter and screen attachments to the screw press system. PT&M has refined the screw press design and produced detailed drawings for the machine. SES will design and manufacture the filter, and PT&M will manufacture the rest of the machine. SES engineers experimentally determined the CO_2 slurry requirements and worked with PT&M to design a more reliable filter.

SES performed additional test runs with an improved control system using a fractional flow control valve made specifically for cryogenic and low flows. This valve replaced a proportional flow control valve and allows finer control of the output of the liquid portions of the screw press. Multiple tests show a significant improvement in the controllability of the liquid output from the separations system.

SES demonstrated the system at 0.5 tonne CO_2 captured/day for 50 hours. The average mass fraction of the solids extruded from the presses was 66.9%. Figure 19 shows the mass fraction during the 50-hour run. The average concentration was slightly lower than the 70% goal; however, this run was deemed, with concurrence from NETL, to have met the success criteria for solid–liquid separations. Multiple subsequent runs demonstrate the system can easily reach 70 mass% solid CO_2 from the screw press (Figure 20).

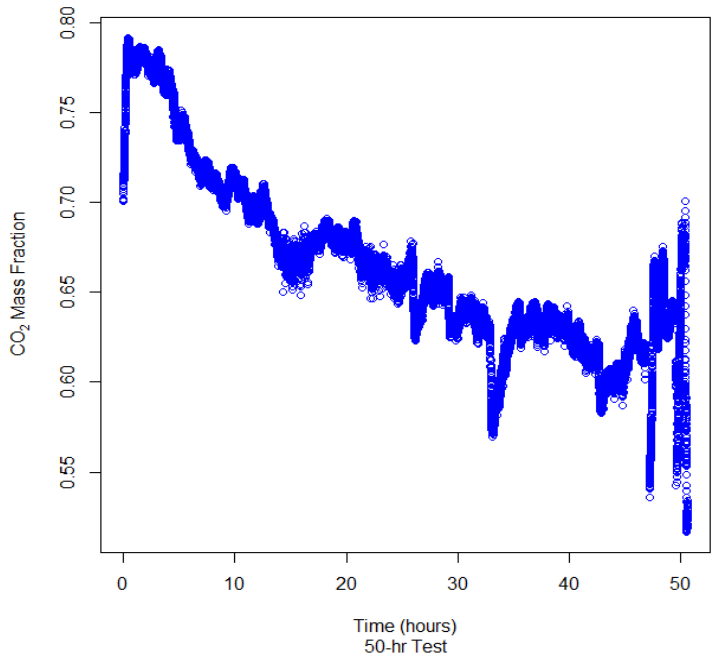

Figure 19. Mass fraction of CO_2 exiting the solid–liquid separations system for a 50-hour test run at 0.5 tonne/day CO_2 [6].

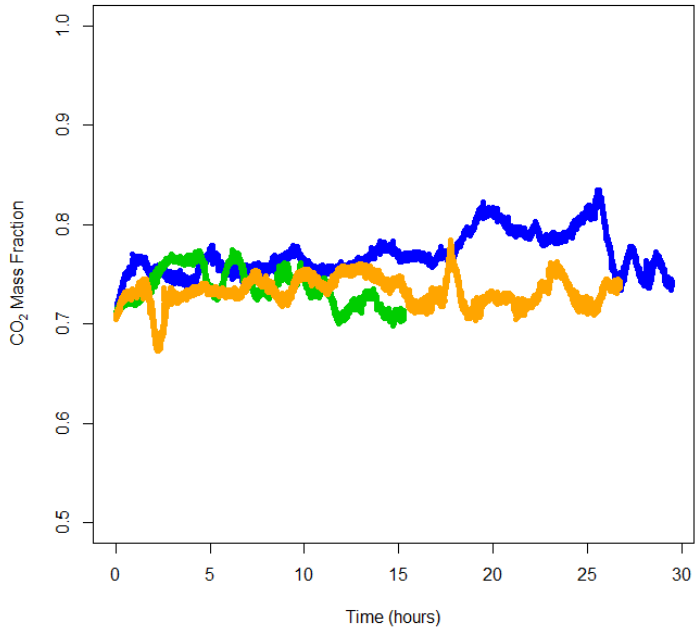

Figure 20. Mass fraction of CO_2 exiting the solid–liquid separations system for representative 15- to 30-hour test runs at 0.5 tonne/day CO_2 [6].

The screw press technology can produce 70 wt% solids and should significantly exceed this level in its final embodiment. The energy demand of the separation process is less than 0.1 GJ_e/tonne of CO_2 processed.

Task 5. Heat Exchanger Testing

Specific Objectives: The objective of this task is to explore the relative merits of the three desublimating heat exchanger designs in a commercial-scale implementation of CCC.

Fluidized Bed Desublimating Heat Exchanger

SES sized a pilot-scale bubbling fluidized bed desublimator and heat exchanger and generated a simple CAD model (Figure 21). The fluidized bed desublimator in this case consists of nine vertical tubes in a circular configuration housed in an insulated standard pipe. Dry flue gas near the CO_2 frost point enters the bottom of the desublimator, fluidizing the CO_2 particles in a bubbling bed mode and exits through the top. Refrigerant passes through the nine vertical in-bed heat exchangers and cools the particles. CO_2 desublimates on both the bed particles and on the tubes. The bed particles scour desublimated CO_2 off the tube surfaces to prevent fouling.

SES decided not to continue development of the fluidized bed in this project, primarily because it is potentially much more complex to operate than the other designs and, while it has advantages, the additional complexity unnecessarily complicates the overall system operation. Once the remainder of the system operation becomes routine, SES may revisit this design.

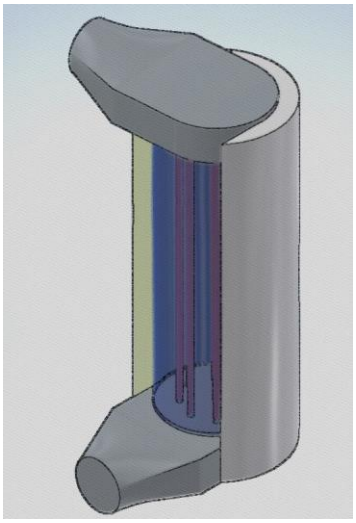

Figure 21. CAD drawing of fluidized bed heat exchanger.

Multi-Stage Desublimating Heat Exchanger

SES installed a camera inside the desublimating heat exchanger near the outlet of the cold treated gas to better understand the fluid dynamics inside the tower (Figure 22). The fittings around the camera are continuously purged to prevent the extreme cold temperatures in the heat exchanger from obscuring the camera view.

Figure 22. Still image taken from the camera feed inside the desublimating heat exchanger showing the cold contact liquid/solid CO_2 slurry entering the heat exchanger (from the left side of the image).

A total of 15 test runs of about ten hours each demonstrated how this primary desublimating heat exchanger reacts to higher flow rates. These tests indicated where insulation needed improvement, such as the placement of vacuum-jacketed tubing for some of the key fluid transfer lines.

Spray Tower

SES reviewed its previous experiments with a spray tower desublimating heat exchanger in the CCC ECL™ process. A previous SES spray tower could fit into the current ECL skid; however, this equipment requires updating the connections to the existing CCC ECL™ skid, updating fabrication drawings for the spray nozzles and/or plates, and contacting vendors for off-the-shelf spray solutions that were not previously available. SES completed the design, construction, and testing of an updated version of the spray tower incorporating lessons learned from previous experience. SES also developed a detailed spray tower model and incorporated this into the process simulator.

The new heat exchanger design is now complete, constructed, and installed in our existing skid-scale CCC ECL™ system (Figure 23). This new heat exchanger can operate in spray tower, bubbling, or hybrid modes.

Figure 23. Spray tower during installation.

In spray tower mode, the heat exchange occurs between cold droplets descending from the top of the tower and flue gas ascending in countercurrent flow. The light gas leaves the top of the tower and solids form on the cold falling droplets. This configuration produces efficient heat exchange with low pressure drop.

In bubbler mode, the heat exchange occurs between bubbles of flue gas passing up through a pool of cold liquid. Solids condense in the liquid as the light gases move toward the liquid surface. The advantage of the bubbler configuration is that the heat exchange occurs over a short distance, resulting in a compact design. However, the mixing that occurs in the liquid results in less-efficient heat exchange because the pool of liquid is well mixed to the point that it approaches an isothermal bath and a large temperature difference is required to sufficiently cool the incoming gas.

The hybrid mode exchanges heat by bubbling a gas through a cold liquid at the bottom and then flowing the gas between cold droplets at the top. The pool of liquid at the bottom forms by allowing the liquid level in the spray tower to rise above the gas inlet. Solids formed anywhere in the heat exchanger exit with the cold liquid at the bottom of the unit. The hybrid heat exchanger provides efficient heat exchange when the flue gas initially cools slowly because components within that gas are condensing. This keeps the temperature profile relatively flat and efficient heat exchange can occur in the well-mixed (isothermal) liquid. Once much of the heat exchange has occurred, the droplets capture the remaining condensable gases as the gas drops significantly in temperature in the top countercurrent spray section.

At full scale, a spray head with a conical spray will be used in the spray tower. These are commercially available and optimized for maximum heat and mass transfer. However, at this scale, it is difficult to test such a device because the size of the desublimating heat exchanger is small enough that a large portion of the spray would hit and flow down the sides of the cylindrical heat exchanger rather than interacting with the flue gas. As a result, we have chosen to only test narrow-cone spray nozzles. These spray nozzles have a uniform distribution of droplets throughout the spray cone. This should result in the best possible heat transfer in the available confined space.

In addition to testing narrow-cone spray heads, SES developed a parallel spray device. The general concept behind this device is that all the droplets will fall parallel to the walls of the cylindrical spray tower. Thus, all the particles will interact with the flue gas, allowing for the best possible heat transfer within the space. This development included photographically measuring the droplet size as a function of hole size and contact liquid temperature (Figure 24). The flowrate of this stream determined the number of holes required to achieve the desired total liquid flow. SES designed, built, and tested a spray plate based on these results. (Figure 25). A half-section view of the new hybrid spray tower/bubbler appears in Figure 26 and features two cameras, redundant level sensing (i.e., continuous and level switches), changeable liquid and gas inlets, a demister at the gas outlet to catch entrained contact liquid, and a conical liquid outlet to prevent solid CO_2 buildup.

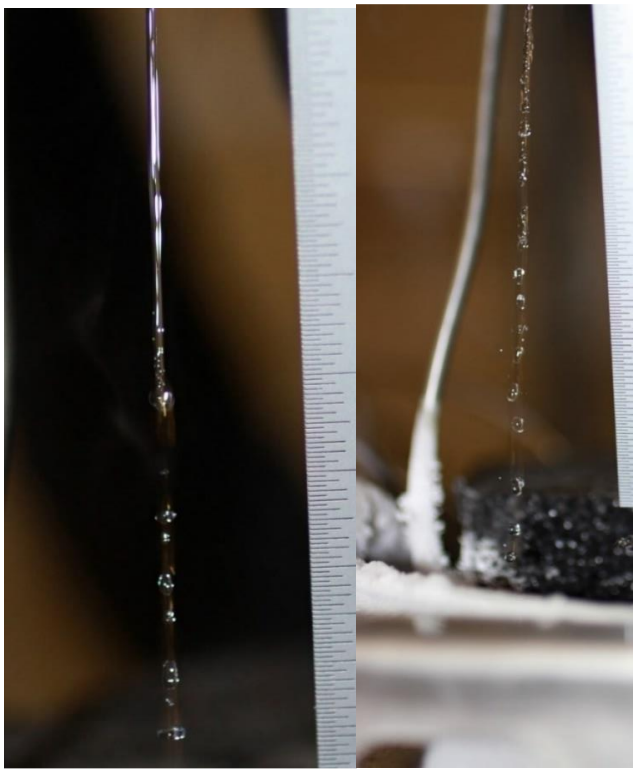

Figure 24. Contact liquid droplet visual measurement.

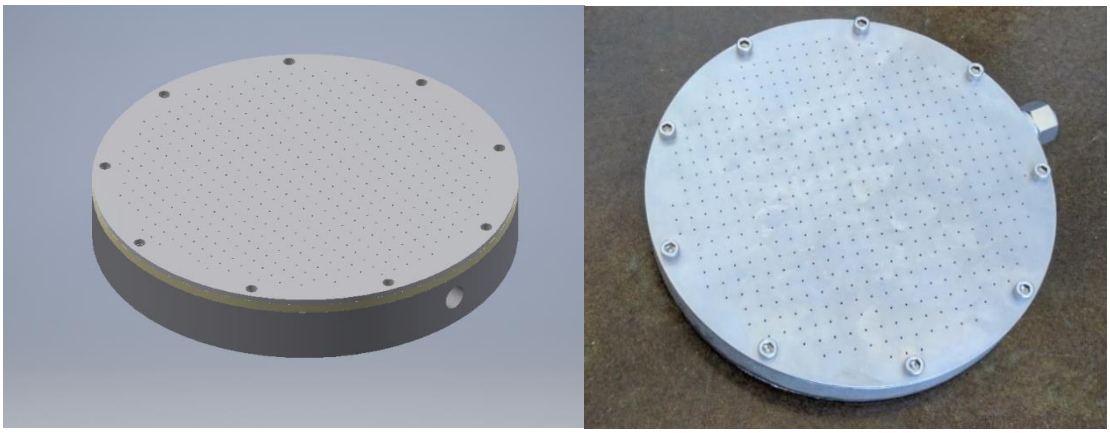

Figure 25. Spray plate for optimal spatial distribution of contact liquid droplets.

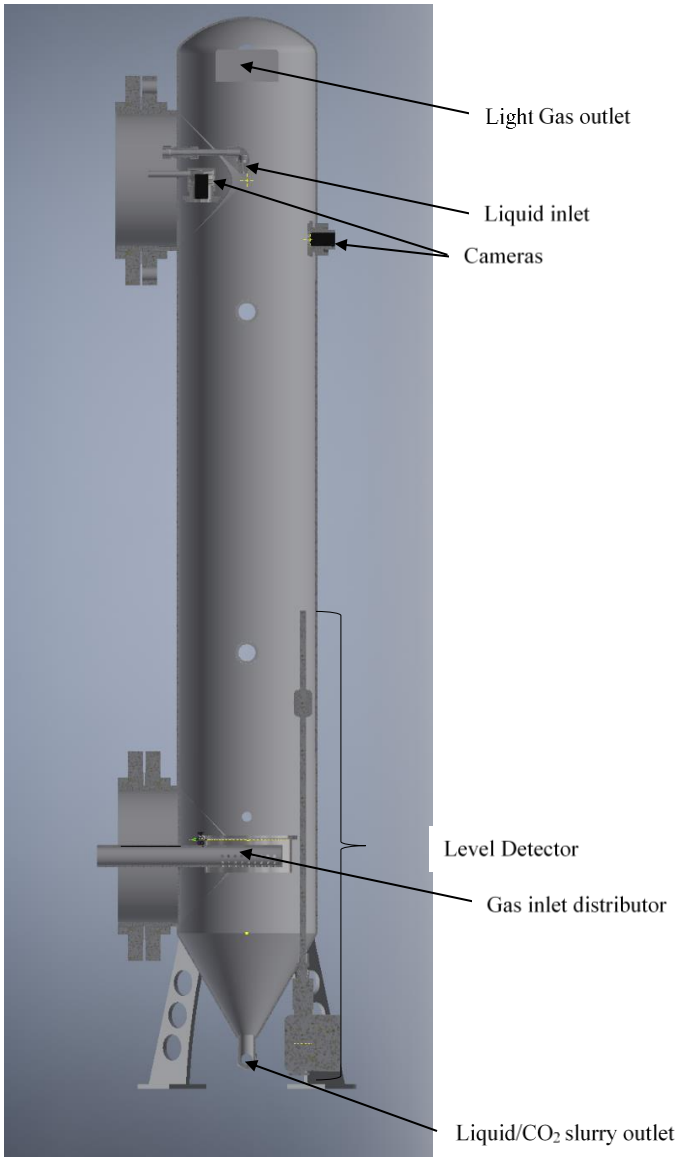

Figure 26. Hybrid spray tower/bubbler half section.

This hybrid desublimating heat exchanger has operated for over 50 continuous hours with a CO_2 flowrate over 0.5 tonne/day and an average CO_2 capture of 90.8%. A plot of the capture data as a function of time appears in Figure 27. Most of the variability in the data involves the heat exchanger cycling discussed earlier under Task 3. The perturbation at 49 hours involved an accumulation of solid CO_2 particles on the walls of the hybrid heat exchanger. This buildup eventually broke free and caused a system upset due to the sudden introduction of a large quantity of solids into the contact liquid slurry. The scale of the skid process exacerbated this upset. Larger-scale systems with larger pipes and volume-to-surface-area ratios would reduce the frequency of and more easily clear this type of upset. Figure 28 shows the cumulative CO_2 mass capture rate and the total mass captured at any given point in the run.

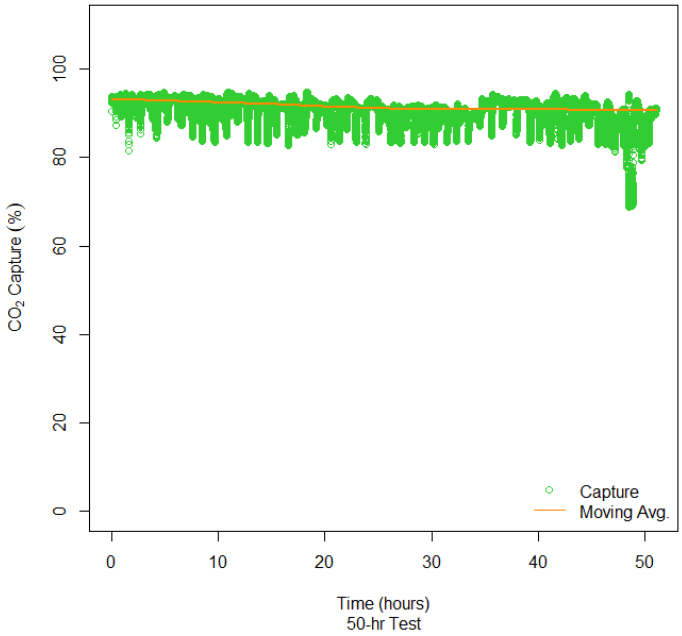

Figure 27. Percent CO_2 capture over 50-hour run [6].

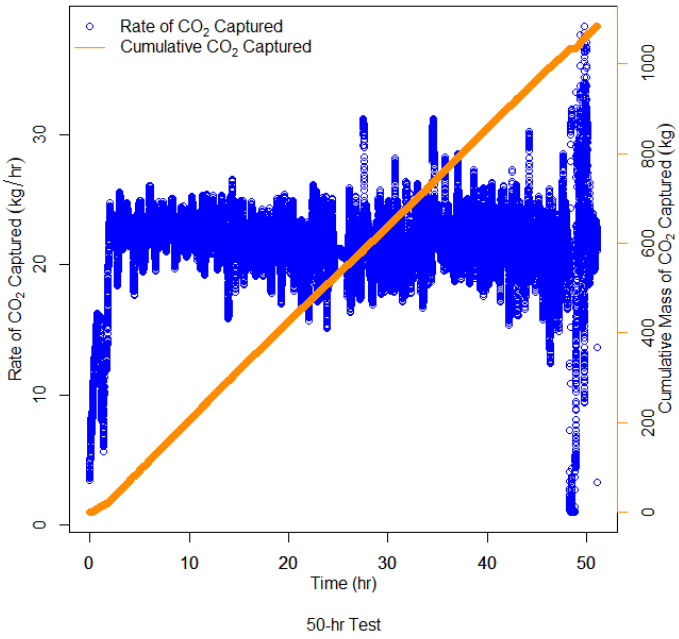

Figure 28. CO_2 capture by mass accumulation rate and total mass [6].

Task 6. Instrumentation and Controls

Specific Objectives: The objective of this task is to extend the skid testing time through improved controls, and instrumentation.

Over the course of this task, SES planned for additional instrumentation to be installed on the ECL skid to improve process performance during this budget period and looking forward to changes to be implemented in Task 10 in Budget Period 2. The new instrumentation includes thermocouples, pressure transducers, level transmitters, flowmeters, and control valves.

SES has purchased and received the new instrumentation and equipment. We have already installed several of the new instruments, including an additional Coriolis flow meter at the inlet feed to the solid–liquid separation system, or dual screw press, and two turbine flowmeters at the liquid output of each screw press. These flowmeters have already improved the screw press reliability.

SES has also installed mass flow controllers for injecting pollutants into our simulated flue gas stream and created new FTIR methods for measuring their concentrations.

This new instrumentation and changes to previous instrumentation support improved process analysis and control algorithms, which is another objective of this task. Higher-level supervisory control will also be considered in preparation for long-term operation.

The new CCC control system has operated for hundreds of hours with the new instrumentation with fewer upsets, both because we are more aware of the conditions in the process and because the controls can better respond to process changes.

Task 7. Light-Gas Dispersal

Specific Objectives: The objective of this task is to explore issues with light-gas dispersal when the gas temperature is near room temperature.

Several dispersal techniques can mitigate the low-oxygen-content hazard of the light gas stream. The simplest of these for a retrofit is to vent the light gas through the existing stack at the plant. SES completed a series of plume dispersion models using AERSCREEN from the EPA [8]. These studies utilize plant characteristics from the Hunter Power Plant in Castle Dale, UT owned by Rocky Mountain Power/Pacificorp and data from in-house models of the CCC process. These AERSCREEN models calculate the gas concentration along the ground to ensure that no areas have pockets with low oxygen content when we vent the clean gas from the CCC process up the stack. The model output uses characteristics of this specific plant, but sensitivity analyses include a variety of factors to ensure that the models robustly account for potential hazards.

The model uses the N_2 emitted as the clean stream exiting the CCC process as an emission rate. The model determines the emitted N_2 concentration as a function of distance from the stack and operating conditions, accounting for season of the year, weather, and other environmental factors. (Figure 29 and Figure 30).

We focused on the effect of plant load on ground-N_2 concentration. When the raw N_2 data and the calculated O_2 concentrations are plotted, there is an obvious trend: the concentration of N_2 on the ground decreases with decreasing plant load (i.e., less gas emitted from the stack). No data set resulted in ground-level O_2 concentrations approaching the hazardous level of 19.5% O_2.

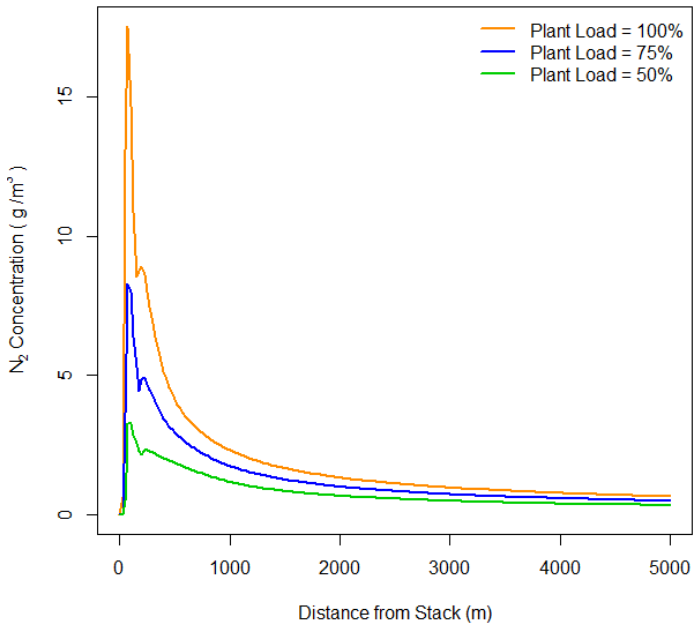

Figure 29. Model output predicting the maximum N_2 concentration at each distance from the stack when emitting the clean CCC gas up the stack at the power plant [6].

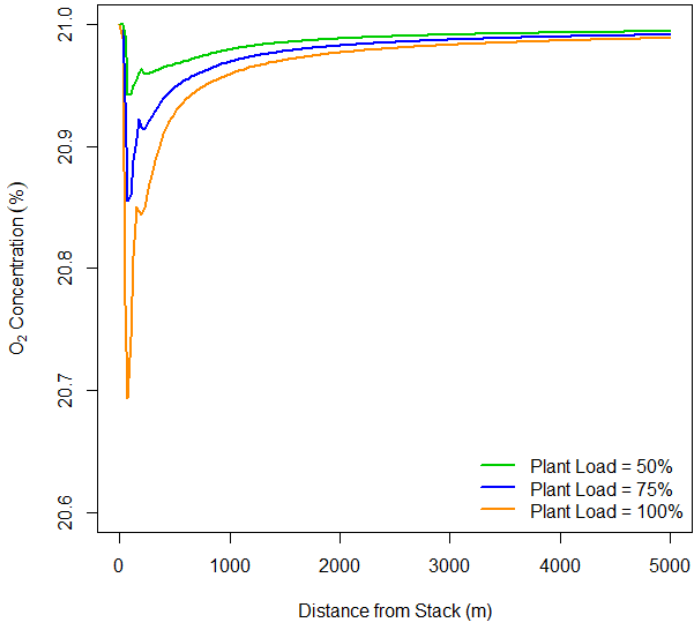

Figure 30. Calculated minimum O_2 concentration using the predicted the maximum N_2 concentration at each distance from the stack when emitting the CCC clean gas up the stack at the power plant [6].

The sensitivity analysis varied each of the model parameters individually while keeping all the other factors at "typical" levels (Table 3). The outcome of the sensitivity analysis is that stack diameter and minimum wind speed have a great impact on the concentration of N_2 on the ground, as expected. The stack diameter needs to be less than 7.43 m and the minimum wind speed (averaged hourly) needs to be greater than 0.45 m/s at this specific plant to maintain a safe concentration of N_2 on the ground; both of which are reasonable

to expect at any full-scale plant. No other variables in the model predicted a hazardous condition for the level of N_2 on the ground.

These simulations indicate that the stack provides adequate dispersal for the clean gas vented from the CCC process additional more-detailed models using the AERMOD model [9] is not required.

SES has decided to vent the clean flue gas into the existing stack at the plant. Sargent & Lundy safety professionals vetted and reviewed the modeling approach as well as the results and the plan for venting the light gas from a full-scale installation of the CCC process. Tri-State also reviewed the information but determined that this task was outside their area of expertise and they requested that we find a more qualified group for final review, which group is Sargent & Lundy.

Table 3. Sensitivity analysis output from AERSCREEN. For each variation, all other factors were held constant at the typical value.

	Max N_2 Concentration at Ground Level		%change
Factor	**Typical**	**Variation**	**Variation**
emission rate	1.75E+07	8.78E+06	−50%
stack height	1.75E+07	1.10E+07	−38%
stack diameter	1.75E+07	6.02E+07	243%
stack temperature	1.75E+07	1.75E+07	0%
flow rate	1.75E+07	6.56E+06	−63%
rural/urban	1.75E+07	1.45E+06	−92%
minimum distance to ambient air	1.75E+07	1.75E+07	0%
building downwash?	1.75E+07	1.75E+07	0%
building height	1.75E+07	1.75E+07	0%
maximum horizontal building dimension	1.75E+07	1.75E+07	0%
minimum horizontal building dimension	1.75E+07	1.75E+07	0%
max building dimension angle to true north	1.75E+07	1.75E+07	0%
angle of stack from building center	1.75E+07	1.75E+07	0%
distance between stack and building center	1.75E+07	1.75E+07	0%
source elevation	1.75E+07	1.75E+07	0%
min temperature	1.75E+07	1.75E+07	0%
max temperature	1.75E+07	3.84E+06	−78%
min wind speed	1.75E+07	2.82E+07	61%
anemometer height	1.75E+07	1.77E+07	1%
dominant surface profile	1.75E+07	4.55E+06	−74%
dominant climate profile	1.75E+07	8.73E+06	−50%

Task 8. Multi-Pollutant Capture

Specific Objectives: The objective of this task is to develop models that describe CCC capture of pollutants other than CO_2 and to validate these models with experimental data.

Pollutant Modeling

SES' in-house process model simulates the capture of condensable gases by solving a solid/vapor/liquid equilibrium (SVLE). The process model describes a CO_2/contact liquid slurry thermodynamically, with transport limitations in several critical processes such as the spray tower. The model predicts CO_2 capture efficiency as a function of temperature, pressure, and composition, as well as all internal stream conditions and equipment performance predictions, including SLVE of CO_2 in contact liquids.

SES recently upgraded our SVLE algorithm to treat not just solid CO_2, but multiple pollutants simultaneously (i.e., CO_2, SO_x, NO_x, Hg, HCl). This upgrade involved generalizing a routine that minimizes Gibbs energy with respect to one variable—the amount of solid CO_2—to a multivariable optimization. The

optimization involves constraints, such as avoiding negative mole amounts and conserving mass and energy.

The multi-component SVLE model predicted nearly the same pollutant concentrations as those predicted by the single-component SVLE solver because the pollutants in the flue gas primarily dissolve in the contact liquid. Hence, the multi-component solver converged to the same solution as the single-component solver, in which all pollutants except CO_2 were just assumed to be fully soluble. However, many of the pollutants condense prior to CO_2 desublimation and therefore prior to the presence of the contact liquid. The multicomponent SVLE is important in understanding their possible fate, especially if they exit the process prior to the primary desublimating heat exchangers. SES compared the single- and multi-component SVLE models with a third, earlier model SES implemented around 2012 called the hybrid VLE/SVE algorithm (i.e., hybrid vapor/liquid and solid/vapor equilibrium). The VLE/SVE predicted the component partitions between the vapor phase and *either* the solid or liquid phases, but not both. Unlike SVLE, this approach cannot predict the solubilities of pollutants in the contact liquid. However, the approach still accurately predicts the vapor-phase composition of the pollutants, including CO_2, which ultimately determines the amount of pollutants captured by the CCC process. SES also compared all models—the multi-component VLE/SVE model, and the incomplete SVLE model—with experimental data (below).

Pollutant Capture Measurements

SES has collected data on pollutant capture through in-house experiments and measurements on the skid at different test sites. These tests have provided important data on SO_2, NO, NO_2, mercury, particulate matter, and others. During this project, SES ran the ECL skid during controlled experiments that validate the thermodynamic models and give other insights on interactions that affect pollutant capture. These tests varied the conditions of the flue gas to better test the new model. A FTIR spectrometer with a long-pass gas cell provided these results

SES ran experiments using simulated flue gas containing the pollutants SO_2, NO, and CO. The pollutant concentration monitoring points include the flue gas inlet, the clean gas outlet, and the purified CO_2 outlet (Table 4).

Table 4. Pollutant concentrations as predicted using the in-house model and measured from pollutant-capture testing of the skid-scale CCC ECL™ process.

Pollutant (inlet concentration)	Predicted outlet concentration (VLE/SVE)	Predicted outlet concentration (single-comp SVLE)	Predicted outlet concentration (multi-comp SVLE)	Observed outlet concentration
CO_2 (5.51%)	0.344%	0.339%	0.330%	0.311%
SO_2 (0.0029%)	2.8 ppm*	0.00085 ppm*	0.00085 ppm*	4.2 ppm
CO (0.0090%)	95.0 ppm	90.3 ppm	90.3 ppm	66.6 ppm
NO (0.0028%)	14.8 ppm	15.0 ppm	15.0 ppm	30.9 ppm
Isopentane (0%)	2.6 ppm	3.6 ppm	3.6 ppm	156 ppm

*** SO_2 vapor pressure was extrapolated**

The observed outlet concentrations of CO_2 and CO agree very well with all models. The models do not agree on SO_2 concentration. Vapor pressure data are not available for SO_2 at these operating temperatures, which is a major contributor to these variations. The two models do agree on NO concentration, predicting that the CCC process captures about half of the NO. However, the experimental data show that almost none of the NO was captured. The measured isopentane exceeded the predictions, due to mist entrainment in the spray tower.

The pollutant concentrations in the purified CO_2 outlet appear in Table 5. We did not attempt to predict these concentrations.

Table 5. Pollutant concentrations in the purified CO_2 outlet.

Pollutant	Concentration in pure CO_2
Isopentane	0.59 %
SO_2	111 ppm
CO	< 10 ppm*
NO	< 10 ppm*

***detection limit of FTIR**

Task 9. Phase 1 Techno-Economic Analysis

Specific Objectives: The objective of this task is to maintain techno-economic analyses during development of the CCC process.

Improved In-House Software

As part of the task to complete the techno-economic analysis, SES has implemented two new unit operations in its in-house simulation software. We plan to test both units in the near-term on the skid-scale process, and we expect to use these units on larger pilot demonstration designs and full-scale installation designs.

A distillation column simulation is now an option in the in-house process design software. The implementation uses an equilibrium, rather than a transport-driven, model. SES is currently building a distillation column for use on the existing skid-scale system to purify the liquid stream of CO_2 from the screw press and melter. The column's design used the new Distillation Column unit operation in addition to similar design tools from more established programs and from the vendor. A sample output from a seven-stage distillation column simulation is shown in Figure 31.

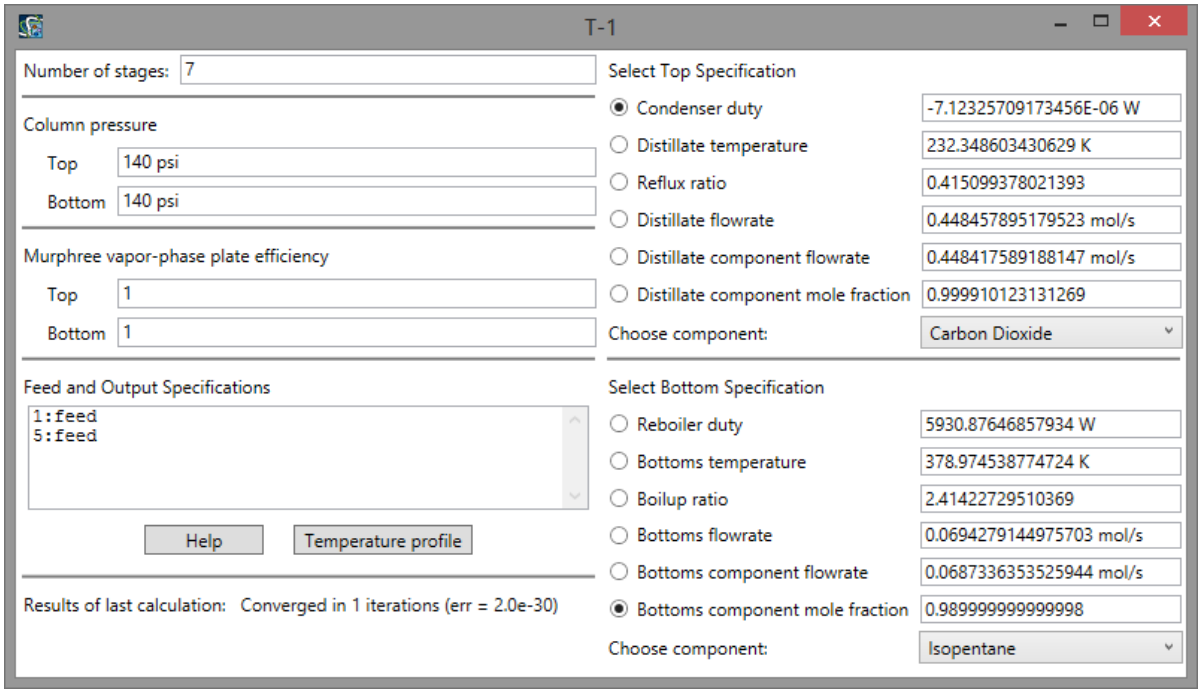

Figure 31. Example output from a Distillation Column unit operation simulation.

Currently, distillation is the preferred method of purification moving forward to the pilot and full-scale systems, so the newly implemented unit will contribute routinely to estimate the energy demands of future CCC systems and processes.

We have also implemented a spray tower unit operation that simulates both counter- and co-current spray towers. Unlike the Distillation Column model, this model is transport-driven, making it substantially more complex. Consequently, the model currently operates only in standalone mode with hard-coded properties for our most commonly used liquids and gases. A sample of the output from this simulator appears in Figure 32. We have integrated the model into our full simulation package to enable general, process-wide simulation.

The simulations continue to be updated with improvements that have been developed during experimental testing. The most notable of these improvements is the development of novel drying techniques from Task 2. The direct-contact dryer described above affects both the parasitic load and capital cost of the pilot-scale and full-scale processes. SES uses the data from Task 2 to simulate a direct-contact dryer on the full-scale process to be able to directly compare the direct-contact dryer and a fixed-bed dryer.

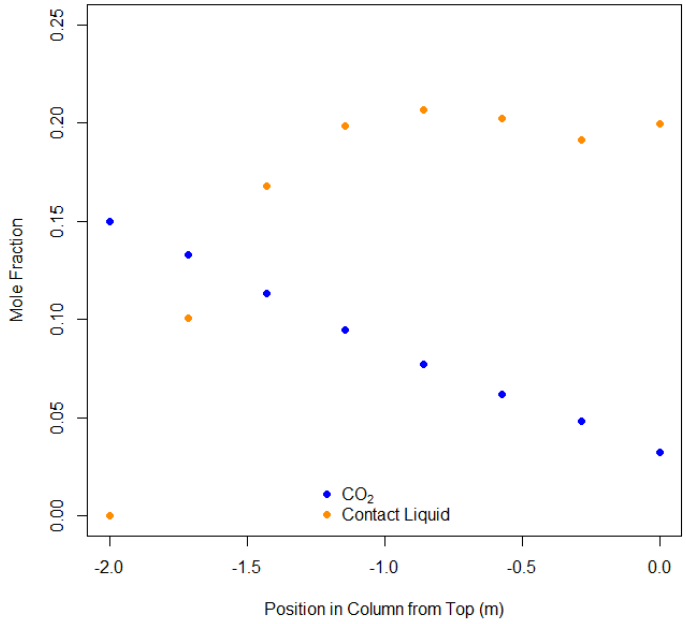

Figure 32. Partial output from SES' standalone Spray Tower simulator calculating the CO_2 and contact liquid content in the clean gas exiting the spray tower.

SES TEA effort

Process Overview

Cryogenic Carbon Capture™ (CCC) exists in two embodiments called the external cooling loop (ECL) and compressed flue gas (CFG) processes. This discussion focuses on the ECL process. The ECL process (Figure 1) boosts flue gas pressure sufficiently to overcome process pressure drop, dries and cools the flue gas, cools it to a temperature slightly above the CO_2 frost point, condenses CO_2 in a desublimating heat exchanger, precipitating an amount of solid CO_2 that depends on the final temperature, and compresses the solid CO_2 to 8–10 bar to remove trapped gases and liquids. The solid CO_2 then melts in a separate vessel as it passes through its melting temperature and a pump pressurizes the liquid to its final delivery pressure. Neither the melter nor the slurry pump appears explicitly in the high-level flow diagram below.

The process ultimately produces CO_2 in a liquid phase at 125–150 bar and a gaseous nitrogen stream at ambient pressure. Both streams are near ambient temperature. The CO_2 capture fraction, generally called capture efficiency, depends primarily on the pressure and temperature at the end of the cooling process. At 1 bar, the process captures 99% of the CO_2 at −207 °F (−133 °C) and 90% at −179 °F (−117 °C).

The CCC process requires less-severe conditions than oxyfuel technologies, which operate with minimum temperatures of about −200 °C with slightly larger volumetric flow rates of gas, require 2–3 distillation columns operating at or near these temperatures, and require substantial post-combustion purification steps. Most alternative processes also exhibit rapidly increasing costs and energy demands as capture increases above 90%. High capture percentages in the CCC process require relatively small changes in minimum temperature (~15 °C between 90 and 99% capture), making the CCC process energy demand less sensitive to capture efficiency. The CCC process also produces high-purity CO_2 since it forms as a solid. A thermodynamic feature of CO_2 in atmospheric-pressure flue gases (< 16% CO_2 on a dry basis in a non-condensable gas) is that the CO_2 will not form a liquid phase at any temperature. Rather, the CO_2 desublimates in a thermodynamically pure solid phase.

The current standard carbon capture process to which new processes are compared is an amine CO_2 capture system. The amine technology involves a classical absorption-desorption process in which the flue gas flows through a column that selectively absorbs CO_2 into an aqueous amine solvent. This liquid stream contains water, amine, and CO_2 and flows to a desorption column that thermally drives the CO_2 back out of solution. This gaseous CO_2 stream passes through a compressor, which typically produces a supercritical fluid at about 150 bar and 40 °C. The main energy loads in this amine process include the heat required to drive the CO_2 from solution, the cyclical heating and cooling of the water/amine stream, and CO_2 compression from atmospheric pressure to 150 bar. Low-pressure steam from the power plant provides the desorption heat. By comparison, the main energy loads in the CCC process include the power required to run the refrigeration loops and the forced draft fan to overcome process pressure drop. The CCC process minimizes the amount of cyclical heating and cooling of process streams through heat integration and process design. Additionally, the CCC process compresses a solid/liquid CO_2 stream whereas the amine compresses CO_2 as a gas, both from nominally atmospheric pressure to about 150 bar. Solid and liquid compression requires only a fraction of the energy and cost required for gas compression over this pressure range. Figure 33 compares the energy demand for the amine and CCC processes.

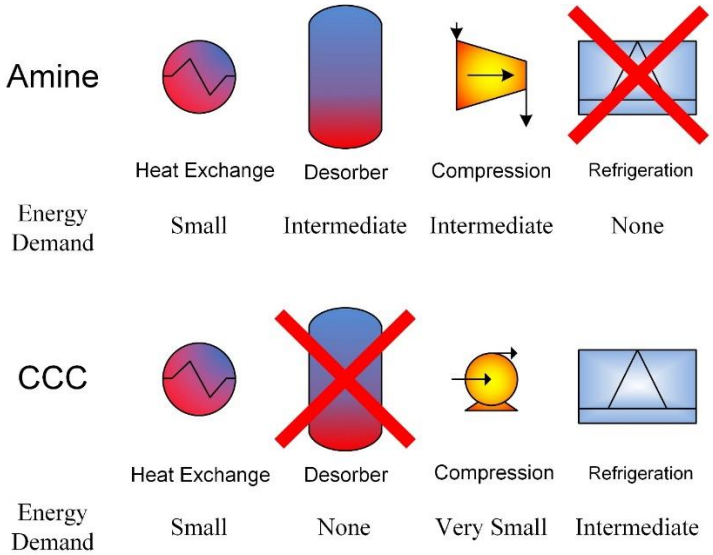

Figure 33. Comparison of the primary energy demands in an air-separation-based unit and in the CCC process

CCC Integration Strategies

While the CCC process requires essentially no changes to the upstream process, there are several integration steps that provide significant ancillary benefit compared to existing systems. These involve either removing existing process steps or simple low-grade heat and cooling integration. For example, CCC can replace current state-of-the-art pollutant removal technologies and capture most criteria pollutants more efficiently

than current best available control technologies, including Hg and air toxics but excluding CO. Figure 34 shows the capture level of key pollutants over the range of temperatures required by the CCC technology. Table 6 gives the predicted capture of these pollutants at the temperature corresponding to 90% CO_2 capture. CCC also captures particulate matter effectively in that it involves several vapor condensation steps in succession (two for water and one for CO_2). These steps remove particulate at all sizes more effectively than current particulate control devices. Nearly all the particulate is captured in the water condensation steps. In these ways, the CCC process is robust to both gaseous and pollutant concentrations and removes them with relatively little process complication. In stark contrast, both gaseous pollutants and particulate significantly affect amine lifetime and amine systems and flue gases require additional substantial treatment prior to the amine system to avoid compromising the amines.

CCC pollutant capture can replace capital equipment in greenfield installations such as flue gas desulfurization (FGD) units for SO_x reduction, selective catalytic reduction (SCR) units for NO_x reduction and activated carbon beds for mercury capture. CCC reduces these emissions to well under current emission standards for SO_x and Hg. In retrofit scenarios, CCC can reduce or eliminate operating and energy costs for these systems. CCC also captures essentially all moisture from the flue gas. CCC removes particulate as well, though these simulations presume that particulate control would remain in place with a CCC installation.

Coal-fired power plants heat boiler feed water by bleeding steam from the turbines. The CCC process can provide much of this feedwater heating by a simple integration. The flue gas in the CCC process cools to ambient temperatures in the first major unit operation. If this heat exchanger is used to heat boiler feed water, the steam flowrate through the turbine increases and improves the cycle efficiency of the power plant. This effect is quantified later in this paper.

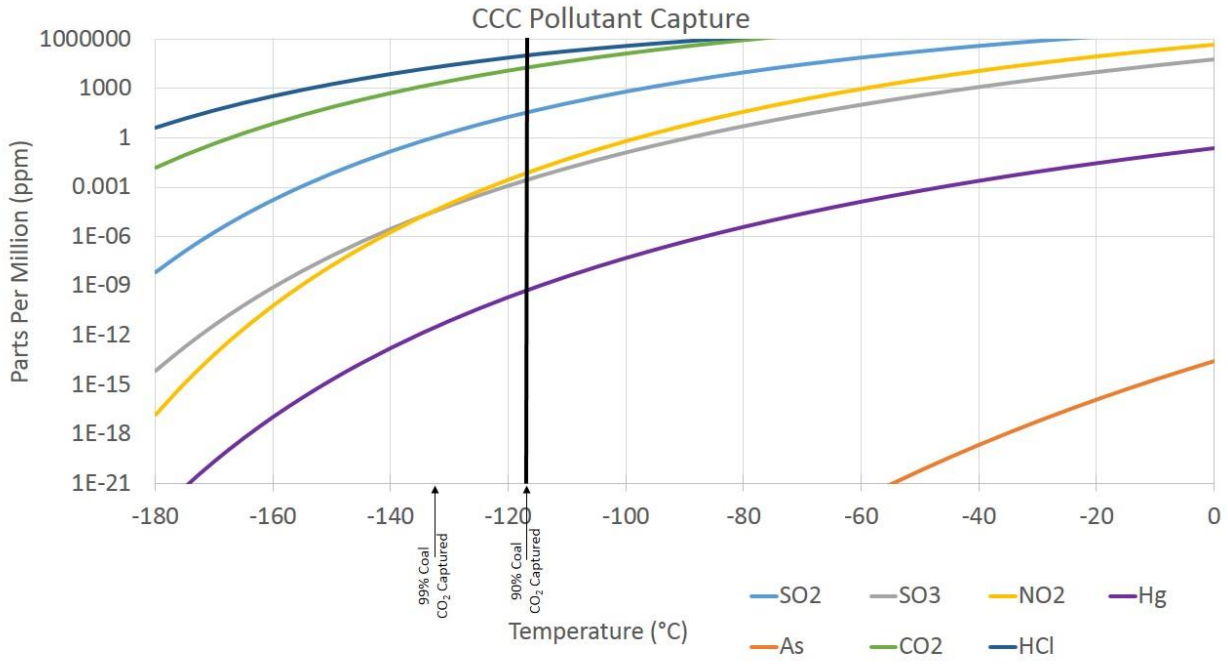

Figure 34. Pollutant Capture at CCC temperatures

Table 6. Pollutant levels at 90% CO_2 capture

Pollutant	Concentration (ppm)
SO_2	32.73
SO_3	0.002
NO_2	0.007
Hg	4.83E−10
As	7.31E−37
CO_2	17882

Similarly, the dry, light gas stream that exits the CCC process can increase the amount of chilled water. The flue gas moisture, which is removed from the flow, can also provide additional water for the process. In this manner, the CCC process can meet its own chilled water demand.

Baseline CCC ECL™ Techno-Economic Modeling

SES has performed detailed cost and energy analyses regarding the CCC ECL™ technology. For all costing calculations, SES utilized the Excel-based costing program Power Systems Financial Model (PSFM) developed by NETL, which program NETL used to report cost estimates for the amine system. This analysis uses the same assumptions as are present in the July 2015 revision of the Cost and Performance Baseline for Fossil Energy Plants [10]. This allows SES to estimate the cost of electricity (COE) and energy penalty without introducing error caused by differing assumptions in the financial models, ancillary costs, and contingencies. We compare CCC with two case studies published and periodically updated by NETL. These are NETL Case B12A, which presents a greenfield 550 MW net coal-fired supercritical pulverized coal (SC PC) power plant without carbon capture, and NETL Case B12B, which presents a greenfield 550 MW net coal-fired SC PC power plant with 90% CO_2 capture achieved via amine absorption. The CCC simulations here correspond closely to those in the NETL report and have net 550 MW_e outputs. The only significant difference is that the CCC process is less energy intensive than the amine process, so a smaller increase in input energy is needed to maintain the net 550 MW_e net output for the CCC process.

Also, the NETL reports provide no estimates for retrofitting existing power plants whereas the analyses below do. The retrofit analysis estimates the energy and financial costs of adding capture to an existing plant and compares this to the cost of existing plant power generation. In contrast, the NETL reports compare the costs of two greenfield plants, one built with and one without carbon capture. In the retrofit analyses below, both the cost for retrofitting the plant (single retrofit) and the cost the retrofit plus the cost of replacing the lost capacity with additional power from a new plant with carbon capture (retrofit scenario).

SES produced all the following results. However, SES has shared process and simulation details with many organizations (American Air Liquide, GE, Linde, Booz Allen Hamilton, national labs, DOE). Most recently, EPRI provided an independent review of these analysis. In all cases, the third-party reviews confirmed that the SES analyses provide accurate process and economic descriptions.

Energy Performance Overview

This section analyzes the energy penalty of CCC and compares it with the published amine system. The first figure of merit presented here is the equivalent electrical energy required per unit mass of CO_2 produced (GJ_e/tonne or MJ_e/kg). This number provides a scalable value that can then be applied to other similar flue gas streams. The effect on the power plant is presented in terms of the percent increase in the net plant high heating value (HHV) heat rate or efficiency. This was chosen because it is a key parameter stated in the NETL report and used in costing simulations. The net plant HHV heat rate is the amount of thermal energy (based on the HHV of the fuel) input per unit of electricity output and is presented in the NETL report in units of BTU/kWh. The system cycle efficiency comes from dividing 3412 Btu/kWh, the number of Btu per kWh, by the reported heat rate. Most people understand relate more easily to an efficiency, which contains the same information than the heat rate. Both numbers describe the effect of changing the total amount of fuel required to achieve the same net power plant output. However, it depends as strongly on assumptions about the power plant as it does on the carbon capture system, so it is not as useful in estimating

costs for alternative power plants. Furthermore, the assumptions made in the NETL report about this plant are extreme relative to operating plants in the US (Figure 35). The assumed estimate of the plant efficiency does not impact the estimated energy consumed for carbon capture in $MJ_e/kg\ CO_2$, but it strongly impacts the estimated energy expressed as a percent parasitic load and it impacts the cost of carbon capture as computed here, where the generation capacity lost to carbon capture is compensated by designing a power plant with a larger gross capacity to maintain the same net output.

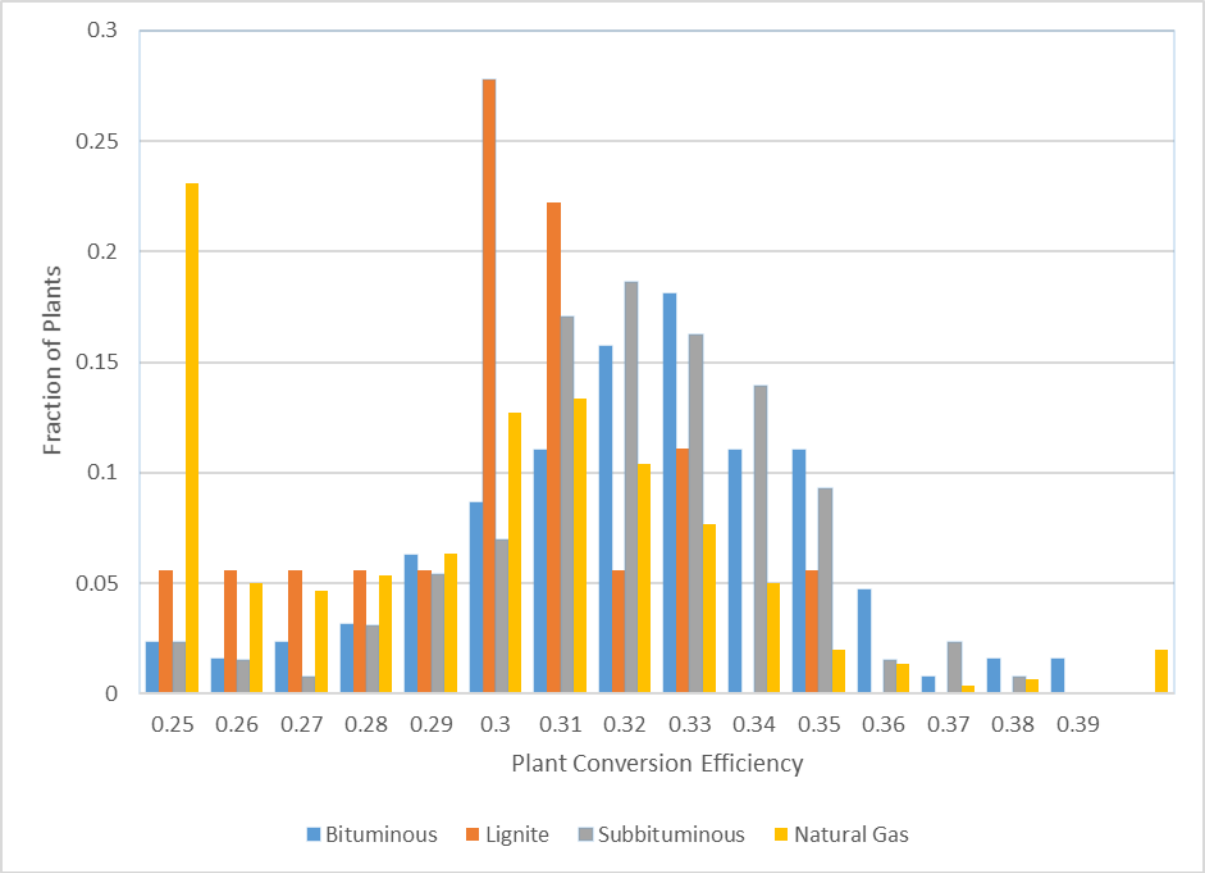

Figure 35. Histograms of overall HHV plant efficiencies for all utility-scale bituminous coal, subbituminous coal, lignite, and natural gas plants operated in the first 8 months of 2017 in the US, with a total of 277 coal plants and 299 natural gas plants. The plant efficiency assumed in the NETL report is 0.41.

The specific energy required to capture CO_2 ($MJ_e/kg\ CO_2$) cited here includes the total amount of energy required for capture. For CCC, this energy is all in the form of electricity or its equivalent (shaft work). However, amine systems primarily consume heat, with relatively smaller power consumption. The numbers cited here for both systems indicate how much the electrical output of the plant changes per unit mass of CO_2 if carbon capture is added to the plant and are therefore directly comparable. This should not be confused with the actual electricity demand for the amine plant, which is much lower because most of the energy in the amine process is in the form of steam, not electricity. However, directing this steam from the turbine influences power plant output, and this is included in the numbers below. The NETL reports list in several places the electricity demand for the amine process and list the numbers from which the overall energy demand can be expressed in terms of a decrease in electrical output. NETL does not actually tabulate the equivalent energy demand directly.

The NETL report indicates an energy demand of 1.05 GJ_e/tonne for Case B12B. The net HHV heat rate is given explicitly in the report as 10,508 BTU/kWh, which indicates a parasitic load of 20.28%. The details of how this is distributed are in that report.

Energy Performance of CCC

For the process simulations detailed in this report, refrigerant compressors were assumed to have 90% isentropic efficiency. All pump efficiencies were assumed to be 85%. Vendors advertise guarantees for compressors at this size and type at 92%. The pump efficiencies are deliberately below those of commercial guarantees because, unlike the compressors, some of the pumps operate at cryogenic temperatures and/or pump slurries rather than pure liquids.

The energy penalty associated with CCC is due almost exclusively to the work needed to power the compressors and pumps in the process. There is also a small load associated with the steam required for running the distillation column. This has been quantified in terms of electric power (MW_e), which is the equivalent power that could be extracted from this stream if it were run through the low-pressure turbine. However, the combined work of the refrigeration compressors and flue gas blower account for greater than 93% of the overall energy penalty. Table 7 contains an itemized list of the parasitic loads in the CCC process with an initial inlet gas matching that reported in the NETL Rev. 3 document [10].

Table 7. List of Parasitic Loads for CCC

Energy Source	Work (MW_e)
Flue Gas Compression	10.4
Refrigerant Compression	88.7
Separations Compression	0.3
Condensed Phase Pumping	4.3
Steam Redirection	2.6
Total	106.3

The real benefit of the CCC numbers can be seen in the established energy metrics stated above. In terms of the processed outlet stream, the energy penalty of CCC is 0.852 GJ/tonne. Its calculated net HHV heat rate is 10,035 BTU/kWh, corresponding to a parasitic load of 16.50%. The parasitic load of the CCC process as-is, without any additional integration, is approximately three quarters of the corresponding parasitic load of the amine process.

Energy Performance of Integrated CCC

As stated above, the CCC technology allows for further integration by removal of capital equipment for pollutant remediation and utilization of the low-grade heat available in the flue gas. Additionally, removal of the FGD unit allows for greater utilization of the low-grade heat, as detailed above. Utilizing "Exhibit 3–47 Case B12A heat and mass balance, supercritical steam cycle" from the NETL report allowed for precise calculation of the energy required for reheating the boiler feed water and the extra power that is generated by the larger steam flow rate through the low-pressure turbine. Utilization of the heat extracted from the flue gas allows for approximately 47% of the boiler feed water to be heated to 298 °F (147.8 °C), the temperature at which it enters the de-aerator before further pressurization and heating. This means that 47% of the steam which was previously extracted and used for feed water heating now passes through the turbine. This additional steam accounts for an additional 5.5% increase in the produced electricity from the low-pressure turbine that would not otherwise be available. In the case of an integrated CCC process, this amounts to approximately 14.3 MW of additional electricity to offset the energy penalty. The additional power results in a lower amount of fuel required to meet the net 550 MW requirement, and further decreases the size and power requirements of the CCC equipment. As every power plant is unique, not every plant will be able to utilize the entire benefit of the CCC pollutant capture value proposition. Therefore, each integration has been considered independently. These independent cases are:

1. CCC with steam cycle integration and including all pollutant removal equipment

2. CCC with removal of the FGD unit but without steam cycle integration or inclusion of the other pollutant removal equipment
3. CCC with the removal of the SCR unit but without steam cycle integration or inclusion of the other pollutant removal equipment
4. CCC with the removal of the mercury mitigation equipment but without steam cycle integration or inclusion of the other pollutant removal equipment
5. CCC with full cumulative benefits of all integration (i.e., steam cycle integration and no additional pollutant removal equipment beyond CCC)

The energy penalty of the SCR and mercury removal are almost negligible (40 kW and 22 kW for Case B12A, respectively), although their capital cost and operating cost are large. There is some parasitic load associated with the operation of the FGD (~3 MW), and its value has been included in the calculations based on the stated values in the NETL report [10]. Table 8 presents a summary of the energy penalties for these differing integration strategies.

Table 8. Summary of Energy Penalty of CCS technologies

	Case B12A	**Case B12B**	**CCC**	**Steam Integration**	**no FGD**	**no SCR**	**no Hg**	**Sum**
Power (MJ/kg CO_2)	0.000	1.047	0.852	0.673	0.810	0.851	0.851	0.630
Plant Efficiency (%)	40.7	32.5	34.0	35.4	34.1	34.0	34.0	35.7
Parasitic Load (%)	0.00	20.28	16.5	13.06	15.48	16.50	16.5	12.24

The Boundary Dam Power Station in Saskatchewan uses the same Cansolv amine process used for the Case B12B calculations. The DOE report was completed before performance results from Boundary Dam were available. The Boundary Dam project now reports a parasitic load of 30% [11], which is a 50% increase in parasitic load from the numbers reported in Case B12B [10]. Additional techno-economic carbon capture reviews also suggest that the findings of Case B12B might be optimistic regarding the energy requirements of amine carbon capture (Table 9) [12]. These techno-economic studies come from the US, Europe, China, and Australia, with similar assumptions as those used in the NETL study (e.g., amine-based processes, flue gas pre-processing to enable amine CCS, compression of the final CO_2 stream). While the parasitic load varies based on report assumptions, the power needed is consistent, and it is about 35% more than the reported value in Case B12B.

The CCC process energy numbers also depend primarily on paper analyses. There are no comparable commercial field data or international comparisons for the CCC process. However, SES has provided DOE and many other third-party reviewers detailed process simulations for their review.

Table 9. Energy requirements for amine-based CCS technologies, based on reports from the US, Europe, China, and Australia [12].

	CMU	**EPRI**	**TNO**	**TPRI**	**CSIRO**
Power Needed (GJ/tonne CO_2)	1.42	1.41	1.52	1.44	1.42
Base Plant HHV Heat Rate (BTU/kWh)	8676	8979	7982	8257	8868
Plant with Capture HHV Heat Rate (BTU/kWh)	11402	12342	11586	11439	12053
Parasitic Load	23.91%	27.25%	31.11%	27.82%	26.42%

Cost Comparison Overview

Cost comparisons proceeded in a similar manner as the energy penalty calculations, using the NETL reports as an outline for all financial assumptions. Additionally, the NETL-developed, Excel-based costing program, PSFM, provided the cost of electricity (COE) calculations used here. PSFM also provided the reported cost estimates for Cases B12A and B12B. Therefore, all COE estimates used identical assumptions and methodology in the financial models, ancillary costs, and contingencies.

Cost of Electricity (COE) for the NETL Cases

All the NETL cost details appear in the reports cited above. The Case B12A COE costs come to 82.3 $/MWh. The corresponding COE for Case B12B, including the transportation, storage, and monitoring (TS&M) of the processed CO_2, is 142.8 $/MWh, which corresponds to an increase of 73.5% compared with Case B12A. This increase includes the extra fuel and increased size of the base power plant needed to achieve the net 550 MW requirement. Additional cost increases come from increased operating and maintenance requirements of the larger plant, including the CCS portion, and an increase in contingencies based around the inherent risks involved with CCS implementation.

Cost of CCC

The cost of CCC uses vendor quotes for major equipment costs and includes increases in fuel, operating, maintenance, and capital costs for scaling up the power plant due to the parasitic load in addition to the cost of the CCC process equipment itself. The resulting COE for CCC is 119.9 $/MWh, which corresponds to an increase of 45.7%, slightly over half the increase in cost of Case B12B. These costs do not include credits for any of the integration benefits or for energy storage.

The benefits of an integrated CCC process improve the COE estimate. Removal of the pollutant mitigation units avoid substantial capital cost, and the decrease in fuel requirements, process chemicals, and corresponding decrease in process equipment size provide additional cost savings. Figure 36 and Table 5 provide a full summary of each scenario. The cost of CO_2 avoided and CO_2 captured are included in Figure 37 and Table 11. The cost of CO_2 avoided is calculated according to the following equation:

$$Avoided\ Cost = \frac{\left(COE_{with\ removal} - COE_{reference}\right)\$/MWh}{\left(CO_2\ Emissions_{reference} - CO_2\ Emissions_{with\ removal}\right)tonne/MWh}$$

The Importance of Retrofit on Cost Analysis

CCC is a minimally invasive bolt-on technology that can retrofit existing power plants. Other competing technologies require significant rebuilding or replacement of existing plant equipment, including amine absorption, oxyfuel, chemical looping, CO_2 cycles, and nearly all other proposed carbon capture solutions.

Retrofitting allows for the energy market to meet enforced carbon restrictions by leveraging existing capital resources rather than having to decommission and replace existing plants. In the United States, most capital of existing power plants has been paid off and has no effect on current COE. The ability to leverage this existing capital resource sets CCC apart from the other core CCS technologies. These numbers have been generated assuming that the boiler feed water integration is in place, which would only necessitate a small change in the current piping of the steam system at any existing power plant.

This analysis assumes that costs for a CCC retrofit equal those of a greenfield installation since the CCC process is essentially a bolt-on technology. Energy penalty calculations indicate that a net 550 MW_e power plant with CCC would produce 659 MW without CCC. Therefore, retrofitting a 659 MW plant with CCC requires the capital cost investment for the CCC process and expanding the cooling water system. Furthermore, it reduces the net power output of the existing plant by 109 MW, or 16.5%, resulting in a 550 MW_e plant. If the plant does not implement the energy storage capability, every 5 plants of this size that are retrofitted require one new plant to replace the lost capacity.

The COE of a single retrofit plant in this analysis equals the COE of Case B12A scaled linearly to a 659 MW_e net plant minus the capital cost portion of this COE to approximate the economics of a fully paid off plant. The operation, maintenance, and fuel costs remained at their scaled values. This single retrofit cost does not account for the loss in capacity. The capacity loss is included in the CCC scenario case by adding one fifth of the COE for a greenfield plant to the single retrofit plant. A summary of the results of these economic evaluations appears below in Figure 36, along with the results from all greenfield scenarios (Table 10). The retrofit numbers do not include any of the integration benefits previously discussed (pollutant capture, boiler feedwater heating, etc.).

CCC costs less than Case B12B and all other comparable amine-based CCS techno-economic estimates (Table 12) for new power (greenfield) generation. The retrofit capabilities of CCC present even greater savings. The table shows that retrofitting an existing plant with CCC provides cheaper power than a new non-capture plant (compare the two columns after the vertical bar with the first cost column for B12A). The carbon capture costs are 11.1% less expensive in the case of a single retrofit and 1.9% less expensive for the retrofit scenario. Nearly all existing coal-fired power plants are beyond their capitalization periods on the books. The capitalization costs typically account for over half of the COE for a new plant. This fraction of the COE drops to near zero after the end of the capitalization period, reducing the COE by about 50%. CCC enables this existing infrastructure and the similar global infrastructure around the world to continue operation at very low costs well into the future.

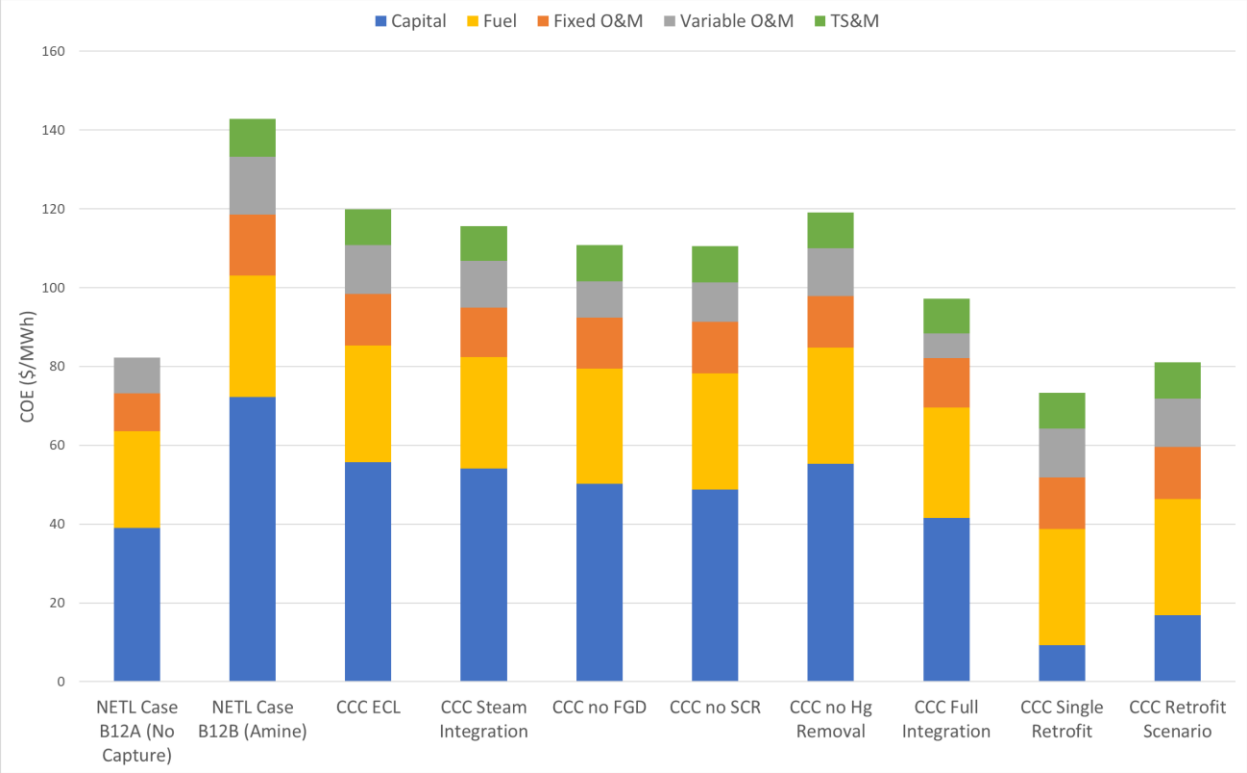

Figure 36. COE of different case studies broken into component parts.

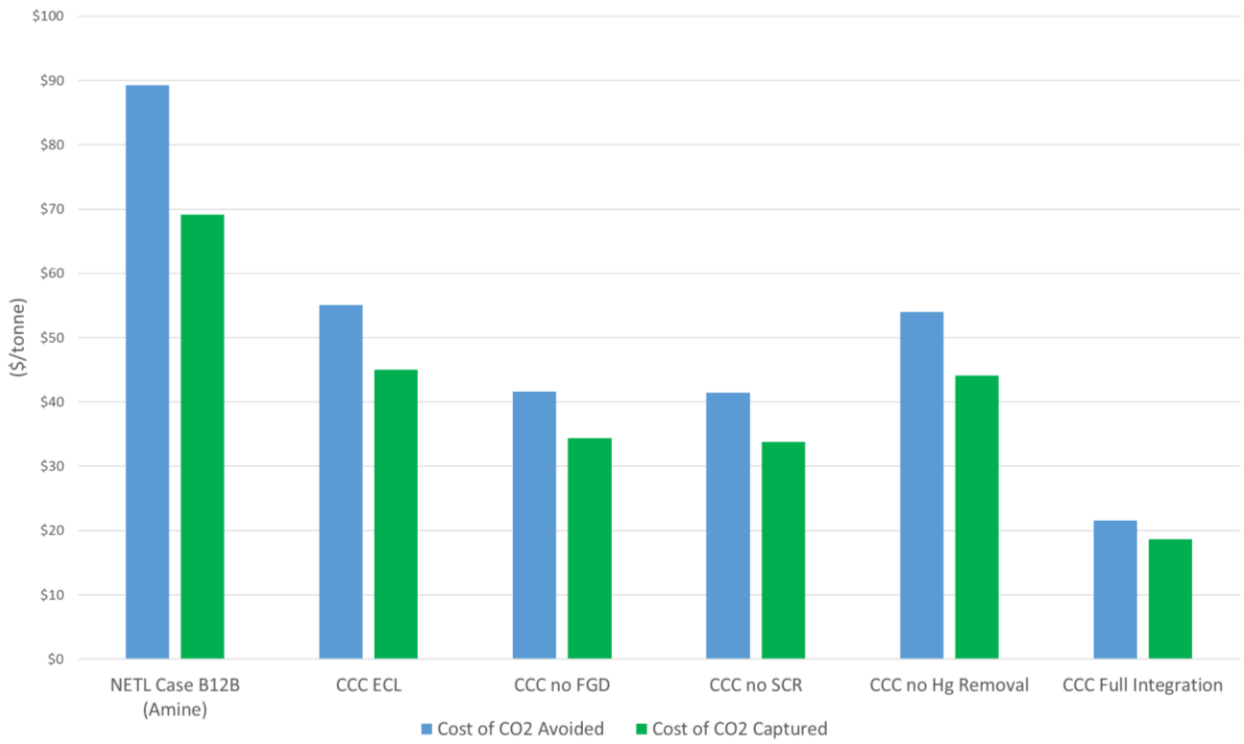

Figure 37. Cost of CO_2.

Table 10. Cost comparison between NETL Cases B12A and B12B as well as estimates for the CCC process, both as a greenfield installation and as a retrofit installation.

Costs $/MWh	Case B12A	Case B12B	CCC ECL	Steam Int.	no FGD	no SCR	no Hg Removal	Full Int.	Single Retrofit	Retrofit Scenario
COE	82.30	142.80	119.90	115.60	110.73	110.55	119.13	97.15	73.37	80.78
TS&M	0.00	9.60	9.17	8.82	9.08	9.17	9.17	8.74	9.17	9.15
Fuel	24.60	30.90	29.50	28.33	29.22	29.50	29.50	28.07	29.50	29.43
Variable	9.10	14.70	12.38	11.83	9.30	10.04	12.06	6.36	12.38	12.35
Fixed	9.60	15.40	13.10	12.58	12.97	13.09	13.10	12.46	13.10	13.06
Capital	39.00	72.20	55.76	54.04	50.16	48.75	55.30	41.52	9.22	16.90
Δ Case B12A	0.00%	73.51%	45.69%	40.47%	34.55%	34.33%	44.75%	18.04%	−10.85%	−1.52%

Table 11. Cost of CO_2 comparison for greenfield cases.

Cost ($/tonne)	Case B12B	CCC ECL	Steam Integration	no FGD	no SCR	no Hg Removal	Full Integration
CO_2 Avoided	89.30	55.1	48.45	41.60	41.40	53.97	21.57
CO_2 Captured	69.17	45.0	41.43	34.35	33.81	44.08	18.64

The reviews of amine performance cited in the energy penalty discussion above also provide COE estimates that can be compared with the NETL results, though they did not provide nearly as much background on the calculations. Table 12 summarizes the results from the comparative documents and includes in the last column the CCC data.

Table 12. Increase in COE for amine-based CCS installations [12] and CCC.

COE ($/MWh)	NETL	CMU	EPRI	TNO	TPRI	CSIRO	CCC
Reference Non-capture Plant	82.3	59.1	73.4	43.9	42.0	53.4	82.3
Capture Plant	143	99.2	121	79.2	62.0	115	120
Increase	60.5	40.1	47.7	35.3	20.0	61.1	37.6
% Difference	73.5	67.9	65.0	80.4	47.6	114	45.7

According to the January 2013 Electric Power Annual released by the United States Energy Information Administration [13], power generation costs in the US average 35.1 $/MWh in 2011—the simulated year of the NETL study [10]. In a greenfield installation, the cost of electricity increases by 81.9% with the addition of carbon capture. However, if retrofits are not an option and the full capacity of existing power plants must be replaced with those capable of carbon capture, the real cost of electricity generation to the utility increases from around 35.1 $/MWh to 142.8 $/MWh, an increase of over 300%. In the low-cost regions of the country, where average generation costs are about 20 $/MWh, this represents an increase greater than 600%. A single CCC retrofit would increase power generation from 35.1 $/MWh to 73.4 $/MWh, a 109% increase. About 26% of this increase is due to transportation, storage, and monitoring. This is a large increase, but it is small in comparison to the alternative of having to replace lost capacity with new installations or significant rebuilds.

Conclusion

The current energy infrastructure still relies heavily on fossil fuel resources for most the world's energy demands. A transitional energy infrastructure is necessary to mitigate the adverse effects of fossil-based energy, such as global climate change. For these reasons, carbon capture and sequestration has become a critical technical challenge. Cryogenic Carbon Capture™ represents a viable alternative to current technologies. Its advantages include:

(a) a lower parasitic load, ~25–50% lower than established metrics for absorption technology, depending on the reference study;
(b) lower cost of electricity, approximately 60% of the increase calculated using established metrics for absorption technology;
(c) minimally invasive bolt-on technology capable of being retrofitted to existing plants;
(d) scalability to largest commercial emitters, such as coal-fired power plants;
(e) ancillary pollutant removal and the inherent integration benefits associated therewith;
(f) ability to capture CO_2 at well above the industry standard 90% capture efficiency; and
(g) equipment and unit operations already familiar to power plant personnel.

By virtually every established metric, CCC outperforms competing carbon capture technologies and represents a potentially paradigm-shifting solution to the current questions facing the energy industry.

Independent TEA Effort

SES has worked collaboratively with EPRI to establish their own independent techno-economic analysis. SES shared a detailed PFD and heat and mass balance with EPRI for review and discussed the details of process assumptions. SES also shared the Aspen simulations with EPRI performed by BYU. EPRI has completed an independent analysis of the CCC technology and documented it in a detailed report. The following is an excerpt from that report:

Overall Performance

The system performance is summarized in Table 13in comparison to the DOE NETL bituminous Baseline rev 3 case 12A – supercritical coal-fired power plant without CO_2 capture.

Table 13. CCC system performance summary.

		Case 12A	Simulated CCC
Gross power	kW_e	580,000	667,900
Impact of steam extraction	kW_e	-	5,755
Plant Auxiliaries	kW_e	29,688	34,187
CO_2 capture auxiliaries	kW_e	-	126,770
Net Power	kW_e	550312	501,187
HHV Thermal Input	kW_{th}	1,350,672	1,555,368
HHV efficiency	-	0.4074	0.3222
LHV Thermal Input	kW_{th}	1,302,740	1,500,172
LHV efficiency	-	0.4224	0.3341
Percent of Load Consumed	-	-	0.2091
Flue Gas Flow Rate	kg/hr	2,165,283	2,493,652
CO_2 Mass Flow	kg/hr	425,409	489,880
CO_2 Captured	kg/hr	-	440,892
Energy Impact of Capture	kJ_e/kg CO_2	-	973.9
CO_2 Intensity	kg CO_2/kWh	0.7730	0.0977

Performance Summary for SES CCC system evaluated using Aspen Plus with Refprop Properties

The components of the CO_2 capture auxiliary load are given in Table 14

Table 14. CO_2 capture auxiliary load.

Unit	Net Power (kW)
C1 – flue gas compressor	33,838
C2 – warm mixed refrigerant compressor	42,952
C3 – cold mixed refrigerant compressor	46,989
C4 – Gaseous CO_2 compressor	413
Pump work – aggregate of all pumps	2,576

The reboiler duty is 29,693 kW at 381 K, which yields a decrease in the steam turbine output of 5,755 kW based on the correlation for steam extraction determined from GateCycle modeling.

Conclusion

Overall, the results from the SES simulations seem to be fairly represented and in good agreement with the EPRI verification and indicate a promising technology with the potential to lower the energy penalty of CCS. As the EPRI heat and mass balance is based on the SES optimized model, but was not optimized for the specific solving methodologies, assumptions, and property methods used, there is the potential to improve the overall performance of the system from the results provided. There are also portions of the process that were not fully modeled that may yield additional loads to system that would diminish the performance.

Further, this evaluation independently verifies the numbers provided by SES but does not optimize the results – either in terms of energy or total cost. Energetically, the process can be improved through maintaining closer temperature approaches in the heat exchangers through refrigerant pressure, composition, and flowrate optimization, increasing the efficiency of the flue gas compressor, and minimizing the pressure drop through heat exchangers and other systems. Impacts to the system that will have to be addressed moving forward include a more rigorous analysis of the dehydration unit and determining the best use of the dry flue gas stream.

Full system optimization will include determination of price/performance tradeoffs for different types of equipment, such as heat exchanger approach temperature or flue gas compressor efficiency. While this

verification simulation does not yet provide insight into these questions, it forms the basis from which sensitivity studies can be performed and equipment pricing can be generated.

Comparison of EPRI and SES Results

Our initial reaction upon review of the EPRI report is that the results were more dissimilar than expected. However, upon further review they agreed quite closely. The only significant discrepancy comes from the shaft work required by the flue gas compressor. EPRI's work is based on a process flow diagram that includes a desiccant dryer as the only drying method, which was considered the state-of-the-art drying method at the beginning of Budget Period 1. SES's work, however, makes use of the dryer concepts and experimental data developed during Task 2. As a result, the total pressure drop of the flue gas in EPRI's simulation is 0.55 bar, whereas the total pressure drop of the flue gas in SES's simulation is 0.134 bar. If one were to take EPRI's simulation and only change the pressure drop of the whole system from 0.55 bar to 0.134 bar, it would decrease the load of the flue gas compressor from 33,838 kW, as is stated in their report, to 8,845 kW. This decrease in the flue gas compressor load decreases the energy penalty from 0.974 GJ_e/tonne CO_2 to 0.767 GJ_e/tonne CO_2. While most of the rest of the system would remain unchanged, this would add slightly to the cooling load of the refrigeration cycles, as discussed in Task 2 above. SES's estimate of the increase in cooling duty of the Task 2 dryer compared to a dry flue gas is 0.0447 GJ_e/tonne CO_2. If this number is included, EPRI's parasitic load would be 0.812 GJ_e/tonne CO_2. This, remarkably, means that rectifying the one major difference between the two simulations should result in a difference in the parasitic load of approximately 1% between the independent analyses.

3. Budget Period 2 – Results and Discussion

Task 1. Project Management & Planning

Specific Objectives: The objective of this task is to manage, coordinate, and report on the technical scope, budget, and schedule consistent with a task-oriented work breakdown structure to accomplish the work effectively and to ensure that project plans, results, and decisions are appropriately documented, and that project reporting and briefing requirements are satisfied.

During Budget Period 2, SES successfully coordinated the preparation and placement of the CCC ECL™ skid equipment for field testing at the Hunter Power Plant.

In discussion with Rocky Mountain Power (RMP), the following objectives were achieved:

- Specific timelines were discussed and the likelihood of any scheduled shutdowns of the unit at the power plant or other issues were considered.
- The locations for the sampling and return of the flue gas were decided.
- On-site logistics and what RMP would provide for support of the on-site testing were discussed extensively.
- A preliminary schedule for SES employees includes continuous tests with two employees on-site. The developed plan resulted in improved operation, safety, and less onerous testing times for the SES team.
- SES also completed the Host Site Agreement with the Hunter Power Plant in Castle Dale, Utah.

All this preparatory work culminated in the placement of the CCC ECL™ skid at the Hunter Power Plant and field testing of the CCC ECL™ skid.

SES also completed and submitted the Test Plan to NETL, and details of the submitted test plan are described in further detail below. During testing, a revision to this test plan was submitted, which included a one-quarter (3-month) extension of the project. This extension request was the result of delays in getting on-site, as well as some initial shakedown concerns. Changes to this test plan and additional details are described further in Task 11.

Task 10. Skid Modification and Shakedown

Specific Objectives: The objective of this task is to modify the existing skid system to incorporate the improvements identified in Budget Period 1 and to shakedown the resulting system.

Planned Approach: The Recipient will incorporate the technologies selected in Budget Period 1 into the skid and shakedown the resulting systems in preparation for long-term, in-house testing. Shakedown testing will include unit and full-skid testing of the modified CCC ECL™ skid. These tests will include a variety of inlet gas conditions to test the updated controls, valves, unit operations, process monitoring devices (e.g., pressure transducers, thermocouples, flow meters, flow rate controllers), etc. Tests will last from a few minutes to over 10 hours to ensure that all modifications to the system are correct and robust.

Finalize Plans to Modify Skid and Complete Skid Modification

Process Layout

While the basic process has remained the same, the many improvements to the desublimating heat exchanger, solid–liquid separations system, contact liquid cooling system, and vapor–liquid separations system have different spatial requirements than previous iterations. The space internal to the CCC ECL™ skid was reoptimized to allow for installation of the new unit ops and to decrease the potential for CO_2 fouling.

Early on, a cryogenic liquid pump was added to pump refrigerant through the various heat exchangers that were being tested. Figure 38 shows the layout of the refrigerant/cooling coldbox with the refrigerant pump.

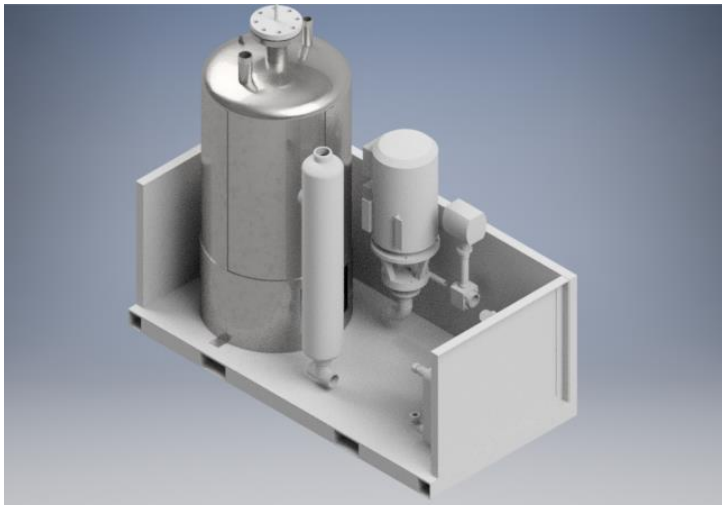

Figure 38. Renderings of the new refrigeration/cooling coldbox.

After removing the cryogenic liquid pump and selecting two heat exchangers (i.e., a brazed plate and a shell and tube) to test and use in parallel, the refrigeration coldbox was again modified. Figure 39 shows the current layout of the refrigerant cold box with the brazed plate heat exchanger in place.

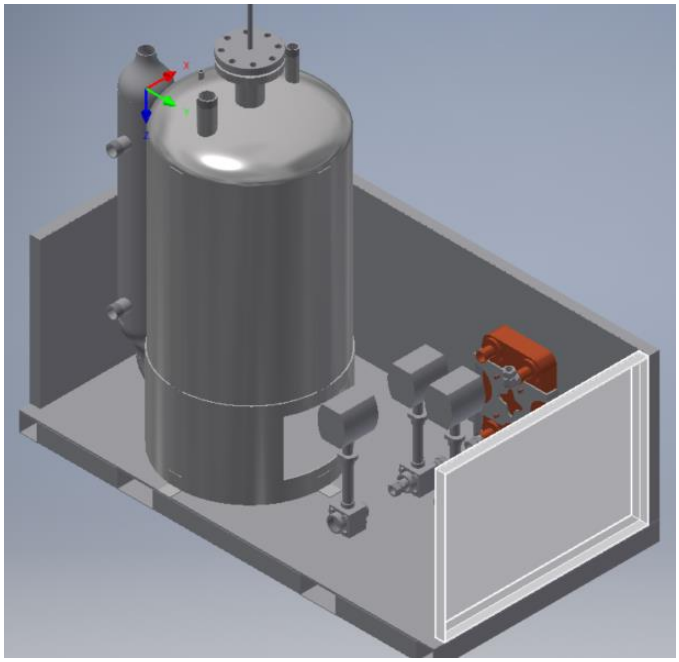

Figure 39. Coldbox after removing the refrigerant pump. The brazed plate heat exchanger is shown in the back (dark orange).

The shell and tube heat exchanger was installed in the skid in front of the refrigerant cold box. Figure 40 shows the layout of the skid from the top and from the front. The walls of the shipping container have been removed and each major cold box or piece of equipment is identified.

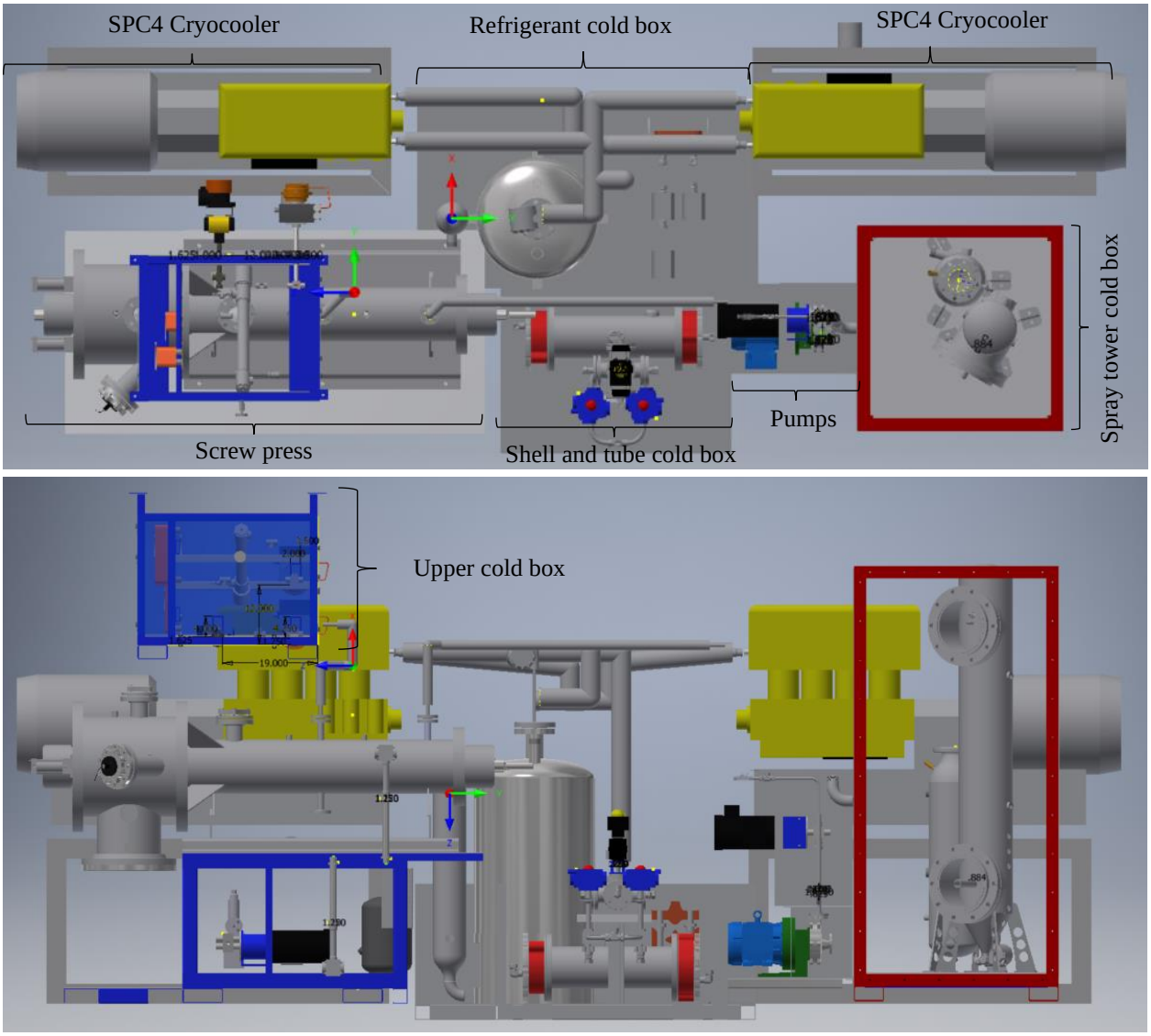

Figure 40. Skid layout without skid walls. Upper panel shows the view from above. The upper cold box is shown in the lower panel and is housed above the screw press.

Dryer Model

The dual-desiccant bed dryer used in the skid was modelled using SES' in-house dryer simulator. The simulator models the operation of one of the desiccant beds. The model works by dividing the bed into approximately 50 zones, then solving the transient heat and mass balances in each zone. The bed adsorbs water when it is drying and desorbs water when it is being regenerated. The inlet conditions and flow direction within the model can be changed mid-run to simulate a dryer switching from a drying state to a regenerating state. Through repeated cycling, the simulation can estimate the long-term trends of dryer performance, ensuring that the dew point of the dried flue gas does not rise to an unacceptable level.

Figure 41 shows a snapshot of the dryer model during a regeneration phase. One feature of interest is the mass transfer zone (MTZ), which is where most of the mass transfer occurs. This is represented by the steepest portion of the curves in Figure 41.

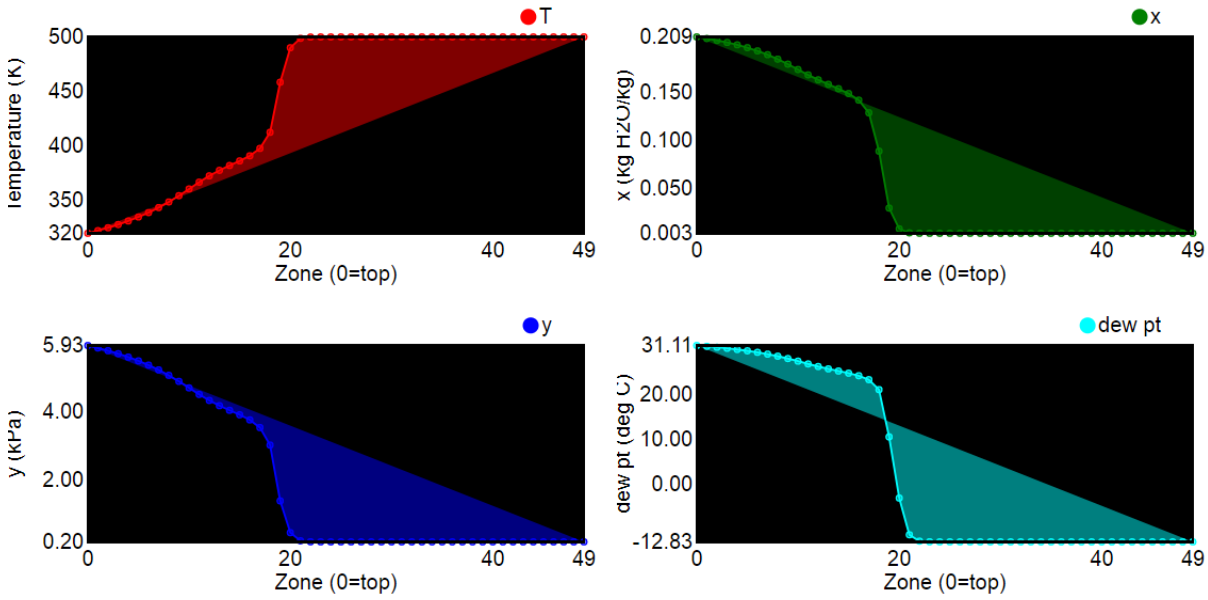

Figure 41. A screenshot from the SES dryer model, showing temperature and moisture profiles of the desiccant bed at a moment in time during the regeneration phase. (top left) Temperature as a function of bed location. (top right) Desiccant loading in kg water/kg desiccant. (bottom left) Partial pressure of water in the gas phase. (bottom right) Dew point of the gas phase. During regeneration, flow enters from the right (zone 49).

Several criteria verify the effectiveness of a proposed program for drying and regeneration. The most important of these is to ensure that after many cycles, the MTZ does not reach the end of the bed, as this would indicate that the entire bed has been saturated, and that an unacceptable quantity of water is leaving the bed with the flue gas.

This model has also helped us verify minimum flowrates and maximum allowable water content during regeneration. Figure 42 shows a simulated dryer that has been regenerated any number of times and it still reached a dewpoint below –100 °C (see bottom right plot). In this case, the regeneration flowrate is low enough to use only part of the available dry nitrogen stream that remains after the CO_2 has been removed from the flue gas.

Using the model, we generated a set of training materials for skid operators to effectively run the dryer. The materials include guidelines that dictate when the active dryer should be regenerated, and how to recognize when regeneration is complete. The model also helped train operators to recognize abnormal conditions. For example, on one occasion the dryer temperatures significantly deviated from the model predictions. Soon it was discovered that a precooler water supply valve had been closed, and that the dryer was absorbing water at a much faster rate than usual. The operators were then able to restore the water supply before the problem became serious.

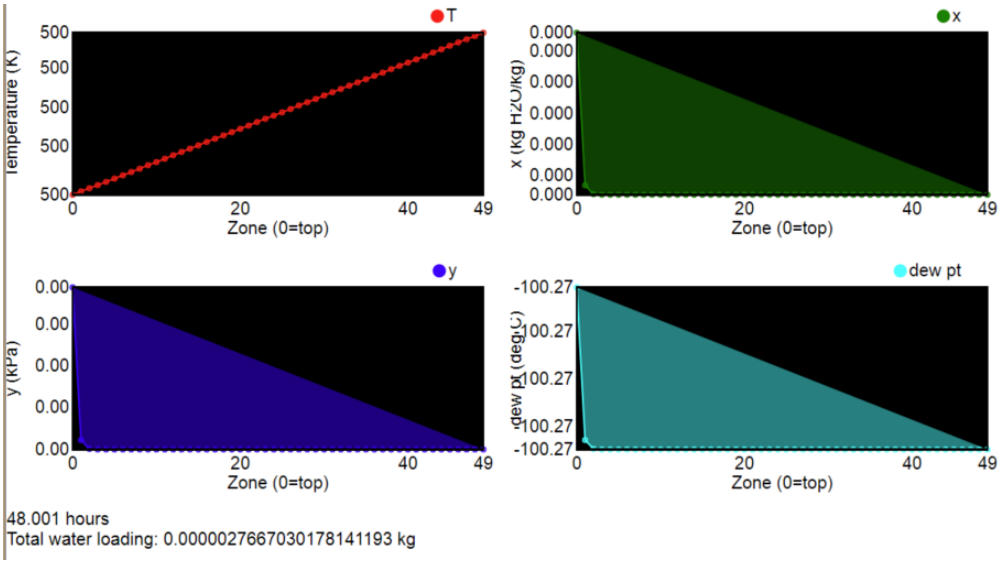

Figure 42. Model output representing the dryer after any number of loading and regeneration cycles at 1 tonne CO_2/day using a portion of the clean nitrogen from the process outlet to regenerate the desiccant.

Future work may include refining the model using data collected during actual operation. This could help us identify the upper limit at which water can be desorbed without oversaturating the beds.

Dryer

After running the dryer simulations with varying flue gas pressures, temperatures, and concentrations, we made several modifications to improve the efficiency of the existing dryer. First, we removed a significant portion of the mol sieve 3A desiccant. The simulations predicted that we could safely remove about a quarter of the desiccant. Removing the unnecessary desiccant reduced the sensible heating requirement, the heat of adsorption, and the pressure loss through the bed. We also changed the piping to flow downwards while active and increased the port diameter to further reduce pressure drop (Figure 43 and Figure 44).

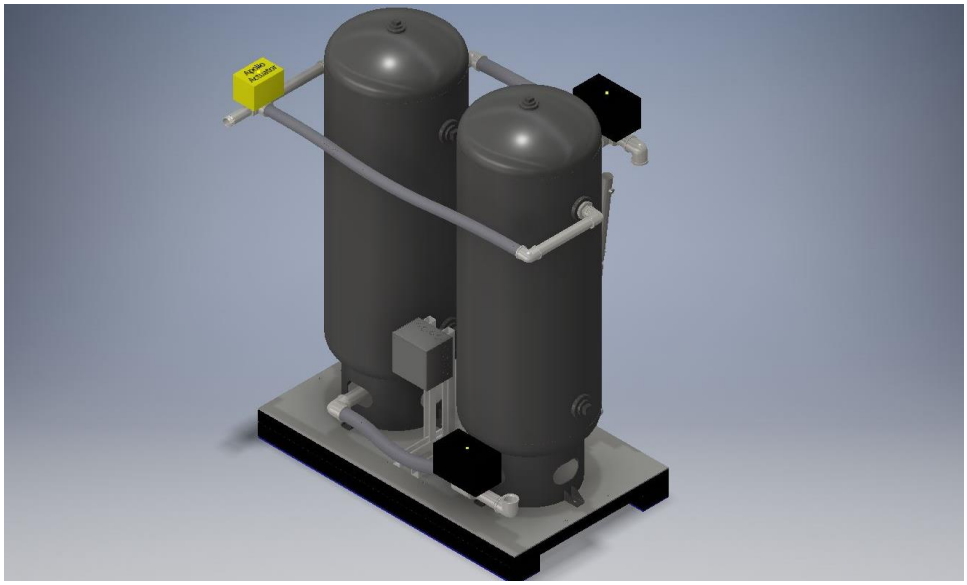

Figure 43. CAD rendering of the mol sieve desiccant dryer.

Figure 44. Mol sieve dryer integrated with the CCC ECL™ Skid. Both beds are covered with blankets of gray fiberglass insulation.

Many of the unit operations in the CCC ECL™ skid were tested in closed-loop mode (i.e., simulated flue gas composed of only N_2 and CO_2) at SES prior to shipment to the Hunter Power Plant in Castle Dale, UT. With no water in the test gas when running in closed-loop mode, however, the dryer had to be tested during the first weeks at the plant. The precooler is a shell and tube heat exchanger that chills the incoming flue gas using plant water with a condensate drain at the bottom. The intercooler and aftercoolers were brazed plate heat exchanges designed for condensing and removing water. These heat exchangers have ports for removing condensates, so no additional separators were installed. During shakedown testing, water was removed via condensate ports on the precooler and aftercooler heat exchangers but there was higher carryover than expected. Since almost 90% of the water in the gas is condensed and removed before the gas reaches the dryers, the water carryover in the stream quickly flooded the dryers and was carried over into the CCC ECL™ process where it condensed in the recuperator and desublimator. Cyclonic separators added after the flue gas precooler and the blower aftercooler heat exchangers (Figure 45) resolved these problems. Areas of the process effected by the water were purged so testing could continue. No other major issues were observed in the dryers for the duration of the testing.

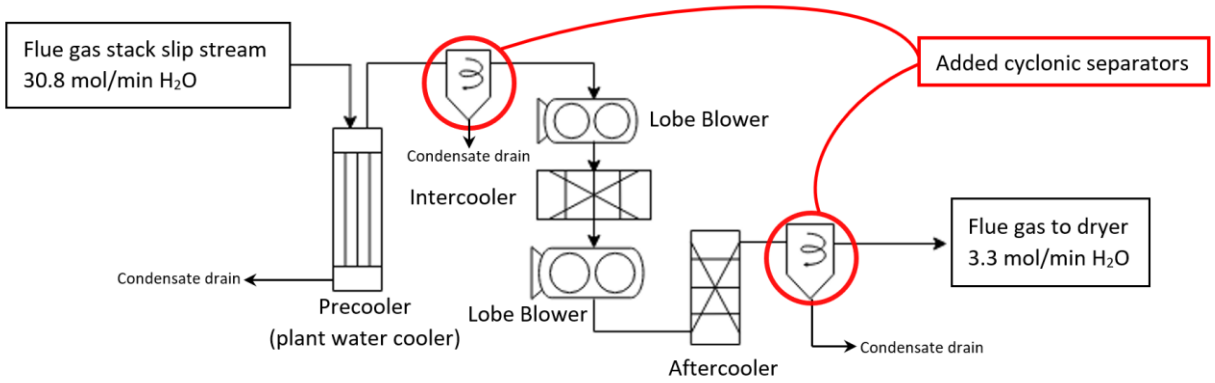

Figure 45. Flue gas conditioning portion of the CCC ECL™ skid. Two cyclonic separators were added during shakedown testing to improve water removal and dryer performance.

Recuperator

During early testing of the ECL system, it was discovered that there was a possibility for the primary recuperator to foul or restrict flow over time. It was originally intended that the recuperator would be oversized, and that if any fouling caused by CO_2 or other materials were to occur, it would simply reduce heat exchange and increase the outlet temperature until it was no longer possible for fouling to continue. However, if the gas enters the recuperator at cold temperatures, it can create a feedback loop wherein CO_2 fouling can reduce heat exchange in the entire heat exchanger, meaning that the outlet going into the spray tower can be well over the temperature at which you would typically see CO_2 desublimation. As this fouling persisted even when operating in closed-loop mode, where the simulant flue gas was made up only of N_2 and CO_2, water or other contaminants were ruled out as a source of fouling. The only possible source of fouling was CO_2.

An early attempt at mitigation was to reverse the flow through the recuperator to sufficiently heat the frozen portions. However, test runs with the recuperator indicated that the partial fouling of the heat exchanger occurred quickly enough that switching the flow would never result in steady-state operation.

To address the issues caused by this fouling, SES developed additional equipment for mitigation (i.e., a “precuperator”, as shown in Figure 46). A basic model of the system indicated that when the outgoing stream from the recuperator into the desublimator remained above −100 °C, fouling would not occur. From this, SES determined that a stream of warm isopentane returning from the distillation column could warm the flue gas. This also had the added effect of improving the system’s heat integration, as it would allow for better cooling of the isopentane stream before it entered the contact liquid cooling loop. As we wanted to be able to control the exact temperature of the returning isopentane stream, we added an inline heater (Figure 47) that would increase our ability to control this stream.

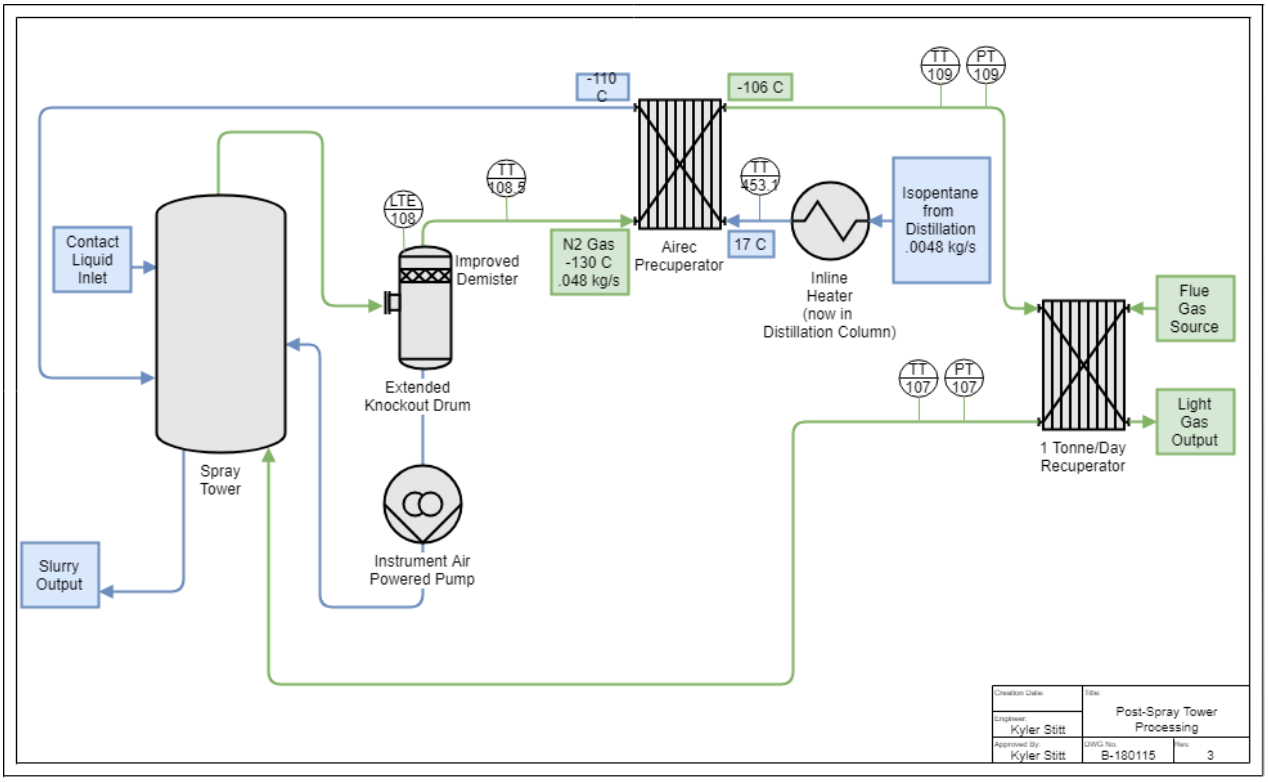

Figure 46. Updated process flow diagram of the recuperator and spray tower for the CCC ECL™ skid.

Figure 47. (left) Recuperator heater casing design, (middle) actual heater, and (right) installed.

To exchange heat with the isopentane stream, SES selected an asymmetrical heat exchanger (Figure 48), which exchanges heat between a small liquid flow and a larger gas flow. This minimizes the pressure drop on the gas side, while also minimizing the amount of contact liquid required to fill the heat exchanger.

Figure 48. Airec asymmetrical heat exchanger.

SES conducted preliminary tests of the modified recuperator system and the new demister/vapor–liquid separator to ensure that the vapor–liquid separator is collecting liquid isopentane and to verify that the asymmetrical heat exchanger is adequately increasing the temperature of the flue gas and cooling the isopentane stream. The final installed heat exchangers are shown in Figure 49.

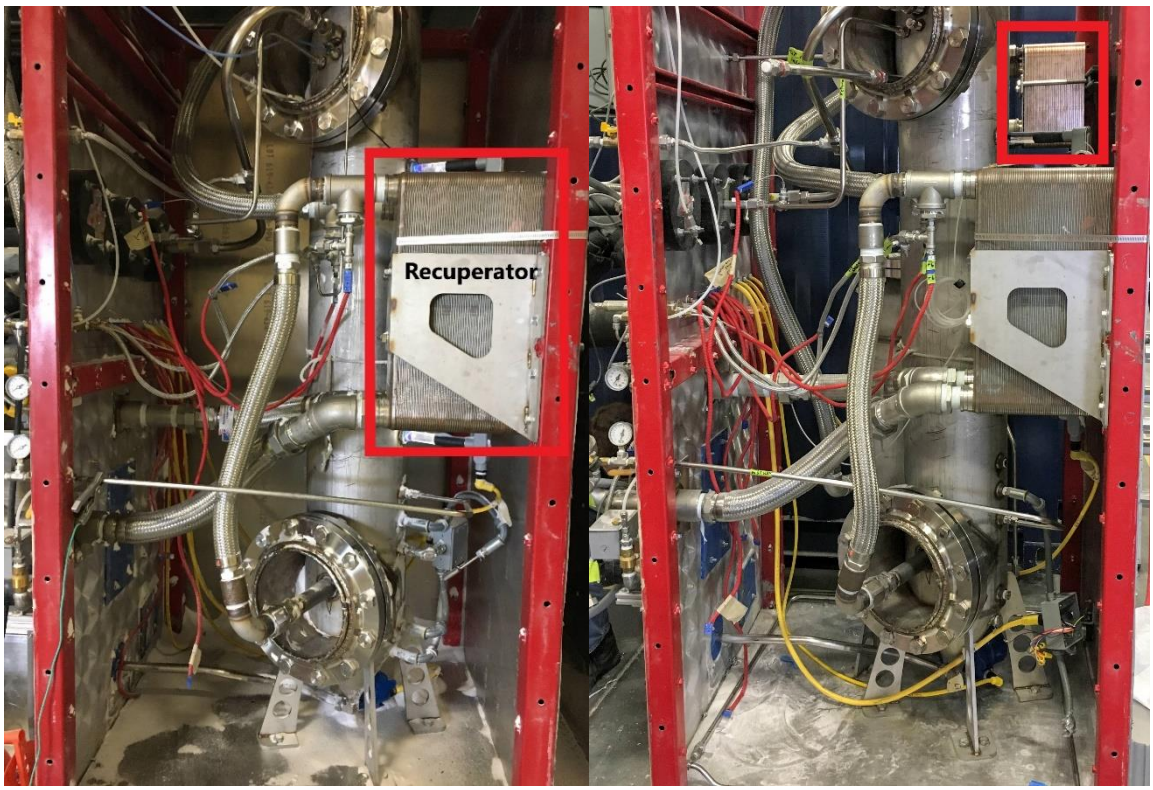

Figure 49. Recuperator (red box, left) and new secondary “precuperator” (red box, right).

SES conducted tests in closed-loop mode at SES as well as field tests with flue gas at the Hunter Power Plant. In both cases, fouling was minimized in the recuperator. SES also discovered during field testing that simply having the incoming stream to the recuperator at slightly warmer temperatures, which occurred naturally at the power plant, removed the fouling issues. This indicates that while this simple system could

be beneficial to integrate at larger scales as a backup, it would likely not be necessary during normal operation at full scale.

Spray Tower (Desublimating Heat Exchanger)

A hybrid bubbler/spray tower (spray tower) direct-contact heat exchanger was installed in the CCC ECL™ skid. This heat exchanger works by spraying a cold contact liquid countercurrent to the flue gas flowing through the unit. A pool of contact liquid stands at the bottom of the spray tower and the incoming flue gas bubbles through the cold liquid prior to coming into contact with the spray. Prior iterations of the spray tower were tested on flue gas from coal, cement, natural gas, and biomass combustion. One observation from these tests was a loss of contact liquid with the outgoing clean gas. The turbulent environment within the spray tower was producing droplets small enough to get entrained into the outgoing light gases. It was therefore necessary to add a vapor–liquid separator with a demister to capture this liquid prior to releasing the light gas stream. Figure 50 shows a CAD drawing of the contact liquid vapor–liquid separator. The flange at the top houses a level sensor that can detect when the level is high, which indicates that the vessel should be drained. The volume of the vessel below the inlet can be used as a buffer to maintain a specific height within the spray tower. Depending on process conditions, liquid can be pumped from this vessel to be added to the spray tower, which would increase the liquid level within the spray tower. Figure 51 shows a CAD drawing of the spray tower and the vapor–liquid separator situated behind and to the left. The tubing has been removed to allow for clear viewing of the spray tower and the vapor liquid separator.

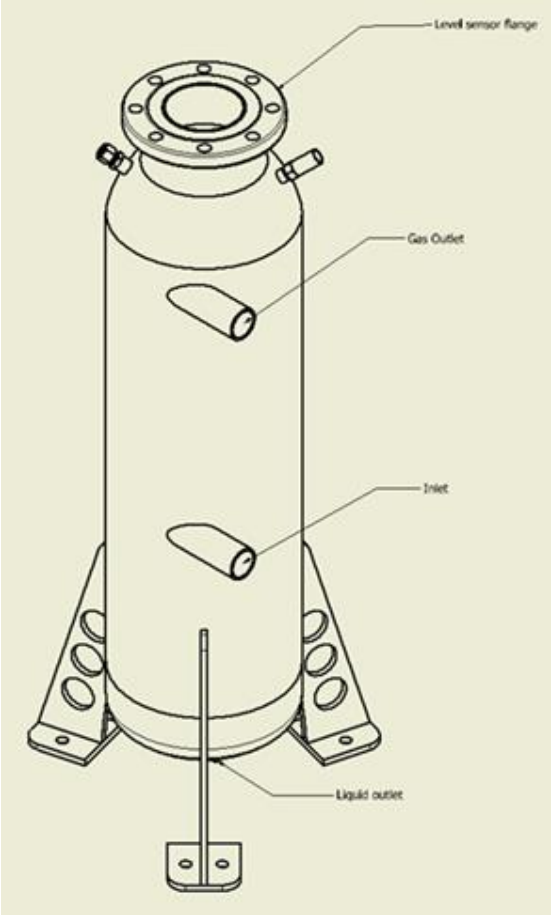

Figure 50. Vapor–liquid separator for removing entrained contact liquid from the clean gas stream.

Figure 51. Drawing of the spray tower coldbox. The vessel in the front on the right is the spray tower. The vessel partially obscured behind and to the left is the vapor–liquid separator.

Longer tests using the spray tower in closed-loop mode had ended because solid CO_2 collected on the sides of the spray tower and then broke off, which overwhelmed the pump and separation system with solids. Three strategies were put forward to mitigate this issue:

1. Polishing the sides of the spray tower would prevent the buildup of solids by reducing the friction between the solids and the sides of the spray tower.
2. A spray cleaning nozzle was employed to spray contact liquid at the sides of the spray tower to dislodge solids before significant buildup could occur.
3. A knocker was added to introduce large vibrations into the tower to physically dislodge solids before the buildup became too large.

Polished Internals

The interior of the spray tower was lined with a thin sheet of polished stainless steel. This was accomplished by designing and cutting a stainless-steel sheet, rolling that sheet and welding it in place within the spray tower. A photo of the polished sides of the spray tower is shown in Figure 52. The sides of the spray tower were now polished, but the cap (top) of the spray tower remained unpolished. This top surface was electropolished at SES using a commercially available electropolishing chemical and DC voltage supplied

by a welder. Figure 53 shows the polished interior of the spray tower prior to attaching it to the body of the spray tower. The bottom cone of the spray tower was not polished because it remains below the contact liquid level and no build-up of CO_2 solids has been observed on surfaces submerged in the contact liquid. An additional surface was not polished above the liquid level within the spray tower (Figure 52). This unpolished surface was left as a control to compare the polished surface to the unpolished surface. During extended tests, the spray tower was observed to operate better and there was less buildup as a result of the polished surface.

Figure 52. Image of the spray tower interior after the polished lining was inserted into the spray tower.

Figure 53. Polished cap of spray tower.

Spray Cleaning Nozzle

We installed a rotating nozzle that sprays every location within the spray tower over a short period of time. The spray nozzle assembly is shown in Figure 54. Figure 55 shows an image of the spray nozzle during operation. It was found that this spray cleaning was very effective and only needed to be employed occasionally to prevent excessive solids buildup. Further, the spray cleaning nozzle was equally effective on both the polished and unpolished surfaces. In future designs, the spray nozzle could be employed alone to prevent solids buildup within the spray tower.

Figure 54. Spray nozzle assembly prior to mounting in the spray tower. The liquid to be sprayed enters at the compression fitting in the center of the image. The air motor that turns the drive shaft is on the left and the spray head and drive gear is located on the right.

Figure 55. Interior of the spray tower showing the cleaning spray.

Impact Knocker

A single impact knocker was installed on the spray tower. The knocker supplied a large vibration to the spray tower to dislodge solids from the spray tower surface. A CAD drawing of the knocker is shown in Figure 56. The knocker was tested with limited success on the spray tower. It was shown that the knocker was able to dislodge solids, but only after buildup became rather significant and when they were dislodged, the resulting upset from the solid CO_2 traveling through the pumps and elsewhere in the process impeded continuous operation.

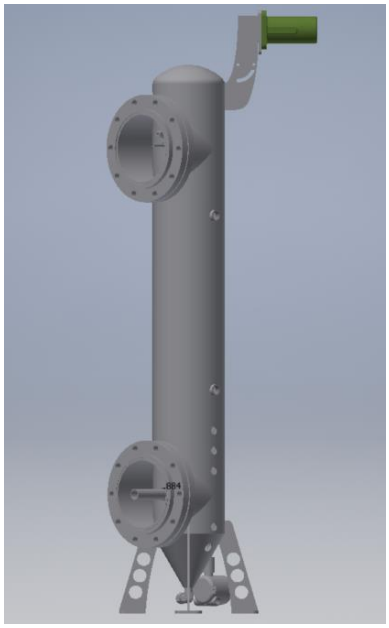

Figure 56. View of complete hybrid spray tower with a single impact air knocker installed at the top (green). The air knocker extends above the insulation surrounding the heat exchanger.

The efforts undertaken during this project to eliminate solid CO_2 build up inside the spray tower were very successful. Moving forward, any desublimating spray tower will be designed with cleaning nozzles and optional polished surfaces.

Pump Modifications

Significant testing and development were done on the process pumps during this project. Two of the process pumps handle low-temperature CO_2 slurry and both pumps are critical to normal operation of the process. The goal in testing these pumps was not only to have sustained operation of the skid but to also find a scalable solution for future operation at pilot and full scales. At the start of the project, we used two magnetically coupled external-gear pumps (Figure 57).

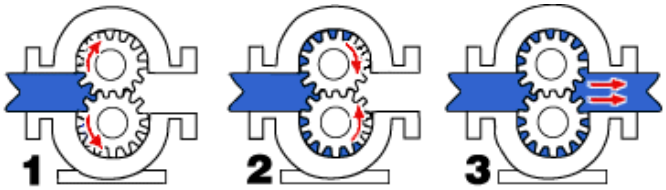

Figure 57. Operating mechanism for the external-gear pumps originally installed on the CCC ECL™ skid.

These pumps are critical to the process; when the contact liquid cooling-loop pump fails, liquid in the contact liquid cooling heat exchanger freezes, causing unwanted pressure drop through the heat exchanger and potentially stopping flow altogether through the heat exchanger. When the separation-loop pump fails, the separation loop loses pressure and the liquid CO_2 in the system flashes and pushes liquid backwards towards the spray tower. Initial testing revealed these failure modes and various mitigation steps resolved them. The PLC safety program was updated to alert the operator and implement safety measures when a pump stopped. The gear pump was replaced with a centrifugal pump that was designed to handle low-temperature slurries.

The centrifugal pump was expected to perform better with the slurry than the external gear pump, but no significant benefit was observed during testing. The centrifugal pump performed as well or better than the

gear pump in some cases; however, it performed very poorly when the slurry CO_2 concentrations were high. It would also periodically lose its prime and would stop. Because of these occasional reliability issues, it was replaced with a gear pump.

The external gear pumps we used experienced accelerated bearing wear during the testing. The discharge pressure of the pump would push the shaft into the bearings with enough force to wear the bearing unevenly (Figure 58). When the bearing and shaft wear too much, the gear-housing clearances become interferences and the pump gear and housing wear excessively.

Figure 58. External gear pump bearing showing uneven wear, as evidenced by the thinner wall towards the upper right.

We investigated needle roller bearings, brass and bronze bearings, and ceramic bearings and discussed the problem with the manufacturer. We decided to test another model of the external gear pump with a different aspect ratio. This pump ran slower and had a larger shaft and larger bearings. However, additional changes were required, including changing the motor and the variable frequency drive (VFD). The original VFD was a sensorless vector VFD that would shut down the motor if the current rose too high during operation. We replaced it with a vector flux VFD, which can maintain torque at maximum motor slip (breakdown torque), thus maintaining power through electrical current spikes during transitional loading from solid CO_2 going through the pump.

P-902 was also modified various times over the course of the project. The size was increased to allow it to pressurize the spray cleaning nozzle in the spray tower. Later the spray cleaning nozzle stream was sourced from another portion of the process and the pump size was decreased again. During regular maintenance and inspection, other small modifications were made to improve the reliability and to better understand the pump.

Development of the process pumps required much more time than expected, but this has provided invaluable insight for the pilot- and full-scale CCC systems. We now have a scalable control scheme and geometry for skid- and pilot-scale pumping.

Contact Liquid Cooling Heat Exchanger

Brazed Plate Heat Exchanger

Relatively extensive tests were completed using standard brazed plate heat exchangers. One advantage of these heat exchangers is that they can transfer a lot of heat with a small profile. This is accomplished by providing a tortuous and turbulence-inducing path. Unfortunately, that path also has the effect of providing a lot of places for solid CO_2 to collect. Further, the temperature change in the contact liquid itself causes a change in the solubility of CO_2 and solids foul the heat exchange surfaces. It would be ideal to have a heat exchanger that could be used continuously or for long periods of time before needing to take the heat exchanger offline to be cleaned.

We experimented with several brazed plate heat exchangers trying to identify one that would provide adequate cooling while resisting fouling to replace the initial setup of two heat exchangers in parallel that we alternated between to cool the contact liquid while the other was defrosted. To accomplish this, we

attempted to find heat exchangers with a low Θ associated with a smoother flow path, as described in Budget Period 1.

One primary brazed plate heat exchanger tested was a low theta cross current heat exchanger from SWEP. Testing at SES revealed that we were able to mitigate fouling by warming or blowing nitrogen through the heat exchanger. However, these techniques became less effective over time and fouling would eventually end testing. In addition to the increased fouling, it was determined that this specific heat exchanger did not have enough cooling capacity to capture one tonne of CO_2 per day.

Currently there is a SWEP brazed plate heat exchanger installed in parallel with the shell and tube heat exchanger. The shell and tube heat exchanger resists fouling more than any of the brazed plate heat exchangers. Therefore, the SWEP heat exchanger is used only when the shell and tube heat exchanger fouls.

Shell and Tube Heat Exchanger

The following discussion describes experiments to determine if a shell and tube heat exchanger better mitigates fouling by solid CO_2. Shell and tube heat exchangers are among the most basic types of heat exchangers. The geometry is simple, and they are commonly used in industry because they are easy to maintain. Initially, it was hoped that the simple geometry would result in significantly reduced fouling and solids buildup. An off-the-shelf shell and tube heat exchanger was tested to see if the heat exchanger would be self-cleaning via the liquid flow in the tubes. This did not prove to be the case. WSA engineered systems, an expert in the field, was consulted and a few guiding principles were communicated. First, the higher the velocity, the higher the shear forces within the heat exchanger and thus the higher the forces exerted on solids building up on the heat exchange surfaces. These higher forces could result in the breakup of solids on the heat exchange surfaces, which would keep the heat exchanger cleaner. WSA also suggested that, if the higher velocity did not result in a self-cleaning heat exchanger, brushes or scrapers could be employed to clean the heat exchange surfaces. This is done by allowing the scrapers or brushes to be driven by the flow from one end of the tube to the other. At the end of the tube, the scraper (or brush) would be stopped in a catch basket specially designed to hold the scraper, but also allow the flow to continue. The flow direction could then be reversed to allow the scraper or brush to traverse the tube in the other direction thereby ending up in a catch basket at the other end of the heat exchange tube. We decided to test a high-velocity heat exchanger that could also accommodate the potential use of scrapers or brushes.

Unfortunately, no off-the-shelf shell and tube heat exchanger was available that could exchange the required heat, maintain the required velocity, and be large enough to allow for the use of scrapers and brushes. Thus, we designed and manufactured a custom shell and tube heat exchanger for the CCC ECL™ skid. Initially the heat exchanger was built with the expectation that we may not need scrapers or brushes. The CAD design and the actual heat exchanger are shown in Figure 59.

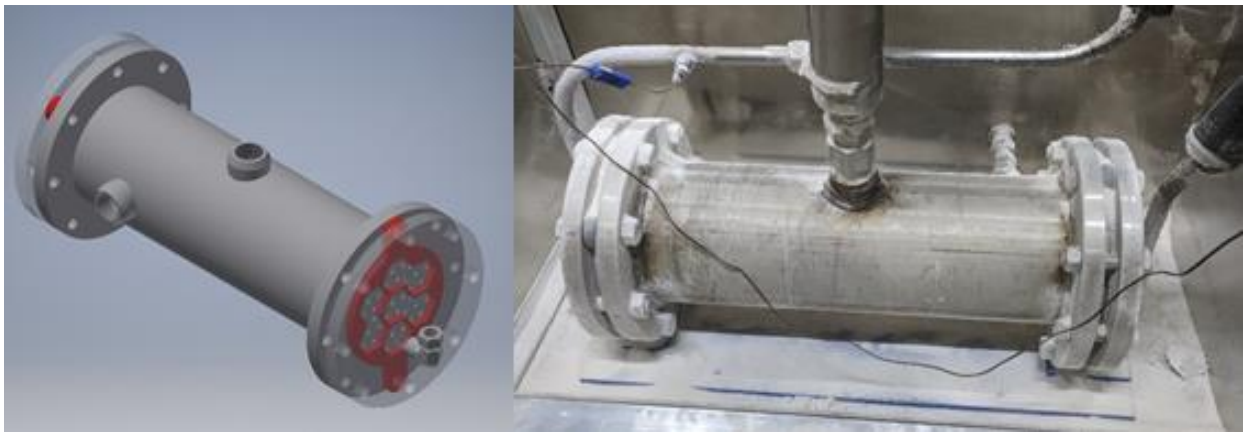

Figure 59. Heat exchanger designed and constructed at SES.

The heat exchanger without scrapers or brushes but with a high velocity within the tubes performed far better than the off-the-shelf heat exchanger. The deterioration of performance was significantly reduced, and we could run much longer, but better performance was still desired, and we decided to add brushes or scrapers. This required a design change and some additional parts. The CAD design of this modification is shown in Figure 60. The brushes were added to the shell and tube and the test did not go well. The brushes were too stiff and got stuck in the tubes. We then fabricated scrapers, which were then placed in the shell and tube assembly and tested briefly prior to taking the skids to the Hunter Power Plant. These brief tests seemed to indicate that the scrapers may not have been traversing the tubes as they should.

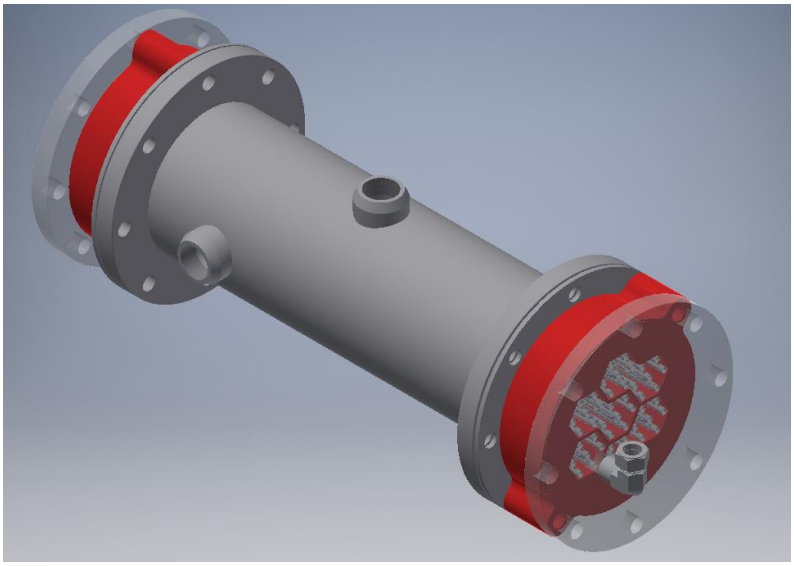

Figure 60. Shell and tube heat exchanger with extended ends for including scrapers or brushes.

Because none of the brazed plate heat exchangers tested were able to function without fouling over a period of 24 hours and because of the promising results from the shell and tube heat exchanger, we decided that we would switch back to the basic shell and tube design (without scrapers) prior to going to the plant. The shell and tube heat exchanger would be the primary contact liquid cooler.

Once the CCC ECL™ skid arrived at the Hunter Power Plant, further tests were completed where the shell and tube heat exchanger did not have scrapers or brushes installed while a plan was formulated to put the scrapers back into the shell and tube. Inserts were designed that could direct the flow in a way that would encourage the scrapers to traverse the tubes properly. The inserts in the shell and tube allowed the shell and tube to clean itself and to operate much longer.

The length of operation of the shell and tube is probably not long enough and remains to be improved. Future work to improve run time on the shell and tube includes:

1. The catch baskets at the ends of the heat exchanger were possibly too long, thus requiring inserts to direct the flow in a way that it would catch the scrapers and direct them through the tubes. If these baskets were shorter, it is likely that the inserts would not be required and would significantly reduce the cost of the heat exchanger is larger designs.
2. Testing new brushes that were ordered to fit through the tubes.
3. The presence of contaminants, which is discussed below in Task 11, within the shell and tube certainly reduced the effectiveness of the cleaning action on the tubes and may have caused the scrapers to become stuck either at the ends or within the tubes themselves.
4. If we decide that we cannot get away from contaminant buildup, a system that could clean the shell and tube in place while a parallel heat exchanger is being used could be developed. This has the benefit of continuous operation but would increase capital costs and could contaminate the contact liquid.

This project significantly advanced the development a shell and tube heat exchanger for use in the CCC ECL™ skid. The shell and tube heat exchanger will likely be used in future CCC process designs.

Screw Press (Solid–Liquid Separations)

The modifications to the solid–liquid separations system discussed below attempt to improve screw press reliability and performance and to decrease its energy consumption.

SES previously iterated on the screw press design and at the beginning of this project was operating two 4-inch presses that could reliably produce solid CO_2 streams at purities over 70% by mass. SES had also performed a series of tests running the CCC ECL™ process at a variety of conditions (e.g., gas flow rates, CO_2 content in the flue gas stream, contact liquid flow rates) to increase the outlet solids fraction exiting the screw press. SES has designed, built, and tested three versions of these screw presses, with two copies of the most reliable design (4-inch screws) currently installed in the CCC ECL™ skid. Instrumentation in these unit operations measures flow rates and conditions. This includes turbine meters, thermocouples, and pressure transducers. SES also continually improved the insulation in these units and their associated piping by immersing them under perlite in a cold box rather than wrapping the screw presses with insulation. In this configuration, the system can easily reach 70 mass% solid CO_2 from the screw press, as described above during Budget Period 1.

SES worked with Press Technology Inc. (PT&M) to design and build a larger 6-inch machine to increase the skid capacity and test new design ideas (Figure 61). PT&M manufactured a version of the screw press that could process 1 tonne/day (6-inch screw). PT&M refined the screw press design, produced detailed drawings, and manufactured the machine. SES designed a custom filter for the larger screw press and designed how the larger system will be integrated into the remaining system.

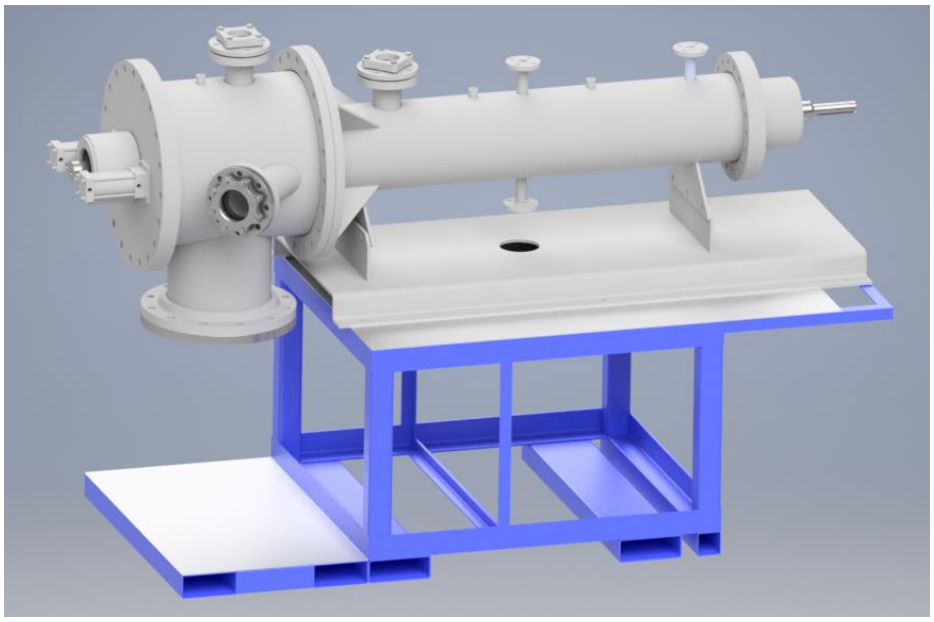

Figure 61. Rendering from PT&M of the 1 tonne/day screw press.

Of note are the following enhancements that have been made to the 1 tonne/day design:

- The solids extrusion process now has the option of using a gas headspace for separating the extremely cold solid CO_2 outlet of the screw press from the warmer melter below. This should decrease the heat load while allowing for greater controllability of the solids.
- The port to the melter port has been widened to allow for solids to freely fall without obstruction, decreasing the possibility of fouling.

- Additional instrumentation ports have been added to the design for both the main screw press section and the melter.
- SES designed and manufactured the filter directly at this scale to focus on the unique requirements that a CO_2 slurry filter must meet, which were discovered through extensive experimentation to date.
- Additional vacuum jacketed tubing has been added to the design, running into and out of the previously designed coldbox.

Filter Design

The filter is made from sintered layers of mesh supported by a filter cylinder. The finest layer of mesh provides filtration, and the filter mesh size was determined by experiments previously conducted at SES. Coarser sintered mesh layers support the fine filter layer. The mesh support cylinder was modeled in CAD and analyzed with finite element analysis (FEA) to ensure that it would support the maximum internal pressure of the filter. An image of some of the FEA results is shown below in Figure 62.

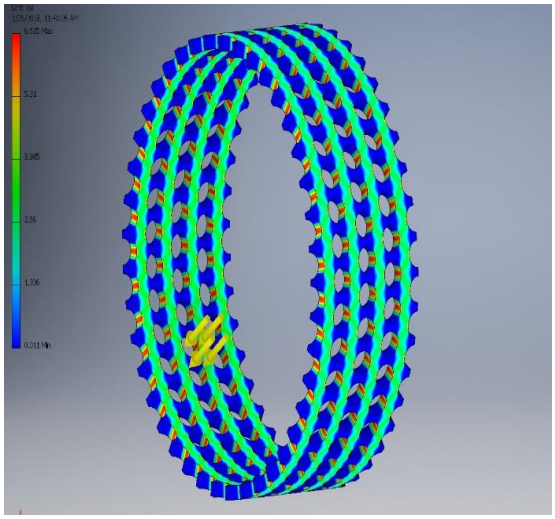

Figure 62. FEA analysis for the filter support cylinder.

SES pressure tested various sintered mesh layups and support hole size combinations. The pressure rating of the hole/mesh combinations was determined by measuring the pressure at which permanent deformation of the mesh occurred. The mesh pressure testing apparatus is shown in Figure 63. The mesh was spot welded to a metal support plate, a thin film of PTFE was placed over the mesh, and the plate was sandwiched between two pipe flanges. A hydrostatic pressure tester was used to apply pressure to the mesh.

Figure 63. (left, center) Mesh pressure testing apparatus. (right) Example of pressure-tested mesh showing permanent deformation.

The results of the FEA analysis and mesh pressure tests were used to produce the final filter support tube design. The final filter assembly halves are shown in Figure 64. The filter support was machined by a local shop in Utah, and the mesh/support assembly was completed at SES.

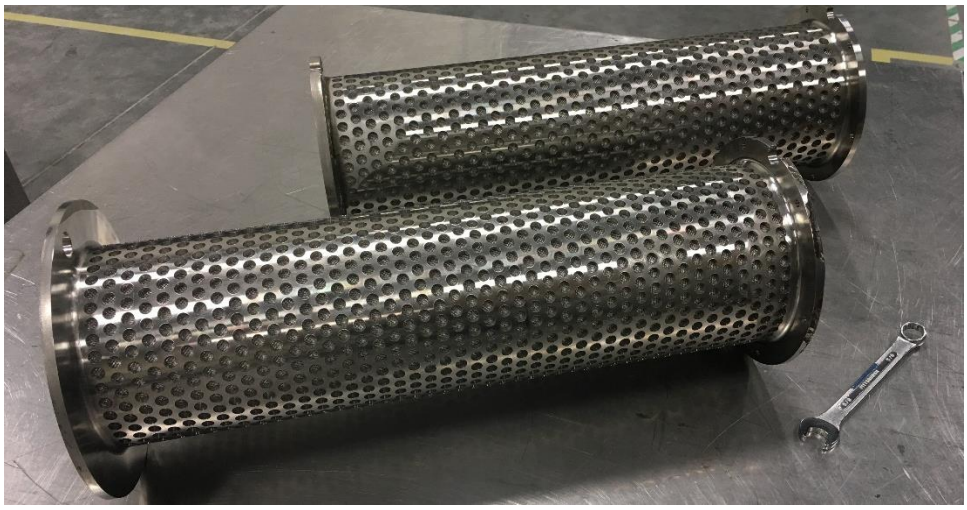

Figure 64. Completed filters for new screw press.

6-inch Screw Press Installation and Modifications

The new screw press required some additional modifications after delivery from PT&M to fix some manufacturing defects including machining new screw bearing supports, replacing the bearings with bearings packed with low-temperature grease, welding caps on holes between the melter and the screw press filter housing, and adding PTFE shaft bushings to support the screw during assembly. We also added expanded PTFE gaskets to fill voids between the filter and the filter housing caused by poor machining tolerances.

More sight glasses and instrumentation ports were added to the melter at SES to provide more information about the melter level and gas space. Cameras and lights were also installed to allow us to visually monitor the screw press filter, the extruding CO_2, and the melter. The screw press was installed on a support frame and in a cold box filled with perlite insulation. A photo of the screw press installed in the cold box with some walls removed is shown below in Figure 65. The cameras and instrumentation installed on the melter is shown in Figure 66.

Figure 65. 6-inch screw press installed on its mount before insulation was applied.

Figure 66. Melter section with cameras and instrumentation attached.

The interface between the filter section and the melter is one of the most novel aspects of this screw press. There are no other known screw presses that melt the solids produced from extrusion on the back end of the screw press in this manner. Figure 67 shows a view from the mounted camera of this interface and the front portion of the plunger.

Figure 67. Internal view of the melter plunger.

6-inch Screw Press Filter Modification

During testing, solid CO_2 leaking past the screw press filter eventually caused plugging downstream. Multiple locations could cause these leaks, including leakage through the mesh itself due to mesh damage, leakage through the seams of the mesh on the filter, leakage around the screw press inlet housing, and leakage around the filter/screw press housing joints. Tasks were completed to address each possible leakage location:

- *Leakage through the mesh.* The mesh we are currently using is composed of four sintered layers of wire mesh. The first layer is the filter layer. The rest of the layers are used to support the filter layer under pressure. After assembling, running, and disassembling the screw press, we noticed more glossy areas of the mesh where the screw likely rubbed on the filter during screw press assembly

and disassembly. There was a concern that the fine mesh was damaged, opening larger holes and causing the filter to leak solid CO_2. The mesh was examined under a microscope, and images typical of the glossy areas are shown in Figure 68. Multiple images of the same location with the focus of the microscope adjusted are shown to resolve all parts of the mesh. At the high points, we see that the mesh was damaged and smeared together, but it does not look like larger openings were created in the mesh. We ordered new sintered mesh material that has a tighter, more durable filter layer. We have both 10- and 26-micron filters that we can test to make sure that the mesh is not the problem.

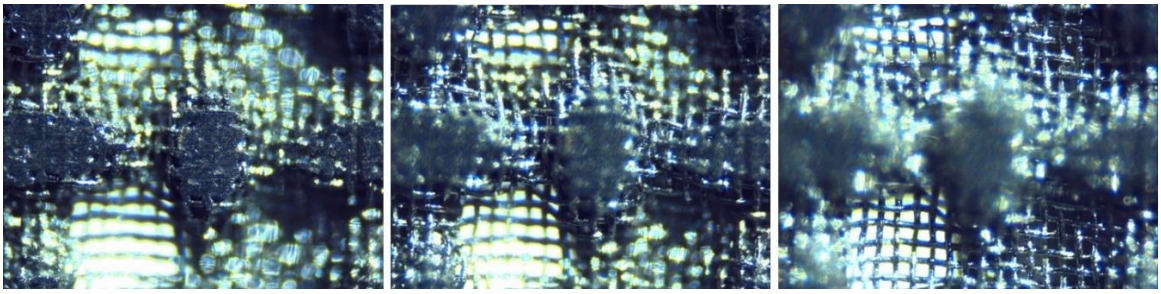

Figure 68. Microscope images of a shiny portion of the mesh with the microscope focus moving down (L to R) through the layers of the mesh.

- *Leakage around the screw press inlet housing.* The inlet housing is a stainless box attached to the inside of the screw press pressure vessel where the slurry enters the machine. The slurry inlet connects via pipe threads to the inlet housing and is then welded to the screw press pressure vessel. The screw passes through the inlet housing, and the inlet housing interfaces with a pressure vessel flange and the filter. Upon close inspection, we found that the inlet housing was not installed straight at PT&M, and it looked like the pipe threads were leaking. The seal between the inlet housing, flange, and filter could also be leaking due to the misalignment. We removed the inlet housing by cutting away the welded inlet pipe. We then welded a new inlet pipe directly to the inlet housing to prevent possible leakage around the pipe threads. The inlet housing/inlet pipe assembly was then welded into the screw press pressure vessel, and much better alignment was attained.
- *Leakage around the filter/screw press pressure vessel joints.* Due to poor tolerances of the screw press parts, the face seals between the filter, the pressure vessel, and inlet housing did not fit well enough to make a seal. Gaps remained when the machine was assembled, and these gaps allowed slurry to bypass the filter. To solve this problem, gaskets were made from compressible PTFE material to fill the gaps in the face seals.

After making these changes, we still had problems with the filter leaking in the 6-inch screw press. While waiting for the new 10- and 26-micron mesh mentioned above, we rebuilt the dual 4-inch screw presses that we used in the past and installed them in the skid. We ran the skid with the 4-inch machines for the last two months of testing and they worked well with a reasonable capacity.

Future work includes:

- Changing the filter material for the 6-inch screw press and reinstalling the machine into the CCC ECL™ skid for testing.
- Modification of the screw press designs to prevent the filter sealing problems encountered on the 6-inch PT&M machine.

Distillation Column

SES upgraded its final vapor/liquid separation unit to a distillation column (Figure 69). The reasons for this were four-fold:

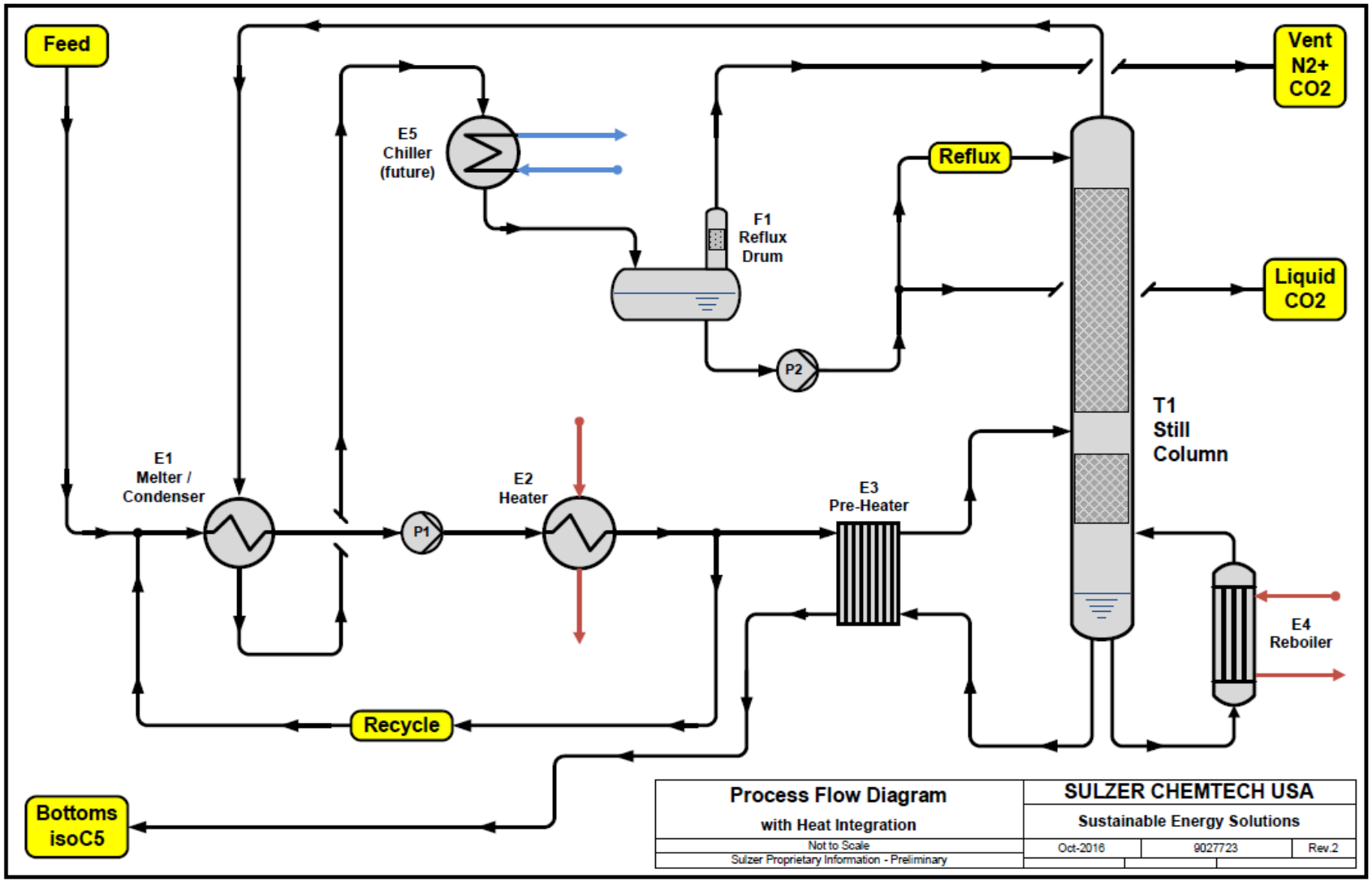

Figure 69. High-level Process Flow Diagram of the Distillation Column and Surrounding Systems

1) Achieve a higher CO_2 product purity
2) Limit the amount of isopentane lost with the CO_2 product
3) Reduce the chance of fouling the isopentane return stream
4) Replicate the process conditions that will be used on pilot- and full-scale implementations.

This last reason is perhaps the most important, as it helps to de-risk the scale up of the skid-scale process. Sulzer Chemtech USA assisted with the design of the column. The column includes heat integration with the screw press, which improved the energy efficiency.

The distillation column is the final stage in the CO_2 separation system. The melted CO_2 that was separated in the solid/liquid separator (screw press) is fed to the column. Any remaining isopentane is stripped out, resulting in a 99.99% pure CO_2 product. The bottom isopentane product is 99% pure and is recycled back into the process. The product purities were chosen based on the anticipated requirements of the pilot- and full-scale CCC processes, which are: 1) the loss of isopentane with the pure CO_2 product should be minimized, and 2) the concentration of CO_2 dissolved in the isopentane returning in the bottoms stream should be low enough to prevent it from freezing when it passes back through the column preheater.

The column contains a partial condenser, whose cooling duty is obtained entirely from the heat of melting of CO_2 in the screw press. Since the relative volatilities of CO_2 and isopentane are so high, only a small reflux ratio (less than 0.4) is required. The reboiler duty is from an electric immersion heater.

The feed to the column is approximately one third of the column height from the bottom of the column. The feed is preheated against the returning bottoms stream to reduce both the amount of required reboiler duty, and to help cool the isopentane returning from the bottoms.

The column is a packed bed three inches in diameter and 18 feet tall, containing seven theoretical stages (Figure 70). The column is supported within a super structure, which forms an enclosure that holds loose perlite insulation. The entire structure can be lowered hydraulically for maintenance and transport.

Figure 70. Fully assembled distillation column before adding side panels and loose perlite insulation.

The distillation column was utilized while testing the CCC ECL™ skid at the Hunter Power Plant (Figure 71). During operation, the CO_2 product was vented back to the stack as an ambient-temperature, ambient-pressure gas. During initial shakedown at the plant, the column operated nominally. However, after several months of testing, minor anomalies began to occur with the reboiler level switches, reflux level float transmitter, and reflux pump. These instruments each contain moving parts which would appear to get "stuck" during startup. This most often occurred after extended periods of shutdown and/or purging, after the system had been emptied of isopentane. We hypothesized that some contaminant had remained behind after purging and caused the mechanical parts to stick together. The possible sources of this contaminant and how it could be mitigated in the future are discussed below in Milestone 11.3.

Figure 71. Distillation column (foreground) installed at the Hunter Power Plant

Several modifications to the distillation column control were implemented during testing at the Hunter Power Plant. Prior to these modifications, the reboiler sump level could only be controlled by opening and closing a proportional drain valve. However, operators discovered an alternate method of controlling the level by increasing or decreasing the column pressure. Lower pressures draw more liquid into the reboiler and vice versa. This method was automated and became the standard operating procedure during the startup phase when the feed CO_2 concentration to the column was low.

Operators also realized that the reboiler temperature must be ramped up more slowly during startup. It normally takes several hours for the CO_2 concentration in the melter to increase to a point where reflux begins. Before that time, if the reboiler is already at its normal setpoint temperature of 100 to 110 °C, the isopentane will boil and condense into the reflux drum, contaminating the product. An additional safety control was placed on the reboiler temperature controller to prevent this from happening.

At the time the column was designed, the fate of pollutants such as SO_2 was not fully considered. After reviewing the models, we discovered that SO_2 may either escape with the CO_2 product, or it may accumulate in the reboiler, depending on the operating conditions. To prevent the possibility of SO_2 accumulation, a task to open the pollutant traps was added to a periodic maintenance schedule.

These operational modifications, as well as other lessons learned from operating the distillation column, have resulted in the revised startup procedure in Table 15 (compare with the original procedure listed in the 2018 Q1 report):

Table 15. Revised stages for distillation startup procedure.

	Action	Milestone
Phase 1	Fill reboiler with liquid	Level is indicated and is controllable
Phase 2	Alternate level control method	Stable reboiler level controlled by adjusting column pressure
Phase 3	Start reboiler heater at low temperature	Reboiler temperature high enough to vaporize some CO_2
Phase 4	Start CO_2 injection	CO_2 is being vaporized in the reboiler and vented to control column pressure
Phase 5	Standard level control method	Stable reboiler level controlled by opening/closing drain valve
Phase 6	Fine tune column pressure	Column pressure is tuned to increase/decrease flow of isopentane through screw press to achieve correct melter CO_2 concentration
Phase 7	Begin reflux	CO_2 is being liquefied in the condenser, is filling the reflux drum, and is being refluxed to the top of the column
Phase 8	Increase reboiler temperature	Reboiler reaches target temperature of 100 to 110 °C
Phase 9	Reach target temperature profile	Top and bottom product purities are within specifications

Pollutant Removal

To remove SO_2, NO_x, and solid particulate matter (pollutants) from the process stream, two settling tanks were designed and implemented in line with the process stream as shown in Figure 72. The pollutant molecules and particles from flue gas processing that end up in the isopentane stream are denser than the isopentane and, given an appropriate location and flow profile, settled out into a tank that was regularly drained. The settling velocity was calculated for these particles and the tanks were designed to remove all the pollutant molecules in the stream.

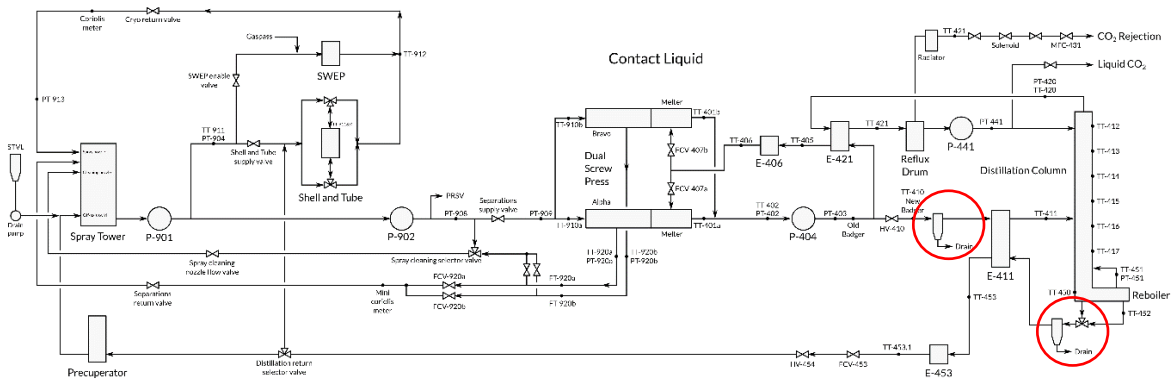

Figure 72. Contact liquid P&ID showing the location of the two pollutant removal and sampling units installed inside the distillation column cold box.

The settling tanks are essentially horizontal tanks that are long enough for pollutants to settle out but not so long as to add excessive pressure drop to the system with a drain at the bottom (Figure 73). The two tanks were placed in two low spots in the process to maximize effectiveness.

After processing flue gas for approximately 24 hours, it was visually confirmed that significant amounts of both water and solid particles had been caught in the drum, as well as evidence of SO_2. Control system reminders were used to drain the pollutant settling tanks every 24 hours. SES originally intended to use FTIR analysis to verify the content of the pollutant settling tanks, but due to unavailability of the FTIR equipment at the Hunter Power Plant, we were unable to test our samples. SES has no reason to suspect

that the pollutant settling tanks were not performing adequately to remove SO_2, NO_x, and solid particulate matter from the process.

Figure 73. One of the pollutant settling tanks with a vapor–liquid separation drain and filter on the bottom.

Supervisory Control and Data Acquisition System

For many years, SES has been developing a novel supervisory control and data acquisition (SCADA) system. This system reached a mature level of development in the second quarter of 2018. Although commercial solutions exist, none contain all the features we thought were necessary. The motivation behind the development of a custom SCADA system has been primarily to give operators better control over the CCC ECL™ skid, allow quicker recognition of problems that emerge during a run, and enable a greater capability to learn from mistakes. An integral part of our SCADA system is a historical data retrieval system, or historian (Figure 74). This displays process variables graphically in real time, or in the past. The historian has proven vital in analyzing runs, troubleshooting issues, and improving the operation of the CCC process.

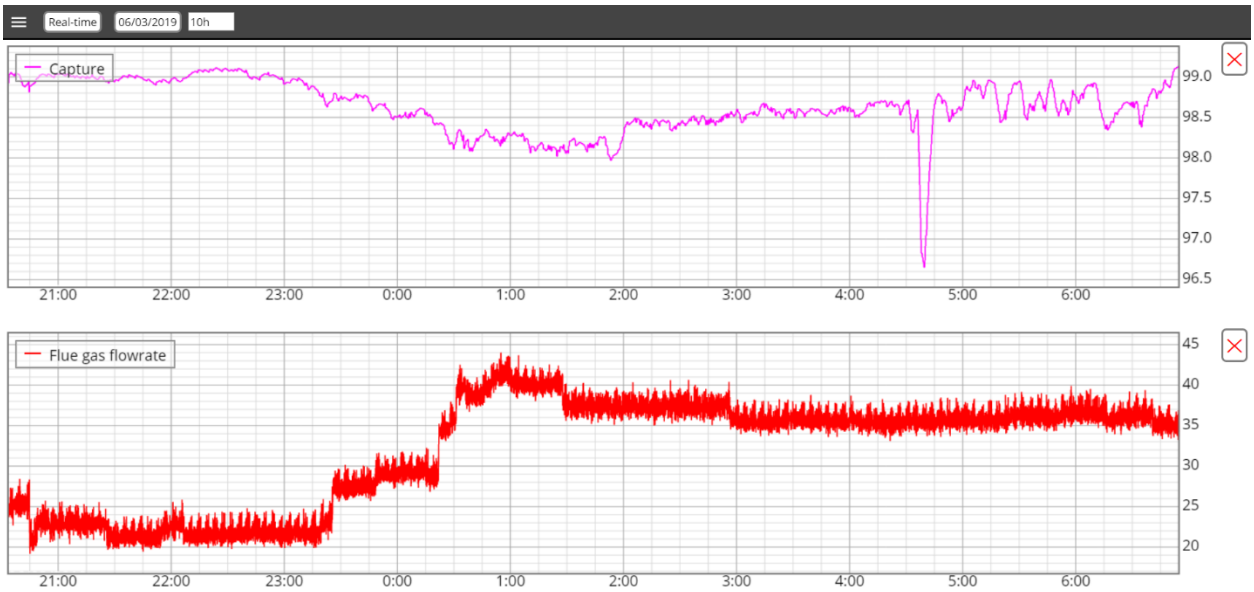

Figure 74. Data output from the SES historian showing data during the test on June 3–4, 2019. Both plots have units of hours and minutes for the x axis. The y axis of the top plot is CO_2 capture (%). The y axis of the bottom plot is flue gas flow rate (kg/hr).

The main portion of the SCADA system contains a flow diagram of the CCC ECL™ skid process with temperatures, pressures, and other process data that are plotted in real-time (Figure 75). Operators can enter values into input fields to change set points, etc. Below this is an area for operator notes and logs. Every action the operator takes is logged, which can help during investigations after unexpected shutdowns. On the right are three additional areas. The first of these are the *Issues*, which lists problems operators have discovered, and communicates important information to the next shift. Below this are the *Watches*, which gives operators a quick view of essential variables. At the bottom are the *Alarms*. These are configurable and can alert operators instantly in the event of a problem.

The complete control system comprises a Siemens PLC, several remote I/O racks, the SCADA system as described above, and a handful of independent ethernet-connected devices, such as Coriolis meters and power meters. The SCADA system gathers all this data and saves it in both local and remote databases for backup redundancy. Complete specifications are given in Table 16.

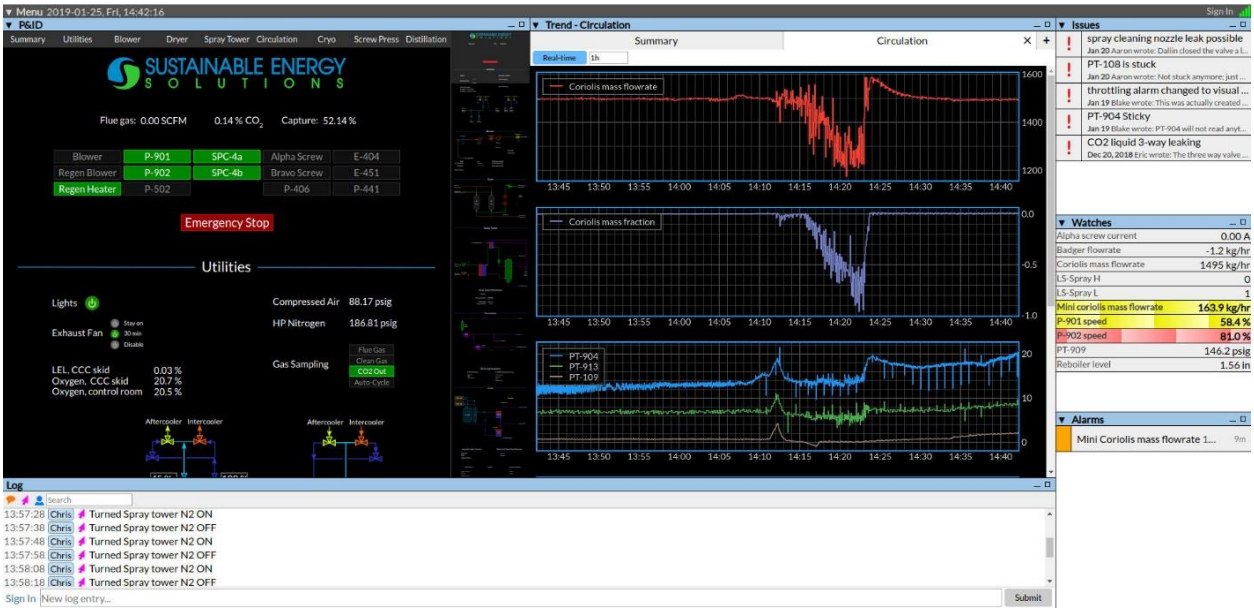

Figure 75. Screenshot of the SCADA software developed by SES. Clockwise from upper-left: process flow diagram, historical trends, issues, watch window, alarm window, log window.

Table 16. Control system specifications

CPU	Siemens S7-300 series programmable logic controller
SCADA	Custom, in-house designed web-based application (Node.js and React)
Historian data storage backend	MySQL
Number of report I/O racks	4
Number of inputs/outputs	150/50
Total number of recorded variables	450
Control system cycle speed	10 Hz
Number of PID controllers	20

Complete Skid Shakedown Testing

Overview

Shakedown tests were conducted until the complete system operated as intended at the beginning of June 2019. During these shakedown tests, SES identified which unit ops needed to be modified to achieve more continuous runs while processing actual flue gas at the Hunter Power Plant. Dealing with manufacturing

delays for the single screw press, overcoming fouling in the contact liquid cooling loop, and addressing CO_2 buildup in the spray tower were all issues that were identified, tested, and successfully resolved during shakedown testing at SES. CCC ECL™ skid testing at the Hunter Power Plant revealed additional issues that we addressed: water accumulation in the system, recuperator fouling, and fouling in the contact liquid heat exchanger.

Figure 76 shows how test length increased after resolving the shakedown issues previously mentioned. Longer and more consistent runs occurred during the last three months of testing. Gaps between the test runs shown in Figure 76 reflect more-significant modifications that were necessary to address issues, such as fouling in the contact liquid heat exchanger and accumulation of water in the system.

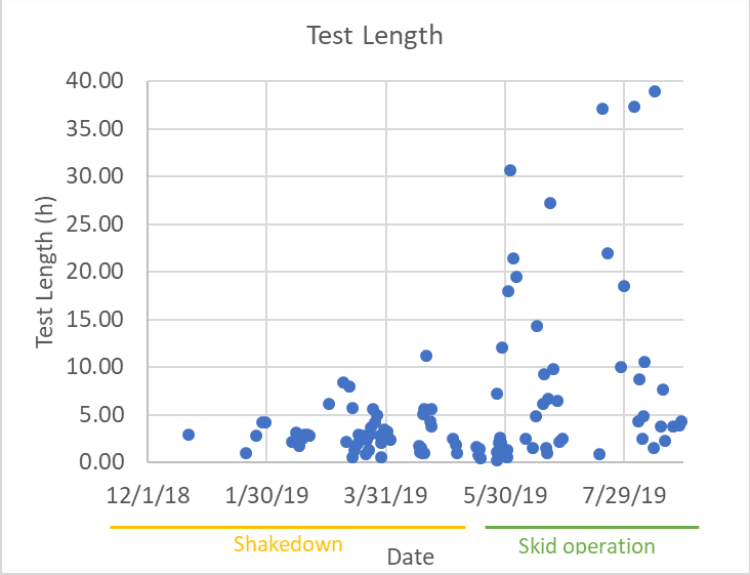

Figure 76. Test duration comparison while conducting shakedown and skid operation testing on site at the Hunter Power Plant

The first significant issue that was apparent from shakedown tests was the need for a robust heat exchanger for cooling the contact liquid. While waiting for the single screw press to be manufactured, SES tested several non-fouling heat exchangers, including a low Θ, cross-current, brazed plate heat exchanger, as well as a custom shell and tube heat exchanger. The shell and tube heat exchanger proved to supply enough cooling for extended test runs when periodically reversing the flow direction through the heat exchanger. Scrapers and brushes were also implemented to clear CO_2 buildup in the heat exchanger as the flow direction reversed. These improvements dramatically improved cooling performance and the longevity of the tests during shakedown.

Another issue identified during shakedown testing was the need to control CO_2 accumulation along the walls of the spray tower. This CO_2 accumulation ultimately and regularly ended test runs as the slurry CO_2 concentration would spike when solid CO_2 broke off the walls into the slurry. This trend is shown in Figure 77. With higher slurry CO_2 concentrations being pumped through the contact liquid cooling loop, the heat exchanger would typically foul despite the improvements that were made. To address this issue, an impulse vibrator was mounted to the top of the spray tower that intermittently knocked off accumulations of CO_2. As shown in Figure 77, this solution occasionally removed certain amounts of CO_2 from the walls of the spray tower, but larger accumulations still caused the slurry concentration to dramatically increase. After testing the intensity and timing of the impulse vibrator, it became obvious that a more robust method of removing CO_2 accumulations was necessary. A spray cleaning nozzle was installed near the top of the spray tower that continuously sprayed clean contact liquid onto the walls of the spray tower. Using the

permanently mounted camera inside the spray tower, we verified that CO_2 was no longer accumulating. A polished stainless-steel sheet was also installed as a lining along the inside wall of the spray tower to keep CO_2 from sticking to the rougher tank walls. The issue of CO_2 accumulation in the spray tower was entirely resolved by these modifications during shakedown testing.

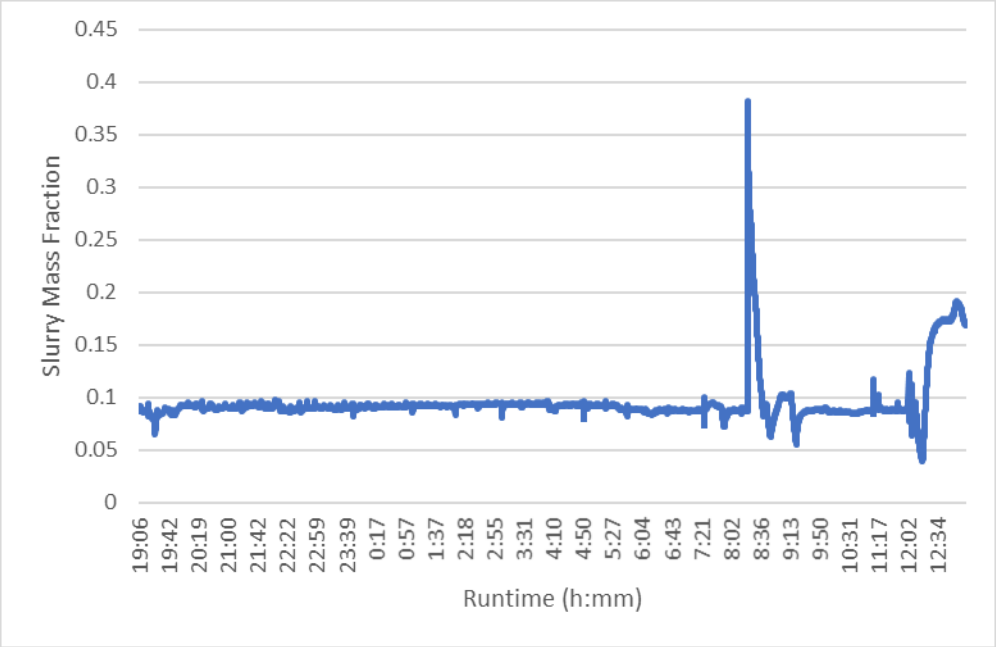

Figure 77. Mass fraction of the slurry over a 24-hour period while the impulse vibrater on the spray tower operates every 10 minutes.

Upon shipping the skid to Hunter Power Plant, we determined that the initial water handling equipment design was insufficient for removing water from the flue gas. An additional cyclonic separator reduced the dewpoint to an acceptable level before the blowers and a water knockout at negative pressure removed the condensing water. The dewpoint and dryer tank status were carefully monitored through the remainder of the on-site testing and a new calculation tool that monitored possible accumulation amounts throughout long-term tests was added to the operating system. After making these changes to the front end of the skid, water accumulation ceased to be an issue that affected our tests.

Fouling in the recuperator was also an issue discovered while testing on site. Injecting flue gas while the recuperator was warm caused problems with cooling capacity and ultimately resulted in rapid fouling in the heat exchangers. A closed nitrogen recycle loop resolved this issue by establishing an appropriate temperature in the recuperator during startup, after which CO_2 could be injected without causing the contact liquid to warm drastically. This more closely resembles the successful startup procedure used while testing in closed-loop mode at SES.

The final issue we encountered while testing on site before longer test runs were possible was that the contact liquid heat exchanger was fouling unpredictably while processing flue gas. SES installed a SWEP brazed plate heat exchanger in parallel with the shell and tube heat exchanger and activated the former if the latter fouls. After testing possible switching methods involving precooling, specific switching timing, and slurry concentrations while switching, it became obvious that this procedure wasn't robust enough to be used in a long test run. In some cases, we were not able to thaw the heat exchanger that wasn't being used, but then we weren't able to maintain the contact liquid at a cold enough temperature while waiting for the other heat exchanger to completely thaw. Ultimately, we implemented new inserts designed to fill the cavities on the ends of the shell and tube heat exchanger. Together with scrapers, the shell and tube heat

exchanger delivered adequate cooling for the long-term tests with drastically less fouling under our test conditions.

SES conducted additional shakedown testing of the non-fouling heat exchanger system. Fouling and subsequent increased pressure drop across the cooling heat exchanger represent key stability and reliability concerns. One mitigation involves temporarily and rapidly increasing the temperature to allow accumulated solids to slough off followed by a return to normal operating conditions. Figure 78 shows results from this process that successfully maintain a low average temperature but with a slowly increasing pressure drop with time. This would eventually result in a pressure drop exceeding the capacity of the pump.

More-recent modifications appear to achieve both a low average temperature and limited or no increase in pressure drop in preliminary results. The modifications involve changes to the timing of the self-cleaning methods and mitigations. Future work includes continued testing of these altered methods, including an alternative mitigation plan that involves using a backup heat exchanger for cooling while a more thorough solids removal of the primary heat exchanger occurs. Preliminary results indicate that this backup solution should be very robust but may slightly decrease the efficiency of the cooling system.

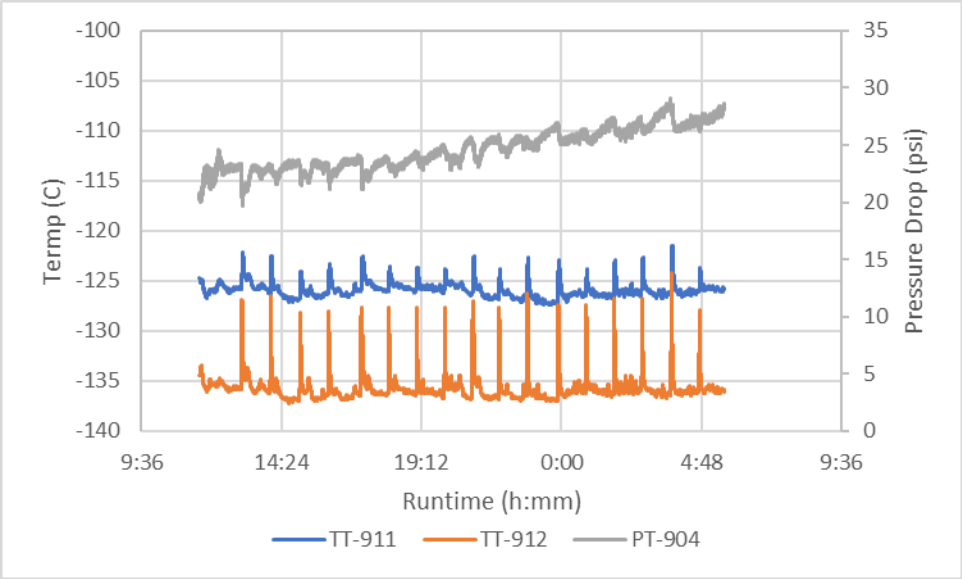

Figure 78. Temperatures into and out of the cooling heat exchanger over time compared with the increase in pressure drop across the heat exchanger.

Task 11. Skid Operation

Specific Objectives: The objective of this task is to test the improved skid in house and in the field, with at least one test consisting of a minimum of 500 continuous hours.

Test Plan

Planned Approach: The Recipient will develop and submit a test plan for the operation of the improved skid.

To successfully execute the field test at the Hunter Power Plant, SES developed a comprehensive test plan that outlined both the requirements of the test site and the key parameters to be tested.

The plan outlined the following items, which are necessary for conducting an effective demonstration:

- Safety requirements from the plant
- Necessary considerations for plant integration

- Field test timeline including:
  - Shakedown
  - Process optimization
  - Long-term testing
- Inlet flue gas conditions from the plant
- Key fixed process parameters to be monitored
- Variable process conditions that would be monitored and controlled
- Measurement methods of process variables
- Management of on-site personnel
- Plans for setup and takedown of the skid units

Following the plant integration plans, in late December 2018, the skids were placed in an area at the base of the stack for Unit 3 that had ready access to utilities and flue gas (Figure 79).

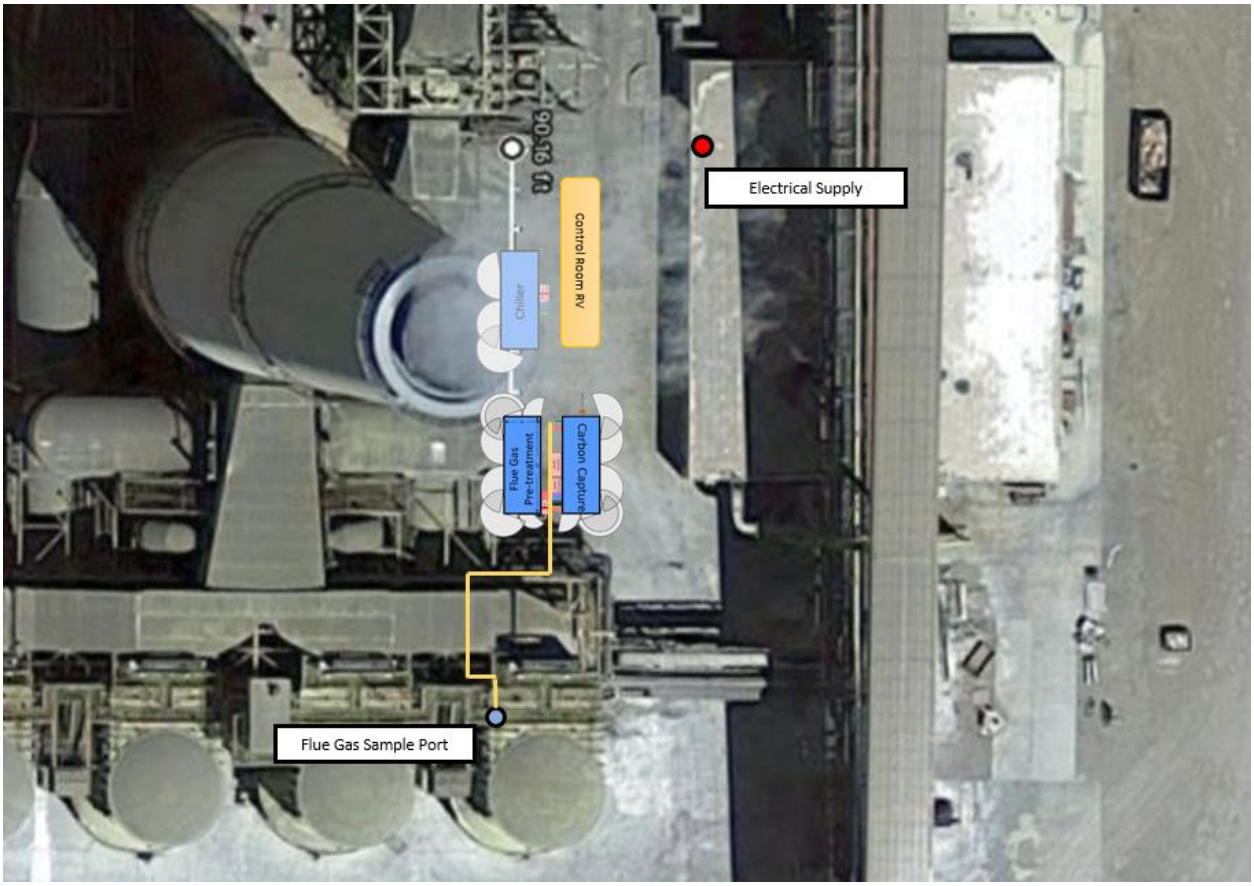

Figure 79. Aerial photograph of Unit 3 at the Hunter Power Station with scale blocks representing the skids.

This test plan was used to structure the on-site testing as well as provide a framework for experimentation with the CCC ECL™ skid (Figure 80). While the plan originally had an end date of March 2019, an extension of the project was proposed and approved to allow for additional testing through the end of June 2019.

The field test was divided into three general periods (Figure 80). Objectives for these periods include:

- On-site shakedown

  - On-site quality check to evaluate leaks, structural issues, equipment alignment, or other problems that occurred during transport and setup.
  - Integration and acceptance testing of power plant flue gas stream, process water, and electrical systems and connections.
  - Process test runs to make sure all safety and controls systems are operational.
  - Thorough testing and setup of pre-treatment systems that could not be tested in a laboratory setting.
- Process optimization
  - Test runs will use lessons from experiments done using the integrated system in the lab and will include longer test runs to ensure that the full system is operating as expected.
  - The method for operating the system may change during this time to adapt to power plant conditions, including temperature and pressure of the flue gas stream and the total available cooling that we are able to achieve.
- Long-term testing
  - This period of testing will be focused on achieving long-term runs and gathering data, including at least one 500-hour test run at nominal 1 tonne CO_2/day at above 90% capture.

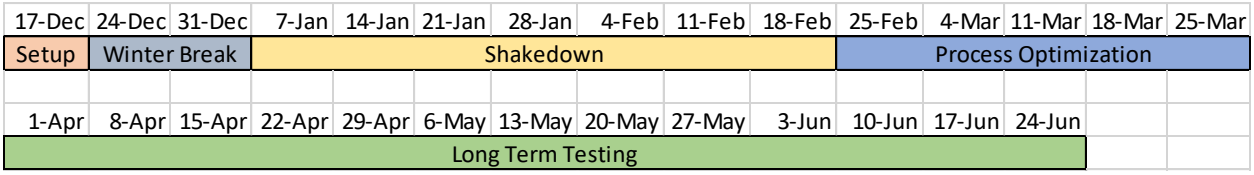

Figure 80. Timeline of the on-site testing.

Part of the intent of the test plan was to allow for flexibility in meeting the objectives of the project. This meant that we would focus on meeting the objectives of each period before the next begins, allowing for shifts in the overall timeline as we progressed. For example, due to delays and difficulties described in other sections, shakedown portions of the testing continued longer than we expected, with some unit operations still being in the shakedown portions into May 2019.

An additional important aspect of the test plan was to ensure that the proper parameters were being measured and that correct instrumentation was in place to measure these parameters. Table 17 lists these key parameters, their purpose, and location, while Figure 81 shows the referenced locations.

Table 17. Key measured parameters and their locations in the ECL skids.

Parameter	Instrument	Purpose	Location
Inlet Flue Gas Composition	Fourier transform infrared spectroscopy (FTIR), Nondispersive infrared (NDIR)	Primarily for CO_2 and other pollutant measurement	(2)
Inlet Flue Gas Temperature	Thermocouples	Comparison to recuperator temperatures for examining effectiveness of recuperative heat exchanger	(1)(2)
Cooling Rate	TC's, Turbine flowmeter	Measure the cooling we get from the Stirling Coolers	LN2 Tank, CL Cooler
Clean Gas Composition	FTIR, NDIR	Determine capture rate in wt% CO_2	(6)
Slurry Composition	Coriolis Meter	Monitor thickness of slurry	(4)
Line Pressure Before and After the Cooling Heat Exchanger	Pressure Transducers	Measuring the pressure drop across the heat exchanger to determine fouling rate	CL Cooler

Parameter	Instrument	Purpose	Location
Melter Liquid Composition	Coriolis Meter	Monitor efficiency of screw press system	(5)
Spray Tower Recirculation Rate	Coriolis Meter, Turbine Meter	Monitor flow into spray tower	(3)
Liquid CO_2 Composition	FTIR	Monitor liquid CO_2 purity	Clean CO_2 Out

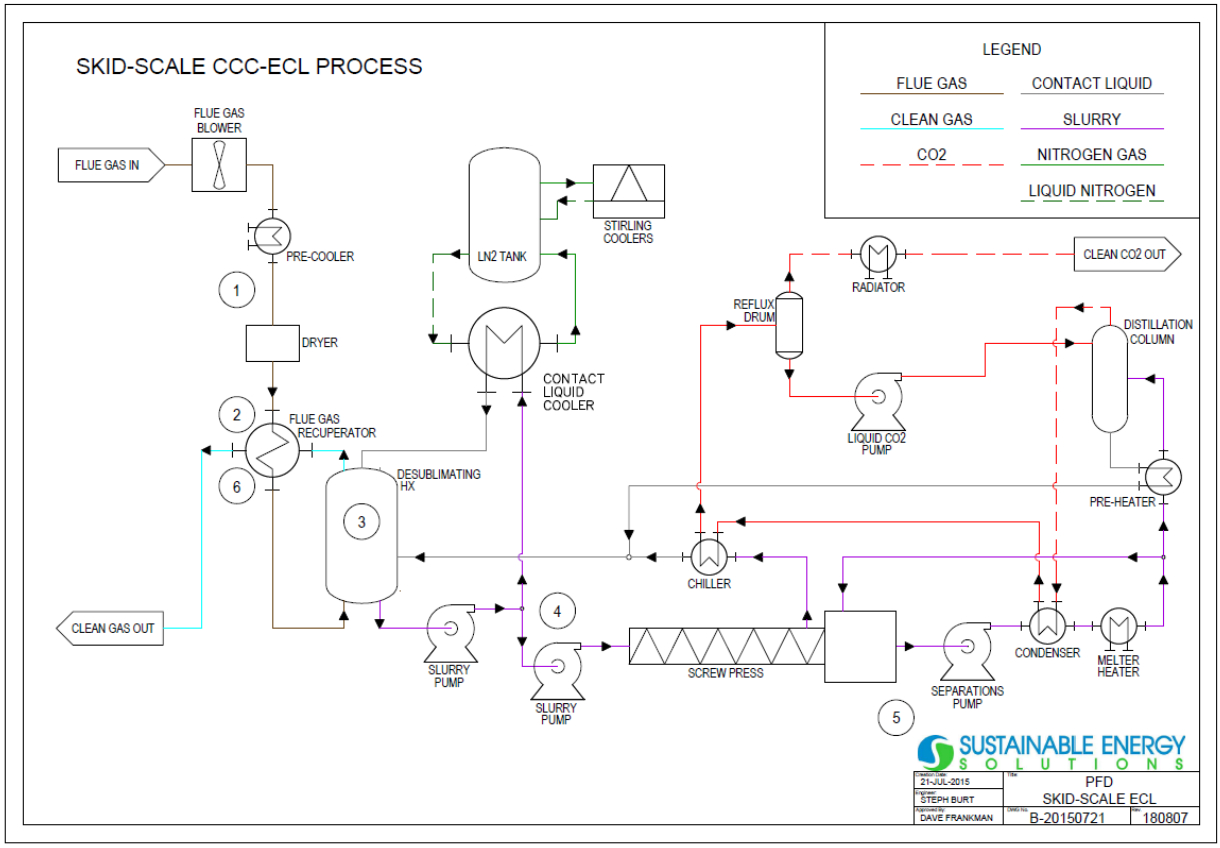

Figure 81. CCC ECL™ skid PFD with instrumentation locations.

Finalize Host Site Agreement

Planned Approach: The Recipient will operate the improved CCC ECL™ skid systems following the test plan developed in Subtask 11.1. Field testing will treat flue gases from a field unit, the precise composition and consistent control of which will depend on the specific field site selected. The Recipient already has an agreement to conduct such tests from Pacificorp, but the specific test location has not been finalized. In-house testing may include mixed N_2/CO_2 gas representative of the compositions found in flue gases from energy production. The Recipient shall conduct a combination of in-house and field tests, at least one of which will involve 500 continuous hours of operation and which shall last a total of at least 4 months.

SES worked with Rocky Mountain Power to develop a host site agreement for the field test at the Hunter Power Plant. As part of the agreement, Rocky Mountain Power agreed to provide administrative support, technical support, operational data, and utilities for the project. This support will include electricity and access to flue gas, support in preparation for the demonstration, on-site supervision and support during operation, and take-down support. Rocky Mountain Power anticipates providing this support for at least

five months, which coincides with the conclusion of the NETL project. SES submitted a copy of the full host site agreement to NETL for review.

As part of their support for this project, Pacificorp and the Hunter Power Plant have made several site modifications. In September and October 2018, electricians from the plant allocated breakers and installed cabling from their electrical building to the location where the CCC ECL™ skid will sit at the plant. They also scheduled the electricians to be available for power connections when the skids were put in place.

SES has also agreed to meet all the safety and operating requirements put forth by the plant. This includes requirements for the use of PPE, operating vehicles on site, and communication requirements. As part of their support for this project, the Hunter Power Plant set up a dedicated plant phone for us for safety and integration into the plant. They provided us with dedicated passes into the facility for the duration of the field test.

Skid Operation

After working through the issues identified during shakedown testing detailed in Task 10, we were able to achieve significantly longer test runs. Shakedown testing lasted until the end of May 2019. Beginning on May 28, 2019 until the end of testing in August 2019, we had 12 test runs of 12 hours or longer (Figure 82). These longer test runs helped achieve a total run time of over 600 hours and capture 6.13 tonnes of CO_2 from flue gas at the Hunter Power Plant.

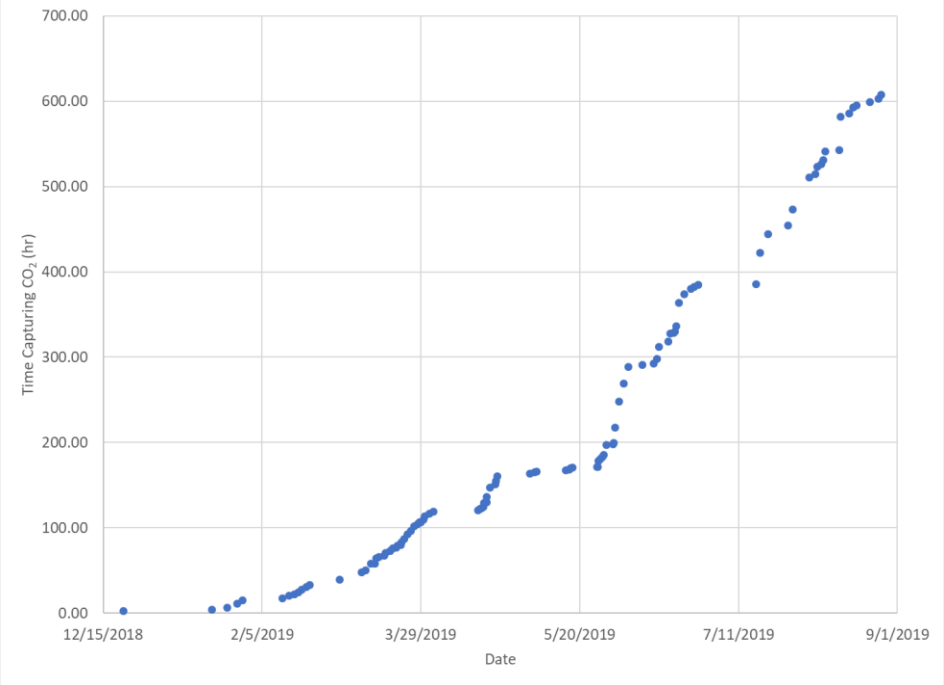

Figure 82. Cumulative hours testing CCC ECL™ skid capturing CO_2 from flue gas at the Hunter Power Plant.

We decided to retrofit the system with the 4-inch dual screw presses. Almost immediately after installing the dual screw presses, we achieved a runtime of 37 hours, which was the longest run to that point.

Several weeks of testing with the dual screws revealed a new challenge that was impeding longer run times. With screw stalling no longer an issue, our contact liquid pump (P-901) began to fail. To overcome this, we changed the motor and the plumbing to make a smoother flow path for the contact liquid.

These changes increased the duration of test runs and limited down time by quickly resetting the system after the end of a test. Over time, despite our attempts to restart quickly, we noticed a degradation in performance. To restore performance after an extended test period, we replaced the contact liquid in the system and purged each unit with nitrogen. While draining the system, we also recovered a foreign contaminant that appears to be oily liquid that is discussed more below. We have concluded that this substance was detrimental to our testing because we were able to have a successful period of testing immediately following each time the system was cleaned and purged, but the performance of the CCC ECL™ skid would degrade with time.

Contaminants

One of the primary issues that impeded a successful continuous 500-hour test run was the accumulation of contaminants throughout the contact liquid cooling loop. The most common symptoms of contaminated contact liquid were dramatic increases in pressure throughout the contact liquid heat exchanger at normal operating temperatures. Figure 83 shows an unsuccessful test during cool down caused by contaminants in the cooling loop.

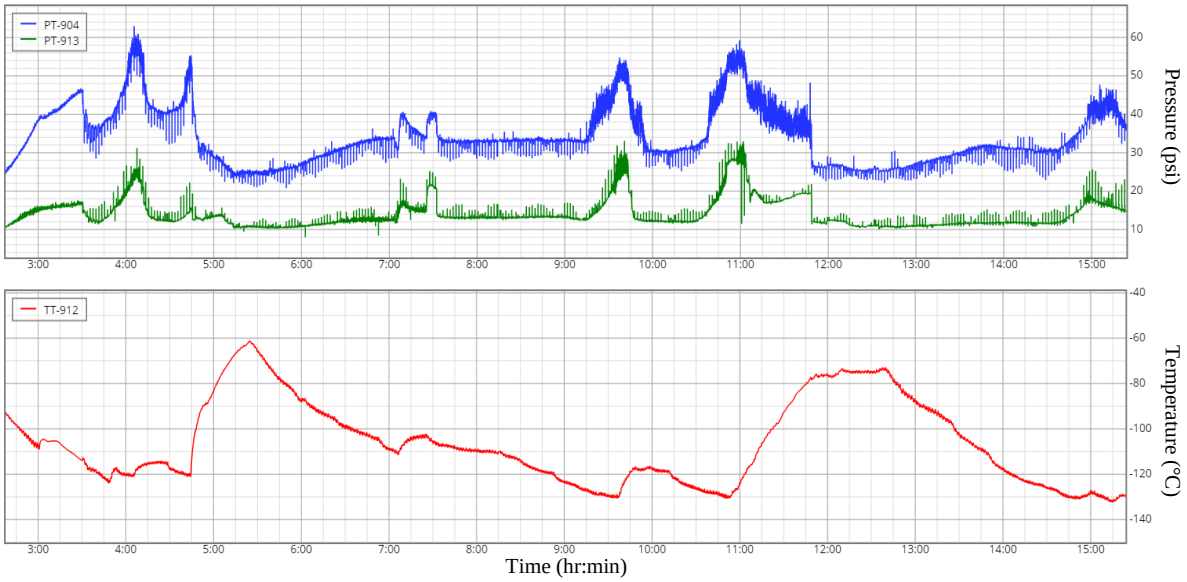

Figure 83. Pressure before (PT-913) and after (PT-904) the contact liquid heat exchanger compared with the contact liquid temperature (TT-912).

The pressure spikes shown in Figure 83 at 4:00, 9:30, 11:00, and 15:00 are representative examples of the contaminant fouling observed during the last part of the on-site testing at the Hunter Power Plant. Normal operating pressures without fouling through the contact liquid heat exchanger were approximately 30 psi (PT-904). Each increase in pressure occurred when the contact liquid was at or near −130 °C, and it occurred even after all the CO_2 was removed from the contact liquid. This indicates the presence of some other substance that freezes or becomes more viscous as the temperature decreases, which causes fouling in either the contact liquid heat exchanger or spray nozzle. We regularly observed increases in pressure just before the spray tower spray nozzle (PT-913), which indicated fouling through the nozzle as well as in the heat exchanger.

To mitigate fouling, SES removed the contact liquid and tested samples from various locations in the contact liquid cooling loop. When we would replace the contact liquid with new clean isopentane, we were often able to achieve longer test results until these contaminants accumulated again. Analytical results from samples of the contaminated liquid were somewhat inconclusive and are still being pursued. Several observations have been made about the contaminants found in the contact liquid despite not knowing the

exact composition or source. There appears to be two different observable contaminants found in the contact liquid cooling heat exchanger: An amber-colored substance (Figure 84) only appears when the liquid is cold (−40 °C) and dissolves back into the contact liquid when at room temperature. This is consistent with what we observed while operating with contaminated contact liquid because fouling was only an issue when the contact liquid temperature decreased. A second, perhaps unrelated, black pollutant appears to coat the surfaces of the entire contact liquid cooling loop. Nuclear magnetic resonance (NMR) tests were conducted on the isopentane that we received from two vendors. These tests indicate this liquid is likely related to contaminants in the feed isopentane. Future work will determine the exact composition of these contaminants to better understand how they behave in our system and how to contain or separate them.

Figure 84. Sample of contact liquid chilled in a freezer to −40 °C. The amber liquid is a separate liquid phase; its composition will be determined by future analytical tests.

Representative Testing Data

We include here a series of plots showing CCC ECL™ skid performance during representative test runs. When describing the test data below, "steady state" is defined from the perspective of CO_2 capture. There is a time offset between when we see the CO_2 capture efficiency reach steady state and when the CO_2 product reaches steady state. We use the CO_2 capture efficiency to define start and stop times. The distillation column continues to produce CO_2 after a test has ended. For all the following plots (from the top): CO_2 capture, flue gas flow rate into the process, flue gas and clean gas CO_2 fraction, temperature into (TT-912) and out of (TT-108.5) of the desublimating HX, CO_2 capturing rate.

Our first run longer than 12 hours was on May 28–29, 2019 (Figure 85). It took about 1.75 hours for the CCC ECL™ process to come to steady state. The drop in CO_2 capture between 7:00 pm and 9:00 pm was caused by the drop in the flue gas CO_2 composition, rather than a decrease in performance in the process. The CO_2 out composition changed very little over the course of this run. The mode of failure for this test is screw press stalling. This run lasted 12.0 hours and captured 204 kg of CO_2 at an average capture efficiency of 93.5%.

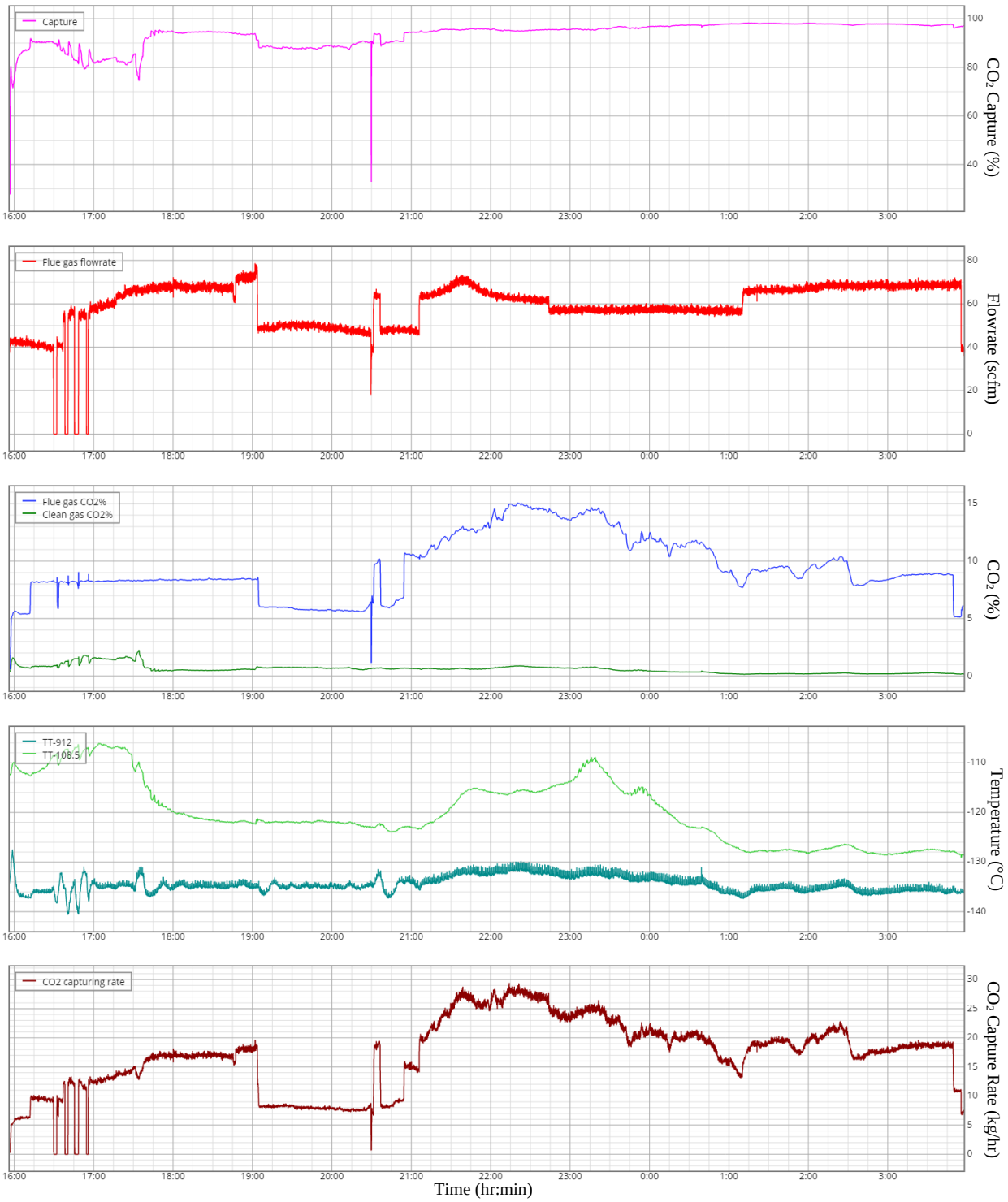

Figure 85. Test data from May 28–29, 2019.

The next long run was on May 31–June 1, 2019 (Figure 86). The process reached steady state very quickly. Minor upsets occurred at 3:00 am and 5:00 am, neither of which ended the run. Rather, the process was able to continue running and regain a high capture efficiency. The mode of failure for this test was screw press stalling. This run lasted 17.9 hours, captured 246 kg of CO_2 at an average capture efficiency of 94.7%.

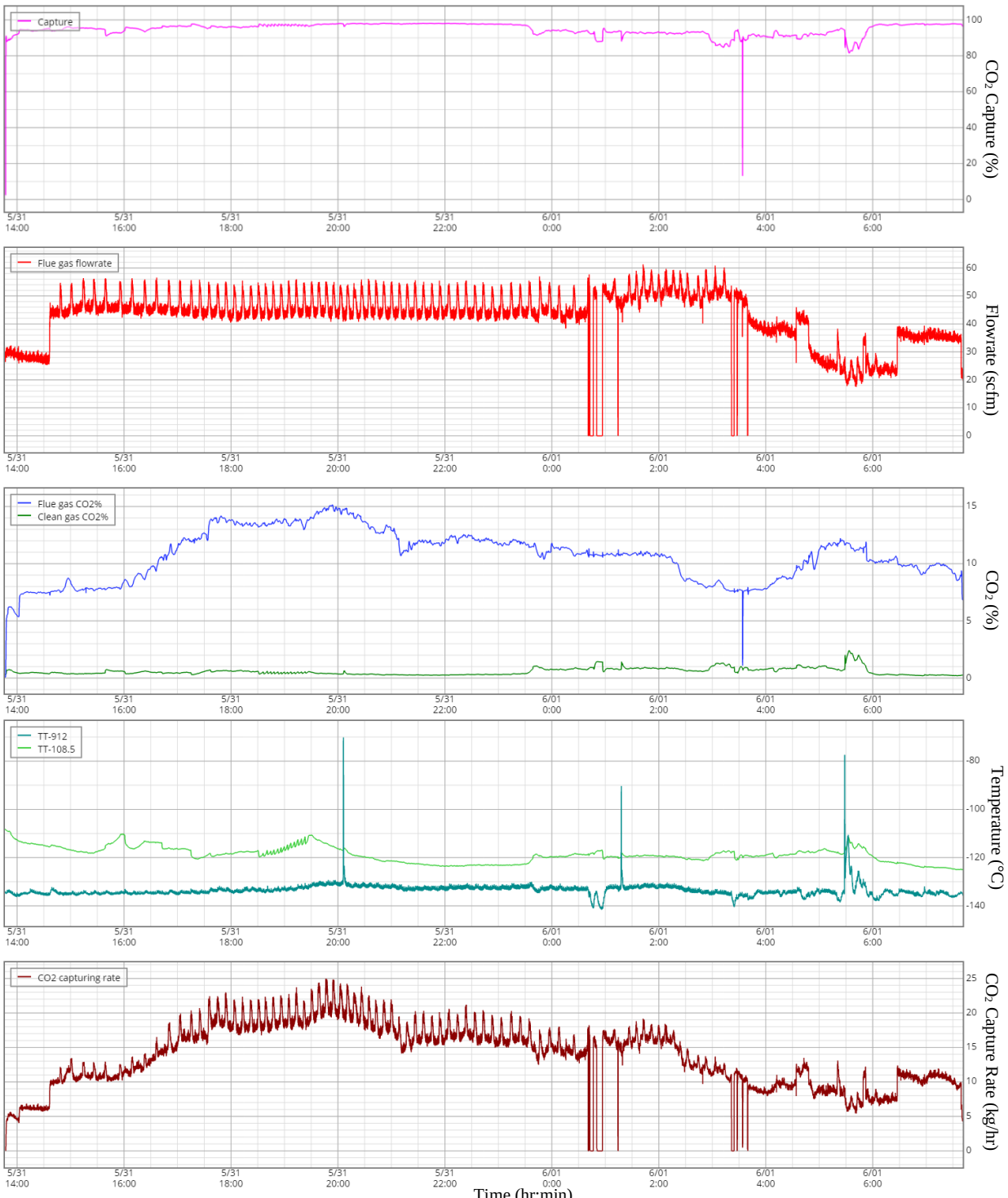

Figure 86. Test data from May 31–June 1, 2019

After resetting the system for about 12 hours, we ran again. This test ran June 1–3, 2019 (Figure 87). Again, the process came quickly to steady state and performed very well. The mode of failure for this run was the loss of the solid CO_2 plug between the screw press and the melter. This run lasted 30.7 hours, captured 281 kg of CO_2 at an average capture efficiency of 97.3%.

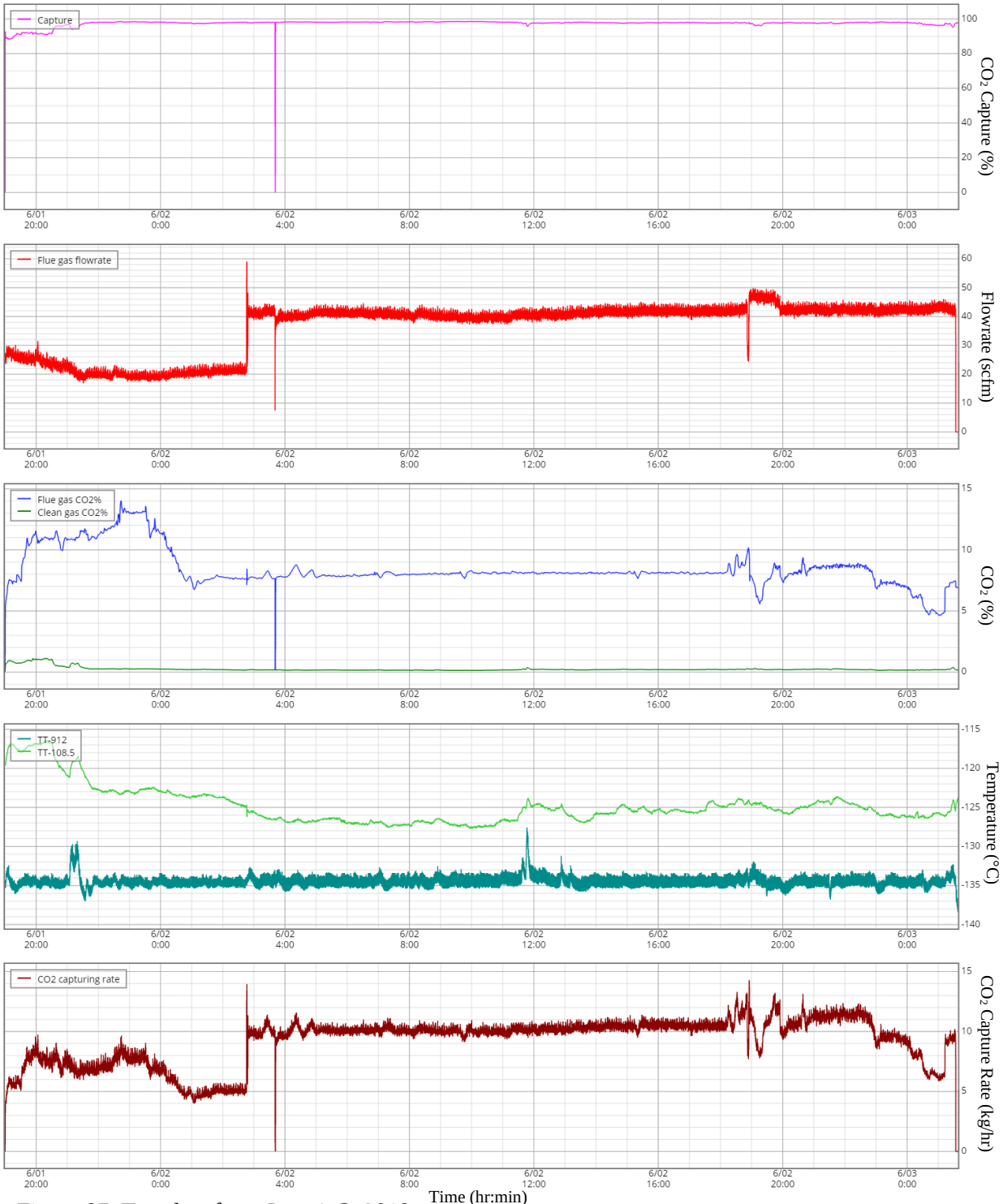

Figure 87. Test data from June 1–3, 2019

We reset for 8 hours, then started a new test (Figure 88). It took about 1.75 hours for the process to reach steady state. The amount of CO_2 in the flue gas nearly doubled in the middle of this test. We could adjust the process on the fly and continue capturing CO_2 without any issues. The mode of failure for this test is

screw press stalling. This run lasted 21.4 hours, captured 211 kg of CO_2 at an average capture efficiency of 96.9%.

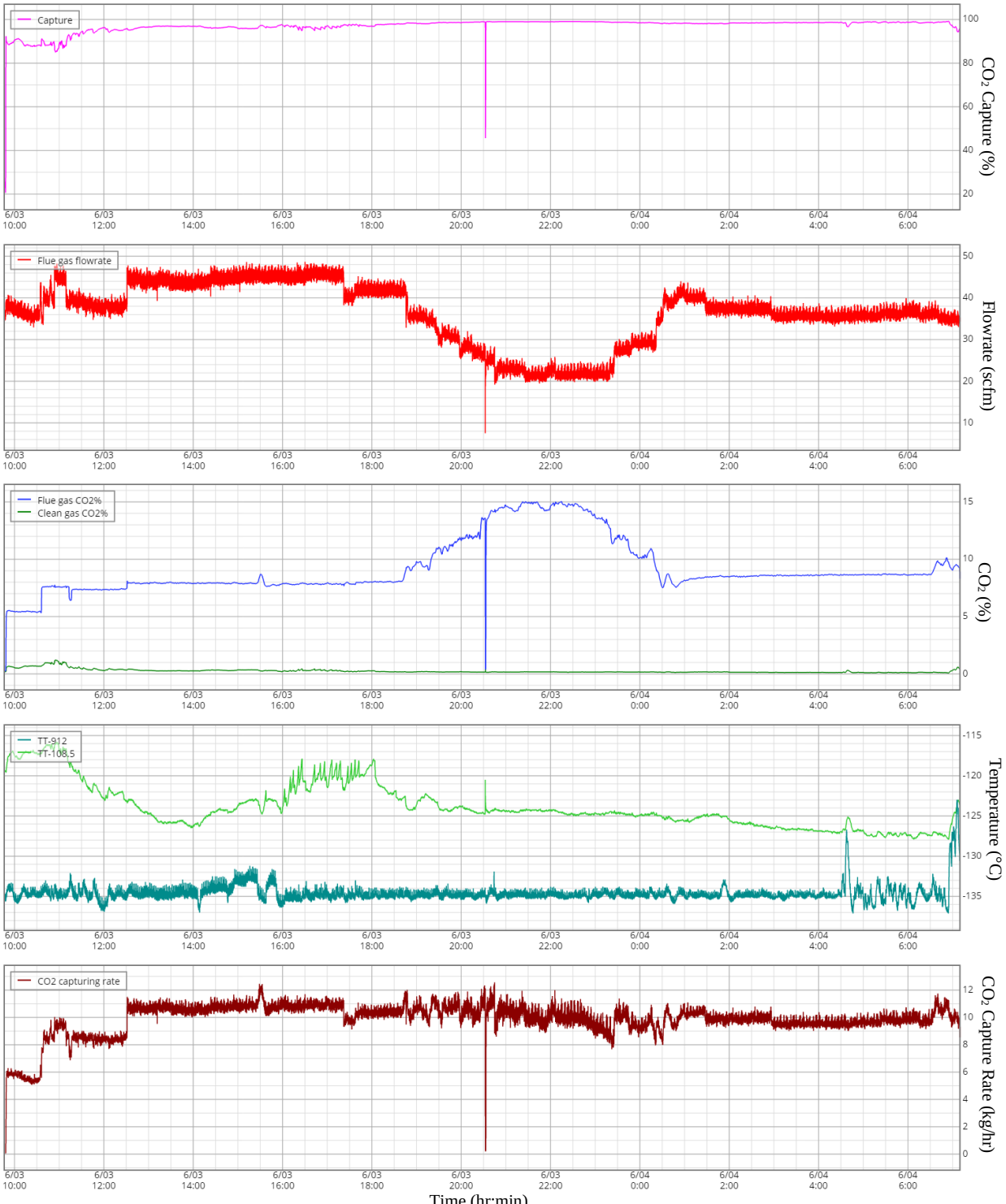

Figure 88. Test data from June 3–4, 2019

Task 12. Quantify System Figures of Merit and Improvement

Specific Objectives: The objective of this task is to quantify the improvements in the skid system and in the unit operations identified above.

Planned Approach: This task will provide summary information on individual improvements in the unit operations identified in Budget Period 1. These will include projected improvements compared to the realized improvements in efficiency, robustness, and scalability and in other figures of merit as indicated in some of the specific descriptions of the unit operation tasks.

Figures of Merit Definition

Table 18 summarizes the figures of merit that quantify unit operation and CCC ECL™ process improvements. For several of the figures of merit, the objective of our testing is to determine the optimal operating conditions for that specific unit operation, thus the figure of merit is "to be determined" (TBD). These specific optimized operating conditions will allow for us to create better, updated designs of unit operations for designing the next iteration of the CCC ECL™ process for the next scale of demonstration and to better model these unit operations moving forward.

Table 18. Figures of merit for individual unit operations and the CCC process as a whole used to quantify the improvements achieved during this project.

Unit Operation	Figure of Merit	Projected Improvement
Desublimating Heat Exchanger	Optimal solid loading in slurry	TBD
	Capture efficiency	>90%
Solid–Liquid Separations	Optimal CO_2 content in melter	TBD
Vapor–Liquid Separations	CO_2 outlet purity	>99%
Non-fouling Heat Exchanger	Pressure drop across unit	TBD
CCC ECL™ Skid	Total hours capturing CO_2	500
	CO_2 capture efficiency	>90%
	Total tonnes of CO_2 captured	20.8

Demonstrate Figures of Merit

The CCC ECL™ skid was tested at Unit 3 of the Hunter Power Plant from December 2017 through August 2018. During this time, we were able to determine optimal operating conditions and parameters, while running for a total of over 600 hours capturing CO_2. Table 19 outlines the quantitative results from our tests and compares these values with those projected at the beginning of this phase of the project. SES did not meet the objective of 500 continuous hours of CO_2 capture from flue gas at the Hunter Power Plant. SES gained important information about how the process works and created an expansive operator handbook that includes the knowledge gained from the testing performed during this project.

Table 19. Quantitative results from operating the CCC ECL™ skid at the Hunter Power Plant for the figures of merit for individual unit operations and the CCC process as a whole.

Unit Operation	Figure of Merit	Projected Improvement	Test Results
Desublimating Heat Exchanger	Optimal solid loading in slurry	TBD	<10%
	Capture efficiency	>90%	91.4%
Solid–Liquid Separations	Optimal CO_2 content in melter	TBD	30–70%
Vapor–Liquid Separations	CO_2 outlet purity	>99%	99.99+%
Non-fouling Heat Exchanger	Pressure drop across unit	TBD	35 psi
CCC ECL™ Skid	Total hours capturing CO_2	500 (consecutive)	607 (non-consecutive)
	CO_2 capture efficiency	>90%	91.6%
	Total tonnes of CO_2 captured	20.8	6.13

These figures of merit show improvements in the process, including:

- Consistent CO_2 capture at rates higher than 91% for all of the tests using flue gas (a total of over 100 tests).
- The heat integration recuperators for cooling and warming the incoming and outgoing flue gas, respectively, performed well and these designs can be utilized in future scales of the CCC ECL™ process.
- The spray tower performed well, consistently reaching high capture efficiencies. The spray cleaning nozzle performed very well, effectively eliminating the need for other methods to ensure that solid CO_2 did not accumulate on the sides of the spray tower.
- We gained invaluable insight into the cryogenic slurry pump performance, which we can utilize for the pilot- and full-scale CCC systems. We now have a scalable control scheme and geometry for skid- and pilot-scale pumping.
- We were able to operate for long periods of time with a consistent pressure drop through the shell and tube heat exchanger, which indicated no increase in fouling of the heat exchanger. Although we found that maintaining a pressure drop of 35 psi or less resulted in optimal performance of the shell and tube heat exchanger, the bottom plot in Figure 89 shows that the shell and tube heat exchanger still performed well and provided the required contact liquid cooling for over 7 hours at with a pressure drop of over 50 psi. The clearly demonstrates how robust this heat exchanger design is and allows the CCC ECL™ process to successfully operate across a broad range of operating conditions.

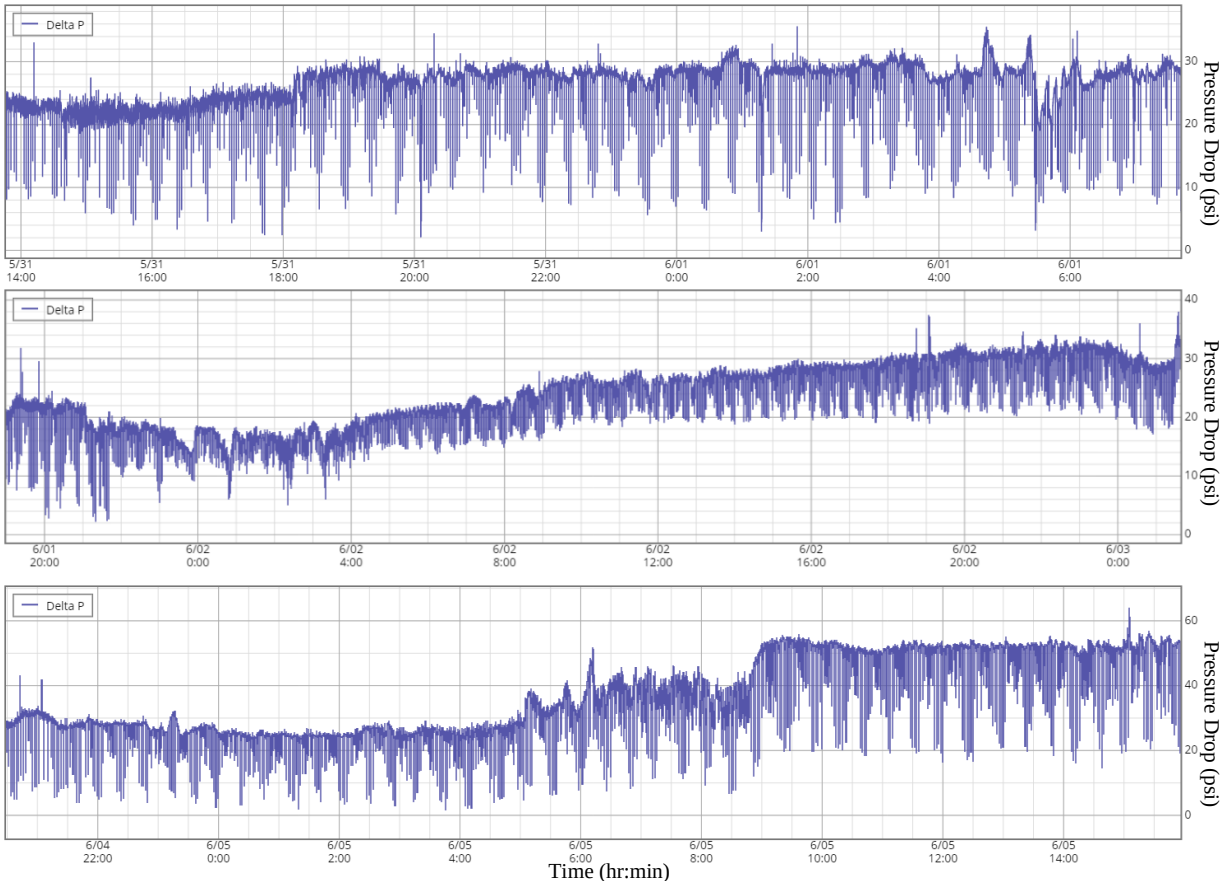

Figure 89. Representative plots of pressure drop through the shell and tube heat exchanger: (top) May 31–June 1, 2019, (middle) June 1–3, 2019, (bottom) June 4–5, 2019

- The distillation column worked as designed for the duration of the field testing. We optimized and improved operational aspects of the distillation column, which resulted in improved performance of the column and other portions of the process.
- We have developed a robust and powerful Supervisory Control and Data Acquisition System that is easy for operators to use. We have compiled a database of test data that is easily accessed and analyzed.

Based in these figures of merit, future work includes:

- Determining the source of the contact liquid contamination that we began to see more and more towards the end of the field testing and eliminating this contamination.
- Improving the single screw press so it performs well at higher capacity and for longer tests.
- Further research into the performance of the pollutant removal settling tanks, including optimizing draining any pollutants and quantifying the pollutant capture of SO_x and NO_x.
- Testing the CCC ECL™ at higher CO_2 capture rates of 1 tonne CO_2/day for continuous tests up to and beyond 500 hr.

Task 13. Phase 2 Techno-Economic Analysis

Specific Objectives: The objective of this task is to quantify theoretical improvements in techno-economic performance of the CCC process based on the work in Budget Period 1 and the results in Budget Period 2.

Planned Approach: The Recipient has maintained an essentially continuous effort in improving technical and economic evaluations of the CCC process. As the other tasks in the project are completed, both the energy and economic projections for CCC will require updates. As process modifications and testing continue in Budget Period 2, The Recipient will continue to use its in-house code and collaborate with project team members to update and improve the techno-economic analyses. The Recipient anticipates continuing to work closely with NETL's process modeling group in this effort.

Updating the CCC ECL™ Techno-Economic Modeling

To expand and update the techno-economic analysis of the CCC ECL™ process, we have continued to optimize both the software used to model the process as well as adjusted the refrigerant profiles and compositions to reduce the energy penalty. These adjustments stem from research into improved alternatives to the refrigerant loops used to cool various portions of the CCC ECL™ process.

Spray Tower Verification

Experimental results have also verified that the spray tower unit operation is working properly. Important parameters such as droplet size have been verified experimentally. Also, the temperature profiles in our spray towers match those predicted by the model. Figure 90 below shows the expected capture from our model based on desublimator gas and liquid input compared with actual test data. While they are similar, the predicted CO_2 outlet percentage is more sensitive to variability in the instantaneous conditions than the actual system. The simulation does not consider the thermal mass of the equipment itself, which we believe accounts for the dampening effect that we see in the system.

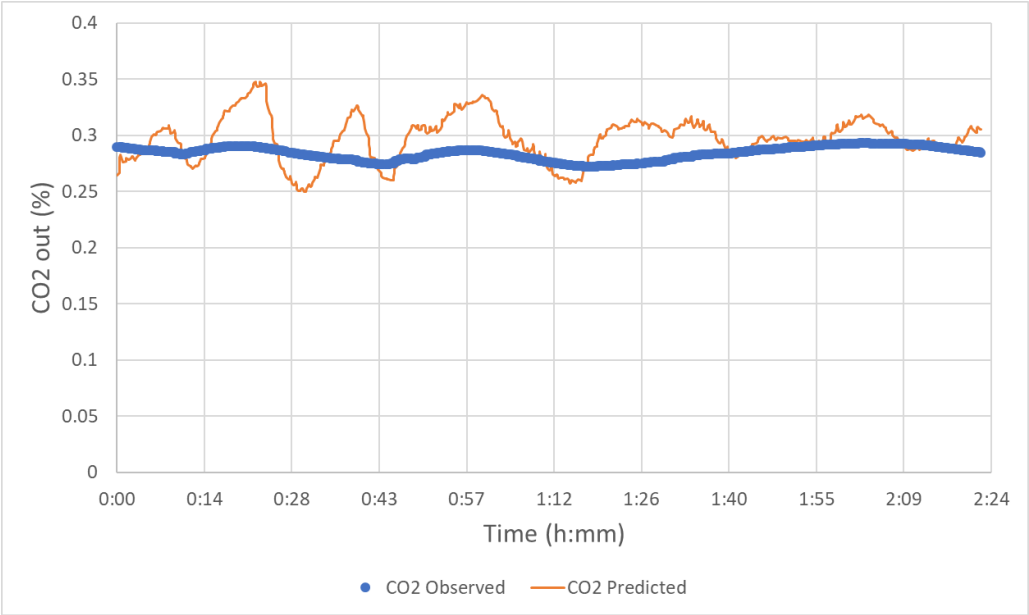

Figure 90. Predicted CO_2 outlet compared with test data

Non-Fouling Heat Exchanger Verification

A non-fouling heat exchanger is critical for this process to be continuous. Fouling has many effects on the system, but the easiest way to measure it is by looking at the pressure drop across the heat exchanger. As fouling occurs, the pressure drop across the heat exchanger increases. Figure 91 shows a full day of continuous data on our non-fouling heat exchanger. The pressure drop does vary in this plot, but these fluctuations are normal and can be attributed to other factors such as solids concentration and slurry temperature. The heat exchanger no longer exhibits the exponential increase of pressure drop that we previously saw that indicates fouling over time.

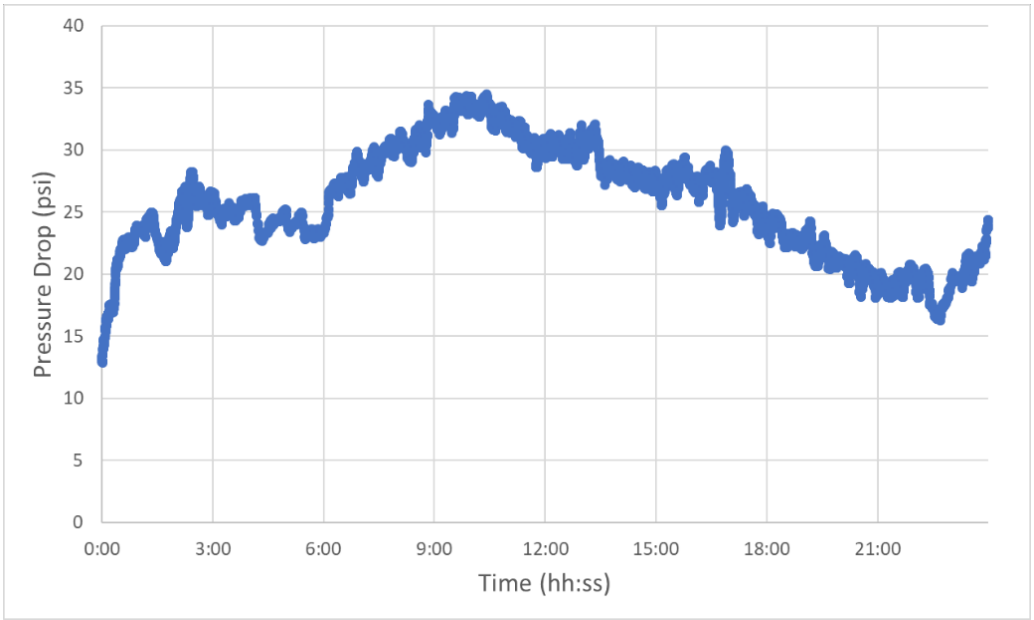

Figure 91. Pressure drop through the non-fouling heat exchanger

Energy Performance Comparisons

This discussion compares carbon capture technologies using the approach of NETL. Specifically, the analysis here compares the energy and economic performance of greenfield plants with the same net output but that use different carbon capture technologies. This internalizes the energy efficiency of each process and provides a way to compare technologies that primarily use heat (amines) with those that primarily use power (CCC). All carbon capture technologies involve substantial parasitic energy loads to separate CO_2 from the remaining flue gas and pressurize the CO_2 stream. The separation and pressurization steps affect the cost of electricity. A power plant with a higher parasitic load requires more fuel to achieve the same output. The plant itself, and all its components, must be larger to handle these larger fuel flow rates. Additionally, the amount of gas that then needs to be processed increases, thus requiring that both the equipment and total loading for the CCS technology be larger.

SES believes this analysis approach most fairly compares technologies. However, it is not aligned with the probable implementation of carbon capture in the US or most of the rest of world. That is, most carbon capture systems in the US and elsewhere will be retrofit rather than greenfield implementations. One of the great advantages of the CCC process is its ease for retrofit, especially in contrast with other carbon capture systems. Most alternative systems require either major upstream modifications to a plant, very large capital expenditures for steam generation, or an entirely new power plant. The CCC process, by contrast, can retrofit any existing continuous CO_2 stream with virtually no change to the existing technology. This leverages existing capital investments and represents a major advantage of CCC in implementing carbon capture in the real world. A discussion of retrofit costs appears after the comparisons to the NETL greenfield scenario.

The NETL report mentioned earlier [10] contains detailed mass and energy balances for six power plant configurations, each labeled with a case number. In addition to mass and energy balances, each case contains detailed estimates for capital expenditures, operating costs, consumables and fuel costs, etc. The report details the resulting cost of electricity, allowing for a financial comparison between the different power plant options on the same terms. All mass balance, energy balance, and cost numbers quoted in this report come from the Revision 3 version of the report [10]. All CCC simulations were carried out at 90% capture, although the CCC process can easily cope with capture efficiencies at and above 99%.

After optimizing the CCC process, many of the tables and figures included in the Budget Period 1 TEA were updated and are shown below.

Energy Performance of CCC

Table 20. List of Parasitic Loads for CCC (updated from Table 7 in the Budget Period 1 TEA).

Energy Source	Work (MW_e)
Flue Gas Compression	8.8
Refrigerant Compression	101.7
Separations Compression	0.7
Condensed Phase Pumping	3.1
Steam Redirection	2.6
Total	**116.9**

The real benefit of the CCC numbers can be seen in the established energy metrics stated above. In terms of the processed outlet stream, the energy penalty of CCC is 0.841 GJ/tonne. Its calculated net HHV heat rate is 10,011 BTU/kWh, corresponding to a parasitic load of 16.30%. The parasitic load of the CCC process as-is, without any additional integration, is approximately three quarters of the corresponding parasitic load of the amine process.

Table 21. Summary of Energy Penalty of CCS technologies (updated from Table 8 in the Budget Period 1 TEA).

	Case B12A (no capture)	**Case B12B (amine)**	**CCC**	**CCC Steam Integration**	**CCC no FGD**	**CCC no SCR**	**CCC no Hg Removal**	**CCC Full Integration**
Power Needed (GJ/tonne CO_2)	0.000	1.047	0.872	0.570	0.845	0.872	0.871	0.563
HHV Heat Rate (BTU/kWh)	8379	10508	10639	9941	10575	10640	10639	9926
Parasitic Load	0.00%	20.28%	16.90%	11.06%	16.40%	16.91%	16.90%	10.93%

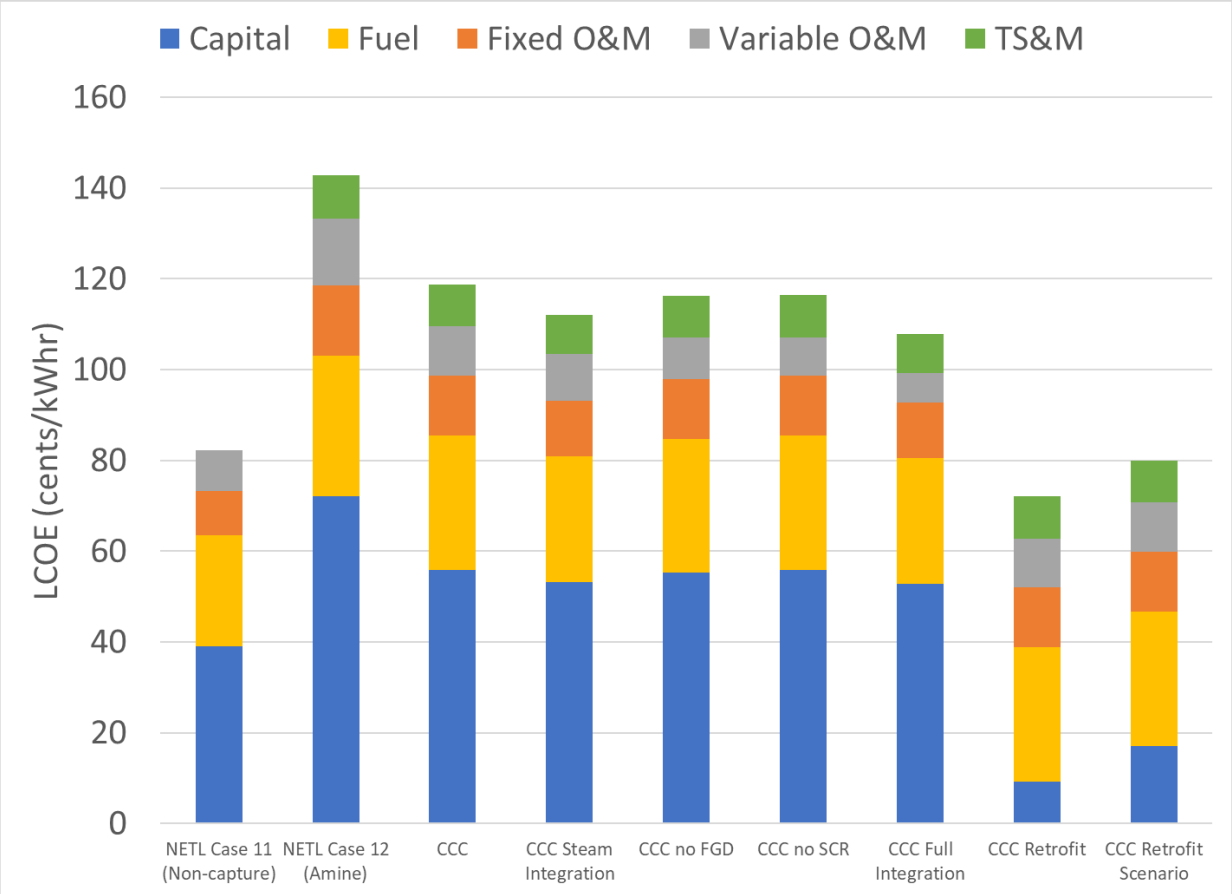

Figure 92. COE of different case studies broken into component parts (updated from Figure 36 in the Budget Period 1 TEA).

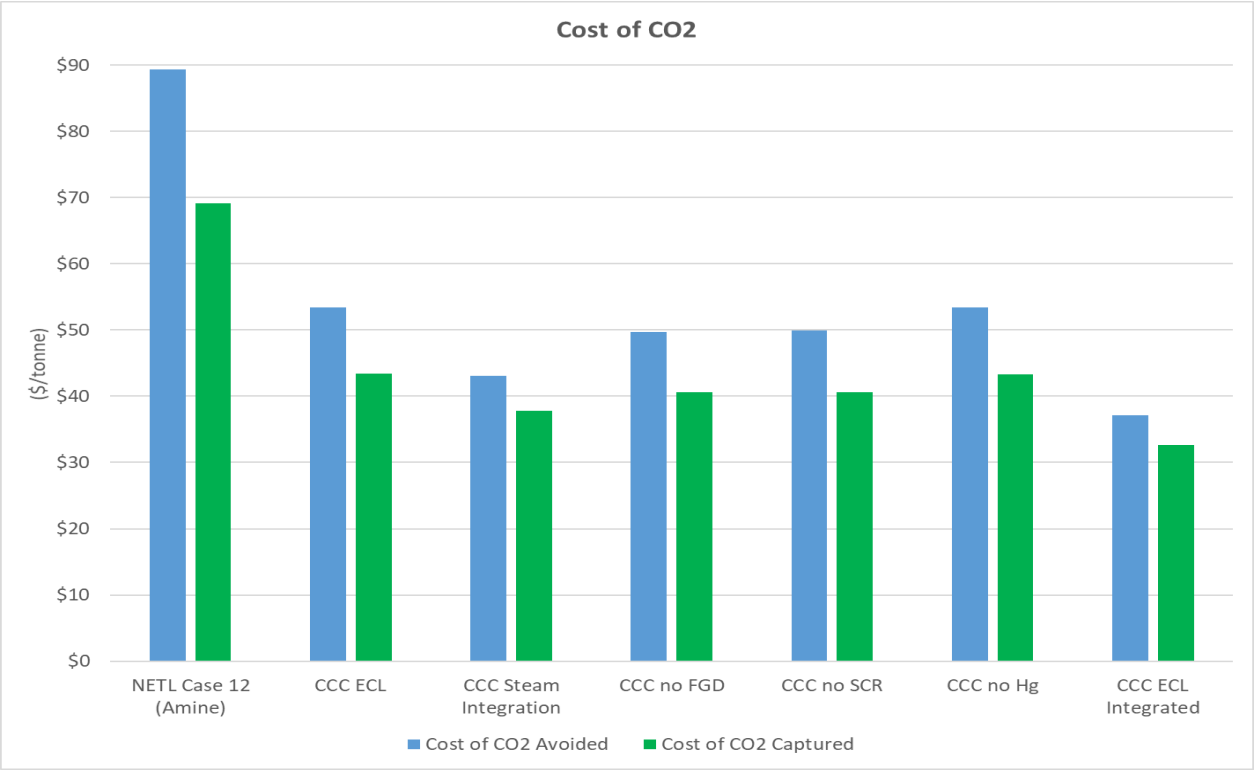

Figure 93. Cost of CO_2 (updated from Figure 37 in the Budget Period 1 TEA).

Table 22. Cost comparison between NETL Cases B12A and B12B as well as estimates for the CCC process, both as a greenfield installation and as a retrofit installation (updated from Table 10 in the Budget Period 1 TEA).

	Case B12A	**Case B12B**	**CCC ECL**	**CCC Steam Int.**	**CCC no FGD**	**CCC no SCR**	**CCC no Hg Removal**	**CCC Full Int.**	**CCC Single Retrofit**	**CCC Retrofit Scenario**
COE ($/MWh)	82.30	142.80	118.72	111.99	116.25	116.39	118.73	107.89	73.21	80.78
TS&M Costs ($/MWh)	0.00	9.60	9.22	8.62	9.17	9.22	9.22	8.61	9.15	9.15
Fuel Costs ($/MWh)	24.60	30.90	29.64	27.70	29.46	29.64	29.64	27.65	29.43	29.43
Variable Costs ($/MWh)	9.10	14.70	10.78	10.14	9.18	8.44	10.78	6.49	12.35	12.35
Fixed Costs ($/MWh)	9.60	15.40	13.16	12.30	13.08	13.16	13.16	12.28	13.06	13.06
Capital Costs ($/MWh)	39.00	72.20	55.92	53.24	55.36	55.93	55.93	52.86	9.22	16.79
Difference from Case B12A	0.00%	73.51%	9.22	40.50%	34.28%	34.07%	44.47%	18.07%	−11.05%	−1.85%

Table 23. Cost of CO_2 comparison for greenfield cases (updated from Table 11 in the Budget Period 1 TEA).

($/tonne)	Case B12B	CCC ECL™	CCC Steam Integration	CCC no FGD	CCC no SCR	CCC no Hg Removal	CCC Full Integration
Cost of CO_2 Avoided	89.30	54.73	48.48	41.28	41.07	53.60	21.60
Cost of CO_2 Captured	69.17	44.83	41.46	34.18	33.64	43.91	18.67

Table 24. Increase in COE for amine-based CCS installations [12] and CCC (updated from Table 12 in the Budget Period 1 TEA).

	NETL	CMU	EPRI	TNO	TPRI	CSIRO	CCC
Reference Non-capture Plant COE ($/MWh)	82.30	59.10	73.40	43.90	42.00	53.40	82.30
Amine-based CCS Plant COE ($/MWh)	142.80	99.20	121.10	79.20	62.00	114.50	119.70
Increase in COE ($/MWh)	60.50	40.10	47.70	35.30	20.00	61.10	37.40
Difference from Base Case	73.5%	67.9%	65.0%	80.4%	47.6%	114.4%	45.4%

This importance of a retrofit technology becomes clearer when comparing alternative power generation systems in a market with saturated fossil capacity. The earlier greenfield analysis suggests that carbon capture could increase COE by about 82%, but this presumes a new greenfield installation. These costs increase significantly if carbon capture technology requires rebuilding all existing infrastructure. The January 2013 Electric Power Annual released by the United States Energy Information Administration [13] indicates an average generation cost of 35.1 $/MWh for 2011—the simulated year of the NETL study—related to operation, maintenance, and fuel costs for fossil steam-generated electricity. This COE using the existing infrastructure provides a baseline with which to compare the cost of new carbon capture technologies. If retrofits are not an option and the full capacity of existing power plants must be replaced with those capable of carbon capture, the real cost of electricity generation to the utility increases from around 35.1 $/MWh to 142.8 $/MWh, an increase of 307%. In the low-cost regions of the country, where average generation costs are about 20 $/MWh, this represents an increase greater than 600%. By contrast, a single CCC retrofit would increase the COE by 85% (26% of this increase is due to transportation, storage, and monitoring). This large increase in COE nevertheless pales in comparison to the alternative of having to replace lost capacity with new installations or significant rebuilds.

Conclusion

The current energy infrastructure still relies heavily on fossil fuel resources for most of the world's energy demands and will likely continue to do so for decades. However, climate change issues become more apparent and acute each year. Climate change mitigation must include technologies that address the adverse effects of fossil-based energy. For these reasons, CCS is not just an important, but an essential part of climate management. Cryogenic Carbon Capture™ represents a viable alternative to current technologies. Its advantages include:

(a) a lower parasitic load, 25–50% lower than established metrics for absorption technology, depending on the reference study;
(b) lower cost of electricity, approximately 60% of the increase calculated using established metrics for absorption technology;
(c) minimally invasive bolt-on technology capable of being retrofitted to existing plants;
(d) ancillary pollutant removal and the inherent integration benefits associated therewith;
(e) ability to capture CO_2 at well above the industry standard 90% capture efficiency; and
(f) energy storage capabilities that could greatly increase the usability of renewables and stabilize the grid.

By every established metric, CCC outperforms competing carbon capture technologies and represents a potential paradigm-shifting solution to the current questions facing the energy industry.

Task 14. EH&S Risk Assessment

Specific Objectives: The objective of this task is to assess the environmental friendliness and safety of the proposed process.

Tri-State Generation and Transmission Association, Inc. (Tri-State) completed an environmental health and safety (EH&S) risk assessment using the details for a full-scale 550 MW net CCC ECL™ process that SES provided (e.g., temperatures, pressures, compositions of each stream). The final EH&S report was completed and submitted to NETL on June 24, 2019.

The specific chemicals included in this risk assessment are isopentane, R14, ethane, methane, ethylene, methanol, propane, n-butane, n-pentane, n-hexane and n-heptane. For the purposes of this toxicological overview, these chemicals will be discussed as the C1–C4 alkane gases, which include methane, ethane, propane and butane; the C5–C7 alkane liquids: pentane, isopentane, hexane, and heptane; and the refrigerant R14. It should be noted that although n-hexane, n-heptane, and R14 do not show up in the streams being analyzed here, they are a part of the refrigerant hence they are being studied as well.

Air, Water, and Solid Waste Identification for a Cryogenic Carbon Capture™ (CCC) System for a 550 MW Coal-Fired Power Plant

The potential air and water emissions and solid waste streams from the proposed technology were estimated for a 550 MW coal-fired power plant. With the exception of isopentane, all other refrigerants are used in closed loop systems and should not result in any air or water emissions under normal operations. Importantly, none of the refrigerants used in the CCC process are included within the Montreal Protocol.

The following tables outline to expected emissions for the streams that exit the process (Table 25–Table 28). It should be noted that all the analysis and stream conditions are representative of an idealized steady-state condition of operation of the SES post-combustion capture system which is installed at the backend of a coal fired power plant.

Table 25. Composition and flow rate for the clean light gas out
Flow rate = 5143563.20 kg/s (3445.39508 mol/s)
Temperature = 16.76 °C
Pressure = 11.0 psia

	mol frac	mol/s	MW	kg/s
CO_2	0.016	308	44.01	13.556
N_2	0.912	17112	28.01	479.307
O_2	0.043	811	16	12.976
Ar	0.011	205	39.95	8.190
C_5H_{12} (isopentane)	2.30×10^{-5}	0.4324	72.15	0.031
NO	4.4×10^{-4}	8.26	30.01	0.248
NO_2	4.53×10^{-8}	0.001	46.0055	4.6×10^{-5}
SO_2	3.7×10^{-5}	0.694	64.066	0.044

Table 26. Composition and flow rate for CO_2 final product
Flow rate = 128.03 kg/s (2908.69 mol/s)
Temperature = 14.25 °C
Pressure = 2214 psia

	mol frac	mol/s	MW	kg/s
CO_2	1	2908	44.01	127.98
C_5H_{12} (isopentane)	2.35×10^{-4}	0.69	72.15	0.05

Table 27. Composition and flow rate of water out after flue gas pre-cooler
Mass Flow rate = 56 kg/s (3143 mol/s)
Temperature = 52.78 °C
Pressure range of loop = 14 psia

	mol frac	mol/s	MW	kg/s
H_2O	0.999	3141	18.015	56.59
SO_2	1.0×10^{-3}	2.43	64.066	0.16

Table 28. Composition and flow rate of pollutant capture/waste stream
Mass Flow rate = 3.26 kg/s (52.45 mol/s)
Temperature = −54.15°C
Pressure Range of Loop = 76 psia

	mol frac	mol/s	MW	kg/s
SO_2	0.895	46.94	64.066	3.01
NO_2	0.105	5.51	46.005	0.25

Toxicological Effects of Components in the CCC Process

A thorough literature search was conducted to examine potential human health effects and eco-toxicity. Where information was lacking for a particular material, the material was either compared to similar substances or Quantitative Structure Activity Relationship (QSAR) models were used to predict toxicity levels of the particular chemical.

The alkane components used in the CCC process are, in most cases, very well studied. These are alkanes that have been used in consumer product applications and thus, have large bodies of research. In many cases, this research includes substantial data on human toxicology from both clinical testing and real-world exposure. According to *Patty's Toxicology* "aliphatic hydrocarbons are practically nontoxic for single exposures below the lower flammability limit. In general, the saturated hydrocarbons from propane through the octanes show increasingly narcotic properties… in general, branched-chain derivatives (isopentane) are less toxic than the parent straight-chain alkanes" [14].

The C1–C4 saturated alkanes will be gases at standard temperatures and pressures, making ingestion of these materials unlikely. As shorter chained alkanes, these components are low toxicity, and in most cases only pose an acute human exposure danger in the case of oxygen displacement and flammability. Central nervous system (CNS) depression and narcotic effects are expected from these gases at varying concentrations, typically seen above the lower flammability limits. In cases of substantial acute exposure, there is no evidence of long-term damage to lungs or other organs. Substantial chronic exposure, seen in the form of intentional abuse or "huffing" of these gases, can cause a variety of mental impairments. These effects would not be expected in a workplace exposure scenario.

The C5–C7 alkanes (i.e., pentane, isopentane, hexane and heptane) are liquids and thus pose two hazards not seen with gases. These can include effects of ingestion such as nausea and vomiting and the more severe

issue of aspiration followed by chemical pneumonitis. When chronic skin contact occurs, dermal irritation and chronic dermatitis can occur due to defatting of the skin. Alkanes generally increase in toxicity as C_n increases, meaning that the C5–C7 alkane liquids are generally more toxic than the C1–C4 gases discussed above. Each of these liquids, except for isopentane, is included in the closed-loop portion of the CCC process, so contact by employees should be isolated to specific maintenance tasks. As noted above, branched-chain alkanes are generally less toxic than their parent compounds.

Carbon tetrafluoride (R14) has been studied far less than the other components of the CCC process. Based on the Safety Data Sheets reviewed, R14 poses little hazard beyond frostbite and oxygen displacement.

Isopentane

Isopentane has been studied for toxicological effects in animals and, to a lesser extent, humans. Isopentane is considered to be irritating to the eyes, nose, and throat and is an aspiration hazard if swallowed. Significant exposures above 9% concentration were required to see any anesthetic or central nervous system effects. No evidence was found to indicate that there is any carcinogenicity associated with isopentane.

Ethane

The primary hazards of ethane are primarily due to the potential for frostbite and flammability. According to the 1986 American Conference of Governmental Industrial Hygienists (ACGIH) threshold limit value (TLVs), ethane produced no systemic effects on the person breathing it at concentrations below 50,000 ppm. While OSHA does not have a specific exposure limit for ethane, it is considered to be a simple asphyxiant. Once the lower explosive limit is reached at 30,000 ppm (3%), the explosive hazard greatly outweighs the inhalation toxicology which, per ACGIH above, does not produce systemic effects. The ACGIH TLV that applies to ethane is the same TLV that applies to all C1–C4 alkanes at 1,000 ppm as an 8-hour Time-Weighted-Average (TWA).

Methane

Methane is considered to be biologically inert. Its toxicity is related to its ability to displace oxygen and its flammability. According to one peer-reviewed study, rabbits can inhale a mixture of one volume of oxygen and four volumes of methane for any length of time without showing any ill effects. For methane, like ethane discussed in the previous section, the flammability and potential for frostbite are the primary hazards. ACGIH does not list any toxicological hazards for methane beyond asphyxiation due to oxygen displacement, which would occur at levels above the lower flammability limit. The ACGIH TLV that applies to methane is the same TLV that applies to all C1–C4 alkanes at 1,000 ppm as an 8-hour TWA.

Propane

Like methane and ethane, propane is primarily a simple asphyxiant. Some anesthetic and CNS depression can be seen at concentrations above the lower flammability limit, which are readily reversible. Propane is non-irritating, but like methane and ethane, contact with the liquid can cause frostbite. Because of its extensive consumer use, the toxicology information on propane is substantial. The ACGIH TLV documentation references a study in which monkeys were exposed to 200,000 ppm propane for 15 minutes. The only toxic endpoint was a depressed breathing rate. The ACGIH TLV that applies to propane is the same TLV that applies to all C1–C4 alkanes at 1,000 ppm as an 8-hour TWA.

n-Butane

Like methane, ethane, and propane, butane is primarily a simple asphyxiant. According to ACGIH, a 10-minute exposure to 10,000 ppm resulted in drowsiness, but no other systemic effects. Contact with butane occurs regularly as it is a common propellant used in consumer products. Exposure to butane has been shown to have no effects on skin, respiratory tract, or eyes, even through direct contact with the gas as a propellant. The ACGIH TLV that applies to propane is the same TLV that applies to all C1–C4 alkanes at 1,000 ppm as an 8-hour TWA.

n-Pentane

Pentane is a skin irritant with the potential to cause a burning sensation and blistering of the skin. In human testing, volunteers exposed to 5,000 ppm pentane for 10 minutes showed no mucous membrane irritation. Laboratory testing of rats exposed to pentane by inhalation over the course of 13-weeks showed a No Observable Adverse Effect Level (NOAEL) of greater than 6,885 ppm.

n-Hexane

Hexane is neurotoxic and irritating to the skin but has not been shown to be carcinogenic. While chronic inhalation of hexane can produce sensorimotor neuropathy, this effect can be stopped and recovery made once the exposure ceases. In studies conducted on human volunteers, exposure to 2,000 ppm showed no effects.

n-Heptane

Heptane is neurotoxic and can cause pain, burning, and itching when in contact with skin, but has not been shown to be carcinogenic. According to Patty's Toxicology, "concentrations of 4.8% heptane (48,000 ppm) caused respiratory arrest within three minutes." Animal exposure studies in rats showed that unlike hexane exposure, which can cause reversible neurotoxicity, the rats exposed to heptane caused severe nerve and muscle damage. As was discussed in the toxicological summary of this process, the toxicity of these straight chained alkanes increases as C_n increases and thus, heptane is the most toxic component in this process.

Ethylene

Ethylene is a colorless flammable as with a sweet musky odor and taste. Ethylene is lighter than air and can displace oxygen starting at higher elevations creating an asphyxiation hazard. Ethylene is a flammable gas with a flash point of -213 deg F, LEL of 2.75%, UEL of 28.6% and an autoignition temperature of 842 deg F. The ACGIH TLV for Ethylene is 200 ppm as an 8-hour TWA. Ethylene reacts with strong oxidants causing fire and explosion hazards.

Carbon Tetrafluoride

Carbon tetrafluoride is a colorless nonflammable gas and is usually shipped and stored under pressure as a compressed gas. Carbon tetrafluoride is heavier than air and can displace oxygen starting at lower elevations creating an asphyxiation hazard. Carbon tetrafluoride is usually stored under high pressure which creates a hazard while handling. Symptoms of exposure are confusion, dizziness and headaches as a result of asphyxiation. Skin contact may result in frostbite. On contact with hot surfaces or flames carbon tetrafluoride may decompose and form hydrofluoric acid. There are no established TLVs for carbon tetrafluoride.

Methanol

Methanol is a common product found in a wide variety of household and commercial products. Methanol is highly flammable and toxic, and people can be exposed through inhalation, ingestion and absorption. Short term exposure to methanol may result in irritation to the eyes, skin and respiratory tract and can affect the central nervous system, resulting in the loss of consciousness. Repeated or long-term exposure with the skin may cause dermatitis, while the substance may have effects on the central nervous system resulting in headaches and impaired or loss of vision. Methanol is flammable liquid with a flash point of 52 deg. F, a LEL of 6%, and a UEL of 36%. Mixtures of methanol vapor and air are explosive, and containers may explode when heated. Methanol also reacts violently with strong oxidants, causing fire and explosion hazards. The ACGIH TLVs that apply to methanol are 15-minute STEL of 250 ppm and 8-hour TWA of 200 ppm.

U.S. EH&S Law Compliance and Regulation Implication for the CCC Process

The compliance of the chemicals used in and potential emissions from the CO_2 capture system with US EH&S regulations are summarized in this section. The applicable laws addressed include: Toxic Substances Control Act (TSCA), Comprehensive Environmental Response and Liability Act 1980 (CERCLA), Clean Water Act (CWA), Clean Air Act (CAA), Superfund Amendments and Reauthorization Act (SARA) Title III, the Occupational Safety and Health Act (OSHA), and the Resource Conservation and Recovery Act (RCRA). The flue gas contaminants come directly from the plant and are not addressed in this regulatory review.

The following individual components are the focus of regulatory review:

- Isopentane
- R14 refrigerant
- Ethane
- Methane
- Propane
- n-Butane
- n-Pentane
- n-Hexane
- n-Heptane

A summary of the application for each component in this review is provided in Table 29. Each regulation in Table 29 is discussed separately in the following sections.

Table 29. Regulator overview for components of CCC system

	TSCA	CERCLA RQ (lbs/day)	CWA	CAA HAP	CAA VOC	SARA 302 EHS	SARA 311/312	SARA 313	OSHA Regulated	RCRA
Isopentane	N	N	Y	No	Yes	N	10,000 lbs	N	No* 1,400 pm	Y
R14	N	N	Y	No	No	N	10,000 lbs	N	No	Y
Ethane	N	N	Y	No	No	N	10,000 lbs	N	No* 3,000 pm	Y
Methane	N	N	Y	No	No	N	10,000 lbs	N	No* 5,000 pm	Y
Propane	N	N	Y	No	Yes	N	10,000 lbs	N	No* 2,100 pm	Y
Butane	N	N	Y	No	Yes	N	10,000 lbs	N	No** 800 ppm	Y
Pentane	N	N	Y	No	Yes	N	10,000 lbs	N	Yes 1,000 pm	Y
Hexane	N	5,000	Y	No	Yes	N	10,000 lbs	N	Yes 500 ppm	Y
Heptane	N	N	Y	No	Yes	N	No	N	Yes 500 ppm	Y

*There are no OSHA regulations for these substances or set values that are maximums. The limits given are 10% of the Lower Explosive Limit.

**This is a vacated 1989 OSHA limit that may still be enforced in some states.

TSCA

Toxic Substances Control Act (TSCA) regulations typically apply to specific chemicals including polychlorinated biphenyls (PCBs), asbestos, radon, and lead-based paint under 15 United States Code (USC) § 2601 et seq. Isopentane, R14, ethane, methane, propane, n-butane, n-hexane, and n-heptane are all

listed on the active TSCA inventory allowing companies to manufacture and use these chemicals commercially.

CERCLA

Comprehensive Environmental Response, Compensation, and Liability Act (CERCLA) regulations apply to spills and releases of hazardous substances, contaminants, and other pollutants into the environment. Reporting and clean-up of spills and releases are regulated under 42 USC § 9601 et seq. Any of the products covered by this process are required to comply with CERCLA regulations.

Clean Water Act

Clean Water Act regulations apply to discharges of all chemical products, petroleum products, and wastewaters to Waters of the United States. State water quality regulations also apply to discharges to state waters. The water streams exiting the process should be evaluated for reuse or recycling in the CCC system, otherwise these water streams should be integrated into the facility's wastewater treatment system for management and/or discharge under a NPDES permit. Any of the products covered by this process are required to comply with CWA and state water regulations.

Spills and releases to Waters of the United States are subject to reporting under 33 USC § 1321(b)(5), 40 Code of Federal Regulations (CFR) § 110.6, and 40 CFR § 153.203.

Clean Air Act

The Clean Air Act (CAA) requirements apply to facilities that emit or have the potential to emit pollutants to the atmosphere. The CAA requires facilities that modify (make a physical change to an existing facility that causes an increase in emissions or the emission of a pollutant not previously emitted) to obtain an air quality permit prior to making the change. In this scenario, the addition of the CCC process to an existing facility will cause the emission of isopentane, which is a volatile organic compound (VOC). The potential uncontrolled emissions of isopentane are estimated to be approximately 867 tons per year. The facility used in this scenario is a Prevention of Significant Deterioration (PSD) major source, which is based on the flue gas consisting of NO_2 and SO_2 above 250 tons per year. An emissions increase of VOCs over 40 tons per year will trigger a major modification that will require the installation of the Best Available Control Technology (BACT) for the VOCs. If controls are installed that reduce the increase in VOC emissions to below 40 tons per year, the modification will be a minor modification requiring only a minor source construction permit.

CAA Section 112(r) Risk Management Plan Requirements (RMP) requires stationary facilities that have over a threshold quantity of a regulated substance in a process to develop a Risk Management Plan. The following listed chemicals are used in the CCC process and are RMP regulated substances: isopentane, methane, ethane, propane, n-butane, n-pentane, and ethylene. Each of these substances has an individual threshold quantity of 10,000 lbs. For regulated substances present in a mixture, the regulated substance must be 1% or greater by weight of the mixture, and the entire mixture must meet the National Fire Protection Association flammability hazard rating of 4 (flash point of 73 degrees F or lower), and exceed 10,000 lbs in a process for the RMP regulations to apply. Isopentane is the only chemical not managed in a mixture and therefore would be considered one process and the RMP threshold of 10,000 lbs may be exceeded depending on the engineering of the system. The remaining chemicals listed will be part of the refrigerant loop 1 and/or refrigerant loop 2 and would be considered mixtures. Depending on the engineered size of each refrigerant system, the percentages of each chemical present, and the flammability of these mixtures, the RMP requirements may or may not apply to each of these systems.

Regardless of the amount of chemical on site, the CAA 112(r) General Duty Clause would apply that requires all owners and operators to identify hazards that may result from accidental releases, to design and maintain a safe facility, and to minimize the consequences of releases when they occur.

SARA

Superfund Amendments and Reauthorization Act (SARA) amended CERCLA in 1986. Title III of SARA requires notifications to state emergency response commissions (SERCs) and local emergency planning committees (LEPCs) of bulk chemical storage. Depending on the quantity stored, any of the products covered by this process are required to comply with the bulk chemical storage requirements under SARA.

Section 313 also requires reporting under the Toxic Release Inventory for manufactured, processed and/or otherwise used chemicals; however, the CCC process does not contain any 313-listed products.

SARA also applies to spills and releases of extremely hazardous substances into the environment under 42 USC § 11001 et seq. and should be evaluated on a facility-specific basis.

OSHA

The C5–C7 liquids (i.e., pentane, hexane, and heptane) are the only components of the CCC process that have specified OSHA limits. These range from 500 ppm for hexane and heptane to 1,000 ppm for pentane. The C1–C4 gases are essentially limited only by the OSHA confined space regulation to prevent dangerous accumulations of flammable vapors above 10% of the lower explosive limit. As all the components of the CCC process except isopentane are in a closed loop system, isopentane is the only component that could be in regular contact with the workforce. As discussed in Section B above, as a branched-chain alkane, isopentane is expected to be less toxic than its straight-chain counterpart pentane. With no OSHA limit published for isopentane, the OSHA limit of 1,000 ppm can be substituted.

RCRA

Resource Conservation and Recovery Act (RCRA) regulations apply to hazardous (Subtitle C) and non-hazardous (Subtitle D) solid waste disposal under 40 CFR 239 through 282. As under any regulations, the applicability of federal (and state) regulations should be evaluated on a facility-specific and state-specific basis. For the purpose of this review, only federal RCRA requirements are considered. This analysis does not include a state-specific evaluation.

All materials should be evaluated for recycling opportunities, prior to determination as a solid waste. Solid wastes include gas, liquid, and solid phases. If the waste does not meet the definition of a hazardous solid waste, it will be handled as a non-hazardous solid waste.

To determine if Subpart C (hazardous waste) applies to a given stream, the following questions must be answered (in order):

1) Is the material in question a solid waste?
2) Is the material excluded from the definition of solid waste or hazardous waste?
3) Is the material a listed or characteristic hazardous waste (see Table 30)?

Table 30. Criteria to be considered characteristic hazardous waste under RCRA Subtitle C.

Characteristic	Criteria
Ignitability	Liquid wastes with flashpoints below 60 °C
Corrosivity	Aqueous with pH ≤ 2 or ≥ 12.5
Reactivity	Explode or cause violent reactions or react to release toxic gas or fumes when exposed to water or under normal handling conditions
Toxicity	Presence of chemical above TCLP regulatory levels

Only three streams were identified as solid waste:

Condensed Water Stream Exiting Process after Pre-cooler

Question 1: Is the material in question a solid waste?

This stream is a liquid product of the direct contact pre-cooler, containing only water and sulfur dioxide. If there is no further use of this water stream, it would be a solid waste unless subject to one of the exclusions.

Question 2: Is the material excluded from the definition of solid waste or hazardous waste?

This stream would be excluded from the definition of solid waste if it is transferred for the purposes of reclamation or remanufacturing. Hazardous waste is a subset of solid waste; therefore, if the stream is excluded from the solid waste definition, it would also be excluded from the hazardous waste definition.

This stream would also be excluded from the definition of solid waste if it is managed and treated under an NPDES permit.

Question 3: Is the material a listed or characteristic hazardous waste?

This stream is not a listed or characteristic hazardous waste.

This stream is not a listed hazardous waste and is not likely to be a characteristic hazardous waste.

Cooling Water Stream Exiting Process after Water Heat Exchanger

Question 1: Is the material in question a solid waste?

This stream is a liquid product (water) of the heat exchanger. If there is no further use of this water stream, it would be a solid waste unless subject to one of the exclusions.

Question 2: Is the material excluded from the definition of solid waste or hazardous waste?

This stream would be excluded from the definition of solid waste if it is transferred for the purposes of reclamation or remanufacturing. Hazardous waste is a subset of solid waste; therefore, if the stream is excluded from the solid waste definition, it would also be excluded from the hazardous waste definition.

This stream would also be excluded from the definition of solid waste if it is managed and treated under an NPDES permit.

Question 3: Is the material a listed or characteristic hazardous waste?

This stream is not a listed hazardous waste and is not likely to be a characteristic hazardous waste.

Pollutant Capture/Waste Stream

Question 1: Is the material in question a solid waste?

This stream contains nitrogen oxides and sulfur dioxide collected in the solid-liquid separation and melter processes. This product should be evaluated for further reclamation and recycling opportunities prior to determination as a waste. If there is no further use of this stream, it would be a solid waste.

Question 2: Is the material excluded from the definition of solid waste or hazardous waste?

This stream would be excluded from the definition of solid waste if it is transferred for the purposes of reclamation or remanufacturing. Hazardous waste is a subset of solid waste; therefore, if the stream is excluded from the solid waste definition, it would also be excluded from the hazardous waste definition.

Question 3: Is the material a listed or characteristic hazardous waste?

This stream is not a listed hazardous waste and is not likely to be a characteristic hazardous waste.

Engineering Analysis and Controls for the CCC-ECL Process

Sustainable Energy Solutions, LLC has designed and put into practice a variety of engineering and controls systems to minimize any release of these materials to environment.

Water

All water collected in the CCC-ECL process is injected into the plant process water cleaning system. This amount of water is very small relative to the plant process water streams, so any contamination, which would be minor in all cases, could be easily removed from the water stream. Typically, plant process water is a closed-loop system that does not release water to the environment, thus further decreasing the impact of any water from the CCC-ECL system on the environment.

Isopentane

Isopentane is used as the direct contacting liquid in the CCC-ECL process. As such, it is a valuable material and SES desires to minimize any potential losses. The CCC-ECL process uses specialized controls for the direct-contact desublimating heat exchanger to maintain proper temperatures when the isopentane is in contact with gases that could entrain or carry isopentane out of the process. The clean flue gas composition is monitored in real time to ensure that any upset that could release isopentane is immediately identified and the loss of isopentane is stopped.

The CO_2 product is also cleaned in a distillation column to minimize isopentane rejection in the CO_2. Although the CO_2 product purity requirements could potentially allow for some contaminants in the CO_2, SES prioritizes the removal of isopentane from this stream to decrease isopentane losses.

Pollutants

SOx and NOx compose the main waste stream from the CCC-ECL process. These streams are kept in proper storage vessels until utilized on site or removed from the site for utilization elsewhere. Monitoring equipment is used to identify and fix possible leaks from these vessels. On-site storage is limited to minimize any possible release.

Refrigerants

All other potential hazardous materials in the CCC-ECL process are used as refrigerants. As such, these refrigerants are all used in closed-loop refrigeration cycles. Monitoring equipment is used to quickly identify and fix possible leaks from these processes.

Handling and Storage for the CCC-ECL Process

In general, the hazards for the CCC-ECL process are flammability and frostbite. With proper storage, engineering controls, monitoring, and personal protective equipment (PPE), these hazards can be minimized. Specialized PPE for each chemical is not required, as each component has similar hazards and similar PPE prescribed by the safety data sheets. Protection of the skin and eyes from thermal hazards and liquid contact will be required when there is potential for contact with these chemicals.

4. References

[1] Grace Davison, "SYLOBEAD® Adsorbents for Process Applications," 2010. [Online]. Available: https://grace.com/general-industrial/en-us/Documents/sylobead_br_E_2010_f100222_web.pdf. [Accessed 2017].

[2] D. Li, D. Zeng, H. Han, L. Guo, X. Yin and Y. Yao, "Phase diagrams and thermochemical modeling of salt lake brine systems. I. LiCl+H2O system," *Calphad*, vol. 51, p. 1–12, 2015.

[3] Blackburn and Associates, "Clear roads study establishing effective salt and anti-icing application rates summary report task 2: Update guidelines," Fountain Hills, AZ, 2014.

[4] E. W. Flick, Ed., Industrial Solvents Handbook, 5 ed., Westwood, NJ: Noyes Data Corporation, 1998.

[5] "NBS Tables of Chemical Thermodynamic Properties, J. Phys. Chem. Ref. Data, vol. 11, suppl. 2, 1982," in *Introduction to Chemical Engineering Thermodynamics*, 7E ed., McGraw-Hill, 2005, p. 459.

[6] R Core Team, *R: A language and environment for statistical computing.*, Vienna: R Foundation for Statistical Computing, 2017.

[7] SWEP, Inc..

[8] EPA, "Support Center for Regulatory Atmospheric Modeling (SCRAM): Screen Models and Documentation: AERSCREEN," 2016. [Online]. Available: https://www.epa.gov/scram/air-quality-dispersion-modeling-screening-models#aerscreen. [Accessed 2017].

[9] EPA, "AERMOD Modeling System," 2017. [Online]. Available: https://www.epa.gov/scram/air-quality-dispersion-modeling-preferred-and-recommended-models#aermod. [Accessed 2017].

[10] T. Fout, A. Zoelle, D. Keairns, M. Turner, M. Woods, N. Kuehn, V. Shah, V. Chou and L. Pinkerton, "Cost and Performance Baseline for Fossil Energy Plants Volume 1a: Bituminous Coal (PC) and Natural Gas to Electricity, Revision 3," US Department of Energy, 2015.

[11] I. Austen, "Technology to Make Clean Energy From Coal Is Stumbling in Practice," *The New York Times*, 29 March 2016.

[12] M. Zhao, A. I. Minett and A. T. Harris, "A review of techno-economic models for the retrofitting of conventional pulverised-coal power plants for post-combustion capture (PCC) of CO2," *Energy & Environmental Science*, vol. 6, no. 1, p. 25–40, 2013.

[13] U.S. Energy Information Administration, "International Energy Outlook 2013," U.S. Department of Energy, Washington, DC, 2013.

[14] E. Bingham, B. Cohrssen and F. A. Patty, Patty's Toxicology, Hoboken, N.J.: John Wiley & Sons, 2012.